Excitation and transport in small scale plasmas

Excitation and Transport in small scale Plasmas

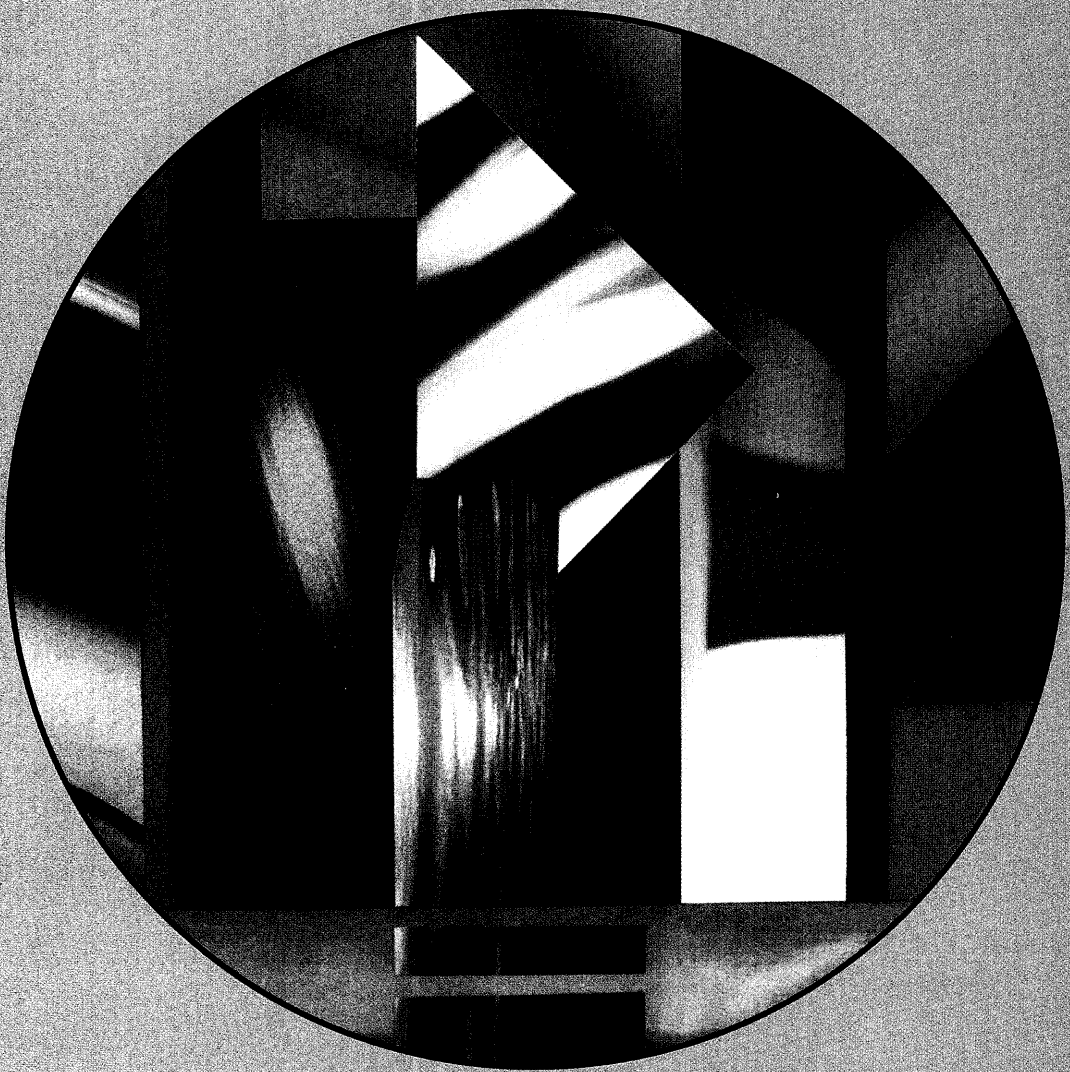

Jeroen Jonkers

Excitation and Transport in small scale Plasmas

Jeroen Jonkers

Omslag: met dank aan Anca Moldovan Feier,
Marco van de Sande en Ger Janssen
Drukwerk: Print Partners Ipskamp, Enschede

CIP-DATA TECHNISCHE UNIVERSITEIT EINDHOVEN

Jonkers, Jeroen.

Excitation and Transport in small scale Plasmas
Jeroen Jonkers
Thesis Eindhoven University of Technology, 1998
With summary in Dutch
NUGI 812
ISBN 90-386-0637-0
Subject headings: plasma diagnostics / plasma torches / fluorescent lamps

Excitation and Transport in small scale Plasmas

Proefschrift

ter verkrijging van de graad van doctor aan de Technische Universiteit Eindhoven, op gezag van de Rector Magnificus, prof.dr. M. Rem, voor een commissie aangewezen door het College voor Promoties in het openbaar te verdedigen op maandag 16 februari 1998 om 16.00 uur

door

Jeroen Jonkers

geboren te Eindhoven

Dit proefschrift is goedgekeurd door de promotoren:

prof.dr.ir. D.C. Schram

en

prof.dr. H.F. Döbele

Copromotor:

dr. J.A.M. van der Mullen

Contents

Dankwoord

Dit proefschrift zou nooit deze staat hebben bereikt zonder Joost van der Mullen. Zijn ideeën, de discussies met hem en zijn humor zijn voor mij van onschatbare waarde geweest.
Of ik iets nu wel of niet kon verklaren, Daan Schram, mijn eerste promotor, wist altijd in een mum van tijd met tenminste drie (alternatieve) verklaringen op te proppen te komen.
De werkgroep ETP vormde een geweldige omgeving voor het verrichten van mijn promotie-onderzoek. Een aantal mensen daarvan wil ik verder specifiek noemen, zoals Eric Timmermans die eerst als afstudeerder en daarna als collega zeer betrokken was bij het TIA werk en Hans de Regt die na zijn vertrek een prachtige opstelling achterliet. Verder heb ik in ruime mate kunnen en mogen profiteren van bijdragen van vele andere studenten: (in volgorde van verschijning) Harald Vos, Igor Martin, Ralph Hanzen, Karel Burm, Marco Bakker, Niels Meelman, Joost van den Heuvel, Harm van der Heijden, Bart Hartgers, Louis Selen, Elwin ter Beek, Micheal Alink en Pascal Herben. De discussies met mijn "theoretische sparring-partners", Dany Benoy, Ger Janssen, Marnix Tas en Jan van Dijk zijn onontbeerlijk geweest. Doet ie 't al, jongens? Van cruciaal belang was tevens de technische ondersteuning van Ries van de Sande, Herman de Jong, Bertus Hüsken en Frans Overberg.
Important "foreign" contributions came from Prof. M. Moisan de l'Université de Montréal, qui m'a gracieusement permis d'utiliser la configuration de la Torche à Injection Axiale, Herman Gielen en Frans Lighthart van Philips Lighting voor de vele discussies over de QL en andere lampen, los tres Antonios de Córdoba, con quiénes he pasado muchas horas agradables, Anca care a realizat coperta si Mariella pentru rabdarea ei deosebita din timpul ultimului an.
En ten slotte wil ik mijn huisgenoten (Ariel en Jan), mijn zus en mijn ouders bedanken voor hun begrip, ondersteuning en geduld.

1

General introduction

The fact that plasmas combine a wide range of operating conditions with a tremendous chemical freedom makes them very suitable for many applications, like deposition and etching of thin layers [1], cutting, welding and spraying [2], spectrochemical analysis [3] and the generation of light [4,5]. However, in order to come to a practical application a plasma should have a limited size. The limited dimensions of artificial plasmas are an essential difference with astrophysical plasmas where the length scales are much larger. The consequences of a small size are that large gradients and corresponding fluxes are created, so that small plasmas can be far from equilibrium.

Deviation from equilibrium has many aspects, of which the most familiar one is the inequality between the temperatures of the electrons T_e and of the heavy particles T_h. This provides the basis for the classification in thermal and non-thermal plasmas, which is often found in the literature [1,2,3,4,5]. In plasmas of the first class, which are also referred to as Local Thermal Equilibrium (LTE) plasmas, the equality $T_e = T_h$ holds, whereas in the second class (severe) deviations can be found. These non-LTE plasmas are generally created in low pressure conditions, so that, due to the lack of effective elastic energy transfer, the electrons are more or less free in kinetic sense and can, heated by an electrical field, reach much higher temperatures than the heavy particles, see for instance [1,4]. It is seductive to proceed classification in the non-LTE conditions by specifying more temperatures, since strong deviations from LTE are indeed accompanied by a wide variety of temperatures. Apart from T_e and T_h also the temperatures associated with the degree of ionisation (T_{ion}), excitation (T_{exc}), rotation (T_{rot}) and vibration (T_{vib}) may be different from each other. In many cases only qualitative statements on the stage of equilibrium departure can be found in which the various temperature values are summed up.

In this thesis we will follow a different route which is based on fluxes and densities rather than temperatures. Due to the small scales of the plasmas, transport of radiation and particles is created, which induces deviations from equilibrium. This may be interpreted as inequalities in temperatures. However, the temperature is only a derivative [6], so that it is more straightforward to study the departures directly; the aim of this study.

One specific goal of this thesis is to achieve a direct relation between the operation parameters by which the plasma is controlled externally, such as pressure, power density and size, on one hand and the internal plasma parameters, like electron density and temperature and the degree of equilibrium departure on the other hand. In this way it can be seen as an extension of the earlier work of Biberman et al. [7], Fujimoto [8] and Van der Mullen [9], who related the non-equilibrium population densities of the excited states to properties of the electron gas.

The main idea behind the study of the direct relation between external and internal parameters is that the dominant local loss mechanism of the free electrons is not volume recombination but diffusion towards the boundaries of the plasma where recombination takes place. This assumption holds for a wide range of combinations of pressures, characteristic sizes and power densities. We will refer to these plasmas as being small or size-stabilised. In this specific class of plasmas the electron particle and energy balances can be simplified, so that a direct relation between the external parameters and the electron temperature and density can be found. In the past this principle has been used to characterise various low pressure plasmas [1,4,10] and in this thesis it is shown that it is also correct to apply it to plasmas which are operated at and around atmospheric pressure. Moreover, together with the density of atoms in the ground state an expression for the departure of equilibrium can be obtained, which can be

used, among others, to determine the validity region of the size-stabilised plasma theory.
The assumption that volume recombination is not important is only valid for atomic plasmas, since the three particle recombination is relatively slow. This picture is changed drastically by the presence of molecules, because they may offer, via dissociative recombination, a fast loss channel for the free electrons. There are three possible sources of molecules:

1. deliberate introduction,
2. entrainment from the surrounding atmosphere in case the plasma is sustained in the open air and
3. created from atoms and ions of the main plasma gas (mostly rare gas molecular ions, like for instance Ar_2^+).

The impact of foreign molecules (the first two sources) depends strongly on the plasma and the kind of molecules in question, so that it can not be treated in a general way. However, the formation (and destruction) of rare gas molecular ions is inherent to (atomic) plasmas at moderate or high pressure. It will be shown that the impact of these molecules on small atmospheric plasmas is not too large, so that the "atomic" low pressure theory can be safely extrapolated to higher pressures.
Besides these theoretical studies, the results and interpretation of experiments on two plasmas are presented. The first one is the TIA ("Torche à Injection Axiale"), which is a microwave induced plasma sustained in the open air. It was developed by the group of Moisan in 1994 [11]. For a typical gas flow of 3 liters per minute (argon or helium) and 1 kW applied power the plasma is 2 mm in diameter and approximately 30 mm long. The TIA is a very flexible, simple and robust plasma source with a relatively low gas consumption and therefore it is an interesting plasma for spectrochemical applications outside a well equipped laboratory such as the on-line monitoring of flue gases [12] and in third world countries.
The other discharge under study is the Philips QL-lamp [13], which was introduced in 1992 as the first commercially available inductive lamp. The QL-lamp is a low pressure argon mercury plasma, which in principle is the same as the well-know fluorescent lamp [4], with one important difference: the power is coupled inductively into the lamp, so that there are no electrodes required. The lack of electrodes benefits the life-time, which is extended to at least 60000 hours compared to 10000 hours for a conventional fluorescent lamp. An other important advantage of electrodeless lamps is that the chemical freedom of plasmas can be fully exploited in the search for more efficient and more environmentally friendly fillings. The QL lamp is 11 cm in diameter and with 80 W power applied to the discharge the partial pressures are typically 100 Pa argon and 1 Pa mercury.

Thesis outline

The first two chapters of this thesis deal with the "early" experimental work on argon and helium plasmas created by the TIA. In chapter 2 the absolute densities of some excited states are presented, obtained by absolute line intensity measurements. It is found that at least two different temperatures can be related to these densities (typically 4000 and 10000 K), which are in good agreement with the temperatures which are often presented in the literature for this kind of plasmas. However, simple calculations show that these temperature values can never be equal to the electron temperature, since they are too low to provide any significant excitation or ionisation of the argon and helium atoms. Our explanation of this paradox (the

temperatures were obtained from the densities of excited states) is that the plasma is far from equilibrium. This is confirmed by the Thomson scattering measurements which are presented in chapter 3. Using this technique it is possible to obtain the electron temperature and density directly. It is indeed concluded that the plasma is not in equilibrium: there is a net production of electrons balancing the losses due to diffusion. Both the production (ionisation) and diffusion losses are larger than the atomic three particle recombination.
In chapter 4 it is shown that excitation temperatures (temperatures obtained from the relative densities of excited states) are by no means characteristic for plasmas far from equilibrium. Especially for helium plasmas this appears to be the case, since these temperatures are almost completely determined by the ionisation potential of the excited states in question.
The non-equilibrium character of the TIA is scrutinised in chapter 5 where a quantitative comparison is made between the ionisation and the losses of electrons due to recombination, convection and diffusion. For a correct estimation of the diffusion losses the spatial resolution of the Thomson scattering setup had to be improved in order to perform measurements as function of the radial position. However, now it is found that there is an overproduction of electrons: the huge ionisation is more than one order of magnitude higher than the estimated losses.
Chapter 6 is devoted to the general relation between the electron temperature and density on the one hand and the characteristic size, power density and gas (helium or argon) of plasmas at atmospheric pressure on the other hand. Moreover, it appears to be possible to predict the conditions under which the temperature related to the excited states is equal to the electron temperature. Besides the characteristic size, power density and pressure this is also determined by the mass of the atom and the ionisation potential of the excited states under study. The molecular rare gas ions are the topic of chapter 7. Their formation and destruction via several reactions is studied and their impact on the plasma is determined.
The investigations of the TIA continue with the hypothesis that the huge production of electrons is necessary to balance the losses of electrons in reactions with entrained foreign molecules (recall that the plasma is sustained in the open air). Chapter 8 deals with Raman and Rayleigh measurements which are used to determine the nitrogen and argon densities and the gas temperature. It is found that the normal, inward diffusion of nitrogen is not fast enough to have any significant influence on the electron particle balance. However, it also appears that the plasma is turbulent and that it is likely that turbulent transport of nitrogen can provide the necessary flux to explain the huge production of electrons. In chapter 9 the various terms of the particle balance are scrutinised. It appears that the TIA can not be described by the general theory of chapter 6, which supports the hypothesis that turbulent transport of nitrogen provides the main loss channel of the electrons.
The last two chapters preceding the general conclusions concern the QL-lamp. In chapter 10 absorption measurements are presented from which the gas temperature and the density of the argon metastable atoms are obtained, both as function of the radius. Chapter 11 deals with two methods to determine the electron density and temperature in the QL plasma: from the experimental results of chapter 10 and using the general theory of chapter 6. A good agreement is found.
The general conclusions concerning the thesis as a whole are presented in chapter 13.

References

1. M.A. Lieberman and A.J. Lichtenberg, *"Principles of plasma discharges and materials processing"*, John Wiley & Sons, New York (1994).
2. M.I. Boulos, P. Fauchais and E. Pfender, *"Thermal plasmas: fundamentals and applications"*, Plenum press, New York (1994).
3. P.W.J.M. Boumans, *"Inductively coupled plasma emission spectroscopy"*, John Wiley & Sons, New York (1987).
4. J.F. Waymouth, *"Electric discharge lamps"*, The M.I.T. Press, Massachusetts (1971).
5. J.J. de Groot and J.A.J.M. van Vliet, *"The high-pressure sodium lamp"*, Philips technical library, the Netherlands (1986).
6. Chapter 4: J. Jonkers and J.A.M. van der Mullen, *"On the excitation temperature in helium plasmas"*, submitted to J. Quant. Radiat. Transf.
7. L.M. Biberman, V.S. Vorobev and I.T. Yakubov, *"Kinetics of nonequilibrium low-temperature plasmas"*, Consultants bureau, New York (1987).
8. T. Fujimoto, J. Phys. Soc. Jpn. **47** 265 and 273 (1979) and **49** 1561 and 1569 (1980).
9. J.A.M. van der Mullen, Phys. Rep. **191** 109 (1990) and J.A.M. van der Mullen, *"Excitation equilibria in plasmas: a classification"*, Ph.D. Thesis Eindhoven University of Technology (1986).
10. C.M. Ferreira, M. Moisan and Z. Zakrzewski, *"Physical principles of microwave plasma generation"*, p11 in *"Microwave induced plasmas"*, ed. by M. Moisan and J. Pelletier, Elsevier, Amsterdam (1992).
11. M. Moisan, G. Sauvé, Z. Zakrzewski and J. Hubert, Plasma Sources, Sci. and Techn. **3** 584 (1994).
12. E.A.H. Timmermas, *"Design of a continuous gas analyser based on MIP-AES for the on-line monitoring of metallic compounds in flue gases"*, report Stan Ackermans Institute, Eindhoven University of Technology (1997).
13. Chapter 10: J. Jonkers, M. Bakker and J.A.M. van der Mullen, J. Phys. D: Appl. Phys. **30** 1928 (1997).

2

On the atomic state densities of plasmas produced by the "Torche à Injection Axiale"

J. Jonkers, H.P.C. Vos, J.A.M. van der Mullen and E.A.H. Timmermans, published in Spectrochim. Acta B **51** 457 (1996).

The atomic state densities of helium and argon plasmas produced by a microwave driven plasma torch called the "Torche à Injection Axiale" are presented. They are obtained by absolute line intensity measurements of the excited states and by applying the ideal gas law for the ground state. It will be shown that the atomic state distribution function (ASDF) does not obey the Saha-Boltzmann law: the ASDF cannot be described by one temperature. From the shape of the ASDF it can be concluded that the plasma is ionising. By extrapolating the measured state densities towards the ionisation limit, a minimum value of the electron density can be determined.

1. Introduction

For several decades microwave induced plasmas (MIPs) have been used as excitation and ionisation sources for atomic emission spectroscopy [1,2,3,4,5]. They have many advantages: apart from being cheap and simple to construct, they are easy to handle. Also, the necessary microwave hardware is cheap and compact nowadays. The versatility in shape as well as in experimental conditions, like pressure, applied power and frequency [6,7,8] is another main advantage.

The various MIPs can be divided in three groups: (1) the surface wave plasmas of which the surfatron is probably the most well known [7], (2) resonance cavities like the Beenakker [3] or the MPCM (integrated microwave plasma cavity/magnetron combination) [9] and (3) torches. The last group is of special interest in analytical chemistry, since torches have a much higher tolerance to injected samples compared to, for instance, the Beenakker cavity [10]. Moreover, due to the absence of a quartz discharge tube no limitation on the power density is imposed by plasma-tube interactions [8]. As a consequence, especially in this field new progress was recently been made. In 1985 Jin *et al.* proposed the MPT (microwave plasma torch) [11,12] and in 1993 the TIA ("Torche à Injection Axiale", i.e. torch with axial gas injection) was developed by the group of Moisan [13]. This paper is devoted to the atomic state densities and the electron densities of plasmas produced by the TIA. The goal is to contribute to the insight in processes taking place in MIP torches.

Two different type of plasmas created by the TIA are investigated: one with helium and the other with argon as main gas. The densities of the excited states are obtained by absolute line intensity (ALI) measurements; the density of the ground state by applying the ideal gas law. A minimum value of the electron density is determined by extrapolating the measured state occupations towards the ionisation limit. The results are compared with the work of Rodero *et al.* who determined the electron density in the helium plasma by the Stark broadening of H_β [14]. They also measured the excitation and the rotational temperatures using relative line intensities [15].

2. Theory

2.1 The Atomic State Distribution Function

The Boltzmann balance describes the exchange of internal energy of atoms with the kinetic energy of free electrons and vice versa. It consists of a forward (excitation) and a backward reaction (deexcitation):

$$A_p + e \overset{B}{\longleftrightarrow} A_q + e \tag{1}$$

Supposing that the number of reactions to the left equals that of the reactions to the right and that there is a Maxwellian energy distribution of the free electrons, the ASDF obeys the Boltzmann relation

$$\frac{\eta_p^B}{\eta_q^B} = exp\left(\frac{E_q - E_p}{kT_e}\right) \tag{2}$$

For the symbols used in this paper we refer to section 7.
The production and destruction of the free electrons is ruled by the Saha balance

$$A_p + e \overset{S}{\longleftrightarrow} A^+ + e + e \tag{3}$$

which links the ASDF to the ionic (ground state) density. In the case that this balance equilibrates, it is found that the ASDF can be described by the Saha formula:

$$\eta_p^S = \eta_+ \frac{n_e}{2}\left(\frac{h}{\sqrt{2\pi m_e kT_e}}\right)^3 exp\left(\frac{E_+ - E_p}{kT_e}\right) \tag{4}$$

Note that two atomic levels which are in Saha relation with the ionic ground state are interrelated to each other by the Boltzmann law. This implies that both balances cooperate by moving the ASDF to a similar distribution. When the whole ASDF obeys Saha (and thus also Boltzmann), the plasma is said to be in Local Saha Equilibrium (LSE). In that case, the production of free electrons equals the destruction by three particle recombination. In other

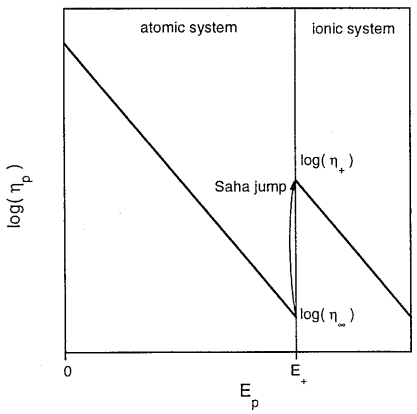

***Figure 1**: The ASDF for a plasma in LSE. At the transition from the atomic to the ionic system the state occupation (η) shows a discontinuity. This is the so-called Saha jump. The size of the jump depends on the electron temperature and density, cf. equation (5) [16,18,19].*

words, the Saha balance is in equilibrium. If only a part of the atomic system is populated according to Saha, this part is said to be in partial Local Saha Equilibrium (pLSE) [16,17,18].

2.2 Electron Densities

In Figure 1 the atomic and ionic state distribution functions according to the Saha relation are depicted. It can be seen that the occupation of the highly excited atomic states is much lower than the occupation of the ionic ground state. This difference is called the Saha jump. By substituting $p \rightarrow \infty$ and assuming $n_e = n_+$ (i.e. no multiply ionised particles), the Saha relation (4) can be written as [19]:

$$n_e = \sqrt{2g_+\eta_\infty}\left[\frac{2\pi m_e kT_e}{h^2}\right]^{3/4} \tag{5}$$

This means that the electron density can be determined from the Saha jump (provided that the electron temperature is known). In this article the electron density obtained in this way will be compared with the electron density obtained by the Stark broadening of H_β [14].

3. Experimental setup

The TIA structure is depicted in Figure 2. It consists of a coaxial structure perpendicular to a rectangular waveguide (WR-340 type, i.e. inner dimensions 86.1×42.9 mm^2). One end of the waveguide is connected to the magnetron and the other end is shorted by a movable plunger. The TE_{01} mode in the rectangular waveguide is transformed into a TEM mode in the coaxial waveguide. Together with the combination of the circular gap and the nozzle the electromagnetic field for sustaining the plasma is shaped. Optimal power coupling is ensured by an impedance transformer (the λ/2 insert) and two moveable plungers [13].
The gas flows through the inner conductor of the coaxial waveguide and the plasma is created just above the nozzle. Note that no discharge tube is used, the plasma just expands in the open

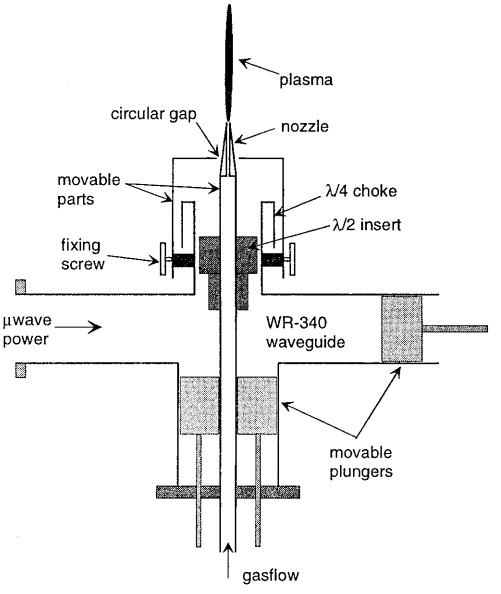

Figure 2: The TIA-structure as proposed by Moisan et al. [13] (not on scale).

Wavelength [nm]	Upper state	Energy level [eV]	Statistical weight	Transition probability $[10^8\ s^{-1}]$
492.19	singlet 4d	23.735	5	0.198
501.57	singlet 3p	23.086	3	0.1338
587.57	triplet 3d	23.072	15	0.7053
667.82	singlet 3d	23.073	5	0.6339
706.52	triplet 3s	22.717	3	0.2786

***Table 1**: The transitions in helium used for the determination of the atomic state distribution functions as presented in this paper. The data are obtained from [22].*

air. The plasma has the shape of a needle: it is approximately 2 mm in diameter and 15 to 50 mm long depending on the carrier gas and applied power.
The light emitted by the plasma is focused by a lens (focal length 24 mm) on a spot-to-line fibre (Ceram Optec, type Optran PUV, transparent from IR down to 200 nm) and guided to a 0.25 m monochromator (Jarrell Ash, type 82-410). Using 25 µm slits and a grating with 1200 grooves/mm the resolution is approximately 0.1 nm. The upper wavelength limit is 800 nm due to the used photomultiplier (Hamamatsu, type RTC XP2233B) and the lower limit is 400 nm due to the blaze angle of the grating (650 nm). The optical system is calibrated by replacing the TIA with a radiance standard [20], a Tungsten ribbon lamp (Thomson lamp, type W2kGV22i). The tables of De Vos [21] give the intensity of the lamp as function of the wavelength.
Since the plasma is very small it is not straightforward to measure radial distributions. Measurements as function of height are obtained by translating the light collection optics.
The spectrum below 470 nm is dominated by molecular bands which arise from association products of molecules from the surrounding air (like the N_2^+ First Negative system, the C_2 Swan system and the CN Violet system). This indicates a strong interaction between the plasma and the open air [8]. Suitable filters are used in order to suppress second order spectra of intense molecular bands.

4. Results

4.1 Atomic State Densities of Helium

The helium plasma is created using an input power of 300 W and a flow of 5.0 slm. The length of this plasma is approximately 15 mm. The upper 3 mm being turbulent is not taken into account in this paper. With our setup only five helium lines can be measured accurately. They are listed in Table 1. The other lines are either too weak, or outside the sensitive range of our detection system, or superimposed on molecular bands.
Using the data listed in Table 1 the absolute densities of the five states can be determined. The result is depicted in Figure 3a. It looks as if the atomic state distribution obeys a Boltzmann relation which results in a temperature $T_{spec} = 3800 \pm 200$ K. This spectroscopically determined temperature is slightly higher than the temperature found by Rodero *et al.* using relative line intensities: 3100 ± 150 K [15].

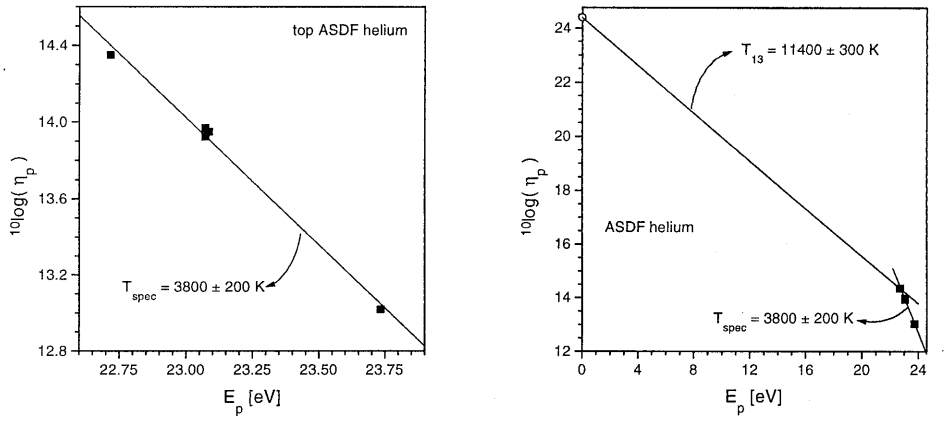

***Figure 3**: The measured ASDF of the helium plasma created by the TIA (measured at approximately 5 mm above the nozzle). The state occupations depicted in Figure a seem to obey a Saha-Boltzmann relation. In Figure b the ground state density based on the ideal gas law (hollow circle) is added to the ASDF. Now strong deviations from Saha-Boltzmann can be observed.*

Since absolute densities were measured, it is possible to include the density of the ground state using the ideal gas law. The gas temperature is unknown, but it can be roughly estimated by the rotational temperature of the N_2^+ molecule: 3000 ± 1500 K [15]. We take a large uncertainty interval since we do not know if the rotational temperature is a good indication of the kinetic temperature. In the next paragraph it will be shown that the exact gas temperature is not that important. So using the ideal gas law the density of the ground state is estimated to be $n_1 \approx (2.4 \pm 1.2) \times 10^{24}$ m^{-3}. Neglecting the electron and ion pressure is justified since the atoms in the ground state are by far the most dominant species (cf. section 5).
In Figure 3b the value of the ground state density is combined with results obtained from the spectroscopic measurements. As can be seen the total ASDF does not obey a Saha-Boltzmann

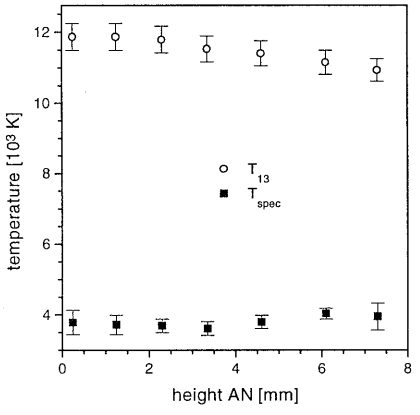

***Figure 4**: The temperatures describing the ASDF (see Figure 3) versus the height above the nozzle (AN). The error bars of T_{spec} correspond to the standard deviations in the fitted slopes; those in T_{13} stem from the uncertainty in the gas temperature.*

relation. The temperature deduced from the ratio of the densities of the lowest measured excited state (i.e. the third level) and the ground state is found to be $T_{13} = 11400 \pm 300$ K. Its accuracy is determined by the unknown gas temperature. However, the influence of the gas temperature uncertainty is very limited. If for instance the gas temperature decreases from 3000 to 1000 K, this results in a decrease of T_{13} from 11400 to 10900 K, i.e. 500 K only.
In Figure 4 the temperatures describing the ASDF are depicted as a function of height above the nozzle (AN). At every point, two temperatures are needed to describe the ASDF. Therefore it can be concluded that at every measured position the plasma is *not* in LSE.

4.2 Atomic State Densities of Argon

An argon plasma is created using an input power of 330 W and a flow of 3.0 slm. This results in a slightly longer plasma (20 mm) than the helium plasma described above. In the argon plasma, much more lines can be measured accurately (cf. Table 2). In this section, measurements at 1 mm AN will be presented.
The measured ASDF is depicted in Figure 5a; in Figure 5b the whole ASDF is plotted including the density of the ground state. The density of the ground state is taken to be equal

Wavelength [nm]	Upper state	Energy level [eV]	Statistical weight	Transition probability [10^8 s^{-1}]
549.59	6d[7/2](4)	15.330	9	0.0176
555.87	5d[3/2](2)	15.136	5	0.0148
557.25	5d'[5/2](3)	15.318	7	0.0069
560.67	5d[1/2](1)	15.117	3	0.0229
565.07	5d[1/2](0)	15.100	1	0.0333
573.95	5d'[5/2](2)	15.312	5	0.0091
603.21	5d[7/2](4)	15.130	9	0.0246
604.32	5d[7/2](3)	15.145	7	0.0153
641.63	6s[3/2](2)	14.838	5	0.121
696.54	4p'[1/2](1)	13.327	3	0.0670
703.03	6s[3/2](2)	14.838	5	0.278
727.29	4p'[1/2](1)	13.327	3	0.0200
738.40	4p'[3/2](2)	13.301	5	0.087
750.39	4p'[1/2](0)	13.479	1	0.472
751.47	4p[1/2](0)	13.272	1	0.430
763.51	4p[3/2](2)	13.171	5	0.274
772.42	4p'[1/2](1)	13.327	3	0.127

***Table 2**: The transitions in argon used for calculating the atomic state densities as depicted in Figure 5 [22].*

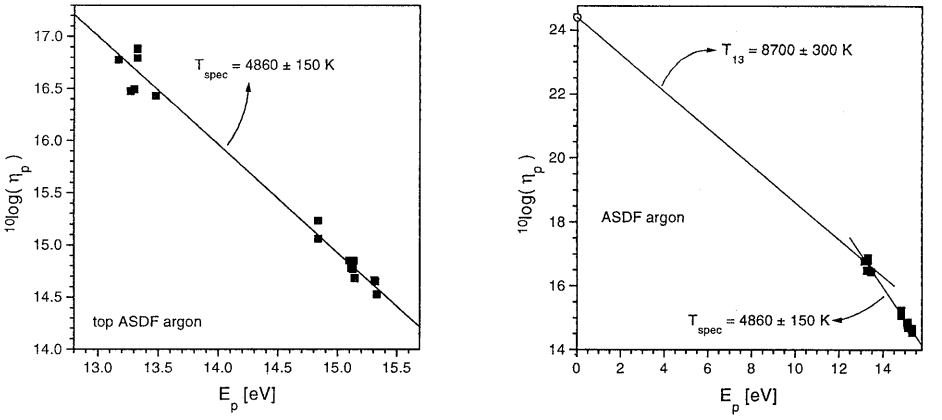

***Figure 5**: The measured ASDF of the argon plasma created by the TIA (measured at approximately 1 mm AN). Just like in the helium plasma the top of the ASDF, depicted in figure a, seems to obey a Saha-Boltzmann relation. However when the ground state density, based on the ideal gas law (hollow circle), is added to the ASDF (figure b), strong deviations from Saha-Boltzmann are also observed.*

to that in the helium plasma, $n_1 \approx (2.4 \pm 1.2) \times 10^{24}$ m^{-3}.
The ASDF in the argon plasma is also described by two temperatures: one for the states determined by spectroscopy $T_{spec} = 4860 \pm 150$ K and one for the ratio between the ground state and the first measured excited state (i.e. the third level): $T_{13} = 8700 \pm 300$ K.

4.3 Discussion

For both the helium and argon plasmas it is found that the ASDF does not obey Saha-Boltzmann. As we stated in the theory section, these relations are only valid when the corresponding balances are in equilibrium: the number of forward reactions has to be equal to the number of backward reactions.
A basic property of plasmas is the presence of charged particles. For a laboratory plasma with small dimensions, this implies the presence of large differences in ion densities. These large gradients will create diffusion, i.e. outward transport of ions and electrons. In steady state this can only be sustained if the number of ionisation processes per unit of volume and time, the so-called ionisation flow, equals the recombination flow *plus* the outward flow of ions in space (cf. Figure 6a). The inequality between the ionisation and recombination flows implies that the Saha balance (3) is not in equilibrium: the number of reactions to the right (ionisation) is larger than the number of reactions to the left (recombination). As a consequence the groundstate must be overpopulated with respect to the density according to the Saha equation. That is

$$b_1 = \frac{\eta_1}{\eta_1^S} > 1 \qquad (6)$$

Since the ionisation flow is mainly stepwise of character, a chain of disturbed Boltzmann balances is needed to generate the flow, which is accompanied by a chain of inequalities:

$$b_1 > b_2 > b_3 > \ldots > 1 \tag{7}$$

i.e. each level has to be more overpopulated than its adjacent higher level, cf. Figure 6c [17,18,19,23].

The monotonically decreasing of b_p as a function of principal quantum number p predicts that b_p approaches unity for $p \rightarrow \infty$. That is, approaching the continuum we will eventually meet with levels for which the number of ionising and recombining processes is much larger than the net ionisation flow through that part of the system. This can be understood by realising that the ionising rate increases with p^2 whereas the flow decreases with p^{-1} [18]. Therefore

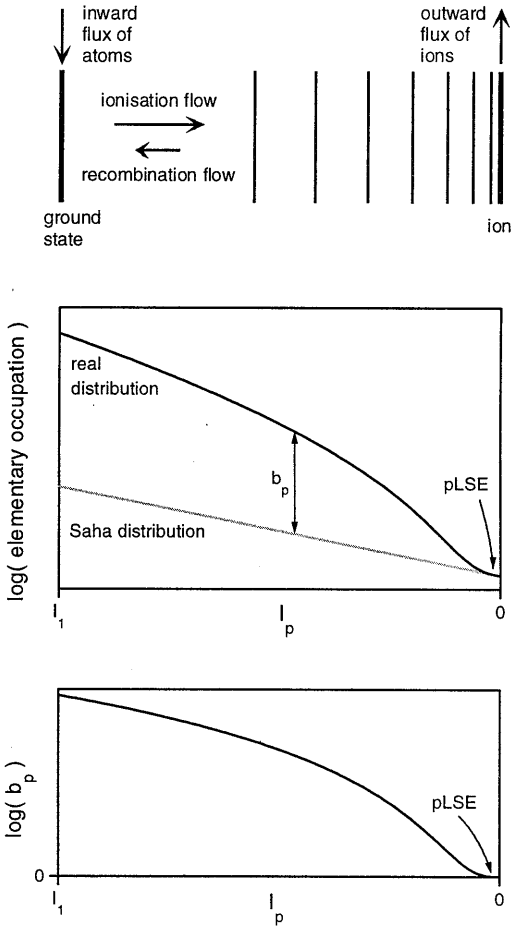

***Figure 6**: The ASDF of an ionising plasma [18].*

a) In steady state an outward flux of ions has to be compensated by a net ionisation flow.

b) Due to the drain of ions the lower lying atomic states are overpopulated with respect to Saha.

c) This overpopulation decreases with increasing effective quantum number. Only the highest levels are in partial Local Saha Equilibrium (pLSE). For strongly ionising plasmas this part of the ASDF is not observable.

above a certain p-value the population is (nearly) according to Saha. This part of the atomic system is said to be in partial Local Saha Equilibrium (pLSE) and the excitation temperature of this region will be equal to the electron temperature [17,18]. Lower in the atomic system the states are not in pLSE and the corresponding excitation temperature will be lower than the electron temperature (cf. Figure 6b).
The shape of the ASDF as depicted in Figure 3 and Figure 5 is similar to the ASDF of an ionising plasma as shown in Figure 6b. However, it should be stressed that *none* of the measured atomic states presented in this paper is in pLSE. Apparently the ionisation flow is so large that pLSE is not yet reached for the highest observable level.
One *could* argue that the upper part of the ASDF as depicted in Figure 3a is in pLSE, since this part looks like a straight line. However, if these states were in pLSE the slope of the line in Figure 3a should correspond to the electron temperature and extrapolation of this line towards the ground state would yield a "Saha" density of $\eta_1^S \approx 10^{41}$ m^{-3} (cf. Figure 3b), so that the ground state would be hugely underpopulated. This would refer to a recombining plasma region. But since everywhere in the helium plasma the ASDF is more or less similar this would imply that the whole plasma is recombining (note that there will be no plasma inside the inner conductor of the coaxial structure of the TIA, since there the EM-fields are absent). This means that there are no regions where charged particles are produced which is in contradiction with the existence of the plasma. Therefore it has to be concluded that (1) both the helium and argon plasmas are ionising and that (2) the temperatures derived from the slopes in the Boltzmann plots are underestimations of the electron temperature.

5. Electron Densities

The Saha jump can be used to determine the electron density as was discussed in section 2.2. For the helium plasma the electron densities obtained in this way are depicted in Figure 7. For the electron temperature 24000 ± 6000 K is taken. This value and a large error interval are chosen, since we only know that the electron temperature has to be larger than the temperatures derived from the slopes in the Boltzmann plot (12000 K).
Note that the top of the measured ASDF is not in pLSE, so that the slope of the fitted line is too steep and η_∞ underestimated, which results in a too low electron density. Compared to the

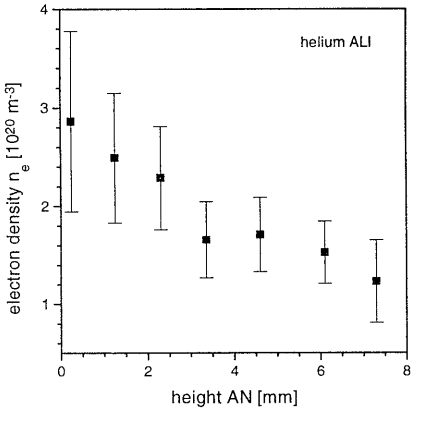

***Figure 7**: The electron density in the helium plasma as a function of height. The values are obtained by extrapolating the measured atomic state densities towards the ionisation limit. The error bars are determined by the unknown electron temperature and the inaccuracy of the fits.*

measurements of Rodero *et al.* [14] the densities presented in Figure 7 are slightly lower: they measured $n_e = (3.8 \pm 0.2) \times 10^{20}$ m^{-3} just above the nozzle.
The resulting densities seem to decrease linearly with height. However, due to the systematic error in the determination of the electron density, other techniques are necessary to confirm this tendency.
In the argon plasma, extrapolating the atomic state densities of the top yields $\eta_\infty = (1.39 \pm 0.16) \times 10^{14}$ m^{-3}. Using an electron temperature of 18000 ± 5000 K (again the only thing we know is that $T_e > 8700$ K), gives an electron density of $(18 \pm 4) \times 10^{20}$ m^{-3} at approximately 1 mm AN.

6. Conclusions

Atomic state densities of helium and argon plasmas produced by the TIA are presented. The plasmas are shown to be out of equilibrium; at least two temperatures are needed to describe the ASDF: one for the ratio between the ground and the first measured excited state (i.e. the third level), T_{13}, and a second, T_{spec}, for the states measured by ALI. These temperatures are listed in Table 3. In helium, T_{spec} is independent of height, whereas T_{13} decreases slightly as function of height.
The similarity between the measured atomic state distributions and the theoretical ASDF for an ionising plasma indicates that these plasmas are ionising. This means that only the excitation temperature obtained from the states which are in pLSE equals the electron temperature. However, the parts of the ASDF which are presented are *not* in pLSE and therefore the temperatures listed in Table 3 are an underestimation of the electron temperature. A different technique as for instance Thomson scattering is necessary to determine the electron temperature.
By extrapolating the measured atomic state densities, an estimation of the electron densities can be obtained. In helium, this density seems to decrease linearly with height: from (2.9 ± 0.9) just above the nozzle down to $(1.2 \pm 0.4) \times 10^{20}$ m^{-3} at 7.3 mm AN. The first value is slightly lower than the densities found by Rodero *et al.* [14]. Unfortunately in this last paper, measurements are not provided as a function of height. In argon, the obtained electron density is approximately $(18 \pm 4) \times 10^{20}$ m^{-3}. However, also in this case, systematic errors occur since the plasma is ionising and the measured states are not in pLSE.
In general it can be stated that the method of absolute line intensity measurements is a relatively simple way of obtaining information from a plasma. It can be done without expensive or complicated apparatus. However, for a plasma which is not in equilibrium, the interpretation of the results is not straightforward.

		He	Ar
T_{13}	[K]	11400 ± 300	8700 ± 300
T_{top}	[K]	3800 ± 200	4860 ± 150

***Table 3**: Typical temperatures which describe the ASDFs as found in this paper.*

7. Nomenclature

E_p energy of level p with respect to the ground state
E_+ energy of the ion ground state with respect to the atomic ground state
g_p statistical weight of level p
g_+ statistical weight of the ion ground state
h Planck's constant
k Boltzmann's constant
m_e mass of the electron
n_e electron density
n_p atomic state density of level p
p effective quantum number
q an other effective quantum number
R Rydberg's constant
T_{13} temperature related to the ratio of the ground and the first measured excited state (i.e. the third level) according to equation (2), cf. Figure 3
T_e electron temperature
T_{spec} temperature describing the ratio of the atomic state densities determined by absolute line intensity measurements, cf. equation (2) and Figure 3
η_p elementary occupation of level p, i.e. n_p / g_p
η_p^B elementary occupation of level p according to Boltzmann (2)
η_p^S elementary occupation of level p according to Saha (4)
η_∞ extrapolated elementary occupation for $p \rightarrow \infty$, cf. Figure 1

References

1. A.J. McCormick, S.C. Tong and W.D. Cooke, Anal. Chem. Acta **37** 1477 (1965).
2. R.M. Dagnall, T.S. West and P. Whitebread, Anal. Chem. Acta **60** 25 (1972).
3. C.I.M. Beenakker, B. Bosman and P.W.J.M. Boumans, Spectrochim. Acta B **33** 373 (1978).
4. K.J. Slatkavitz, P.C. Uden, L.D. Hoey, R.M. Barnes, J. Chromat. **302** 277 (1984).
5. Q. Jin, F. Wang, C. Zu, D.M. Chambers and G.M. Hieftje, J. Anal. At. Spectrom. **5** 487 (1990).
6. A. Granier, E. Bloyet, P. Leprince and J. Marec, Spectrochim. Acta B **43** 963 (1988).
7. M. Moisan and Z. Zakrzewski, J. Phys. D: Appl. Phys. **24** 1025 (1991).
8. E.A.H. Timmermans, J. Jonkers, I.A.J. Thomas, A. Rodero, M.C. Quintero, A. Sola, A. Gamero and J.A.M. van der Mullen, *"The behavior of molecules in microwave induced plasmas studied by optical emission spectroscopy: 1. plasmas at atmospheric pressure"*, in preparation.
9. H. Matusiewicz, Spectrochim. Acta B **47** 1221 (1992).
10. J.F. Camuña-Aguilar, R. Pereiro-Garcia, J.E. Sánchez-Uría and A. Sanz-Medel, Spectrochim. Acta B **49** 545 (1994).
11. Q. Jin, G. Yang, A. Yu, J. Liu, H. Zang and Y. Ben, Pittsburgh Conference Abstracts #1171 (1985).
12. Q. Jin, C. Zhu, M.W. Borer and G.M. Hieftje, Spectrochim. Acta B **46** 417 (1991).
13. M. Moisan, G. Sauve, Z. Zakrzewski and J. Hubert, Plasma Sources, Sci. and Techn. **3** 584 (1994).

14. A. Rodero, M.C. Quintero, M.C. García, A. Sola and A. Gamero, Europhysics Conference Abstracts **18E** *ESCAMPIG XII*, 203 (1994).
15. M.C. Quintero, A. Rodero, A. Gamero and A. Sola, Europhysics Conference Abstracts **18E** *ESCAMPIG XII*, 342 (1994).
16. J.A.M. van der Mullen, Spectrochim. Acta B **44** 1067 (1989).
17. J.A.M. van der Mullen, Spectrochim. Acta B **45** 1 (1990)
18. J.A.M. van der Mullen, Phys. Rep. **191** 109 (1990).
19. J.A.M. van der Mullen, I.J.M. Raaijmakers, A.C.A.P. van Lammeren, D.C. Schram, B. van der Sijde and H.J.W. Schenkelaars, Spectrochim. Acta B **42** 1039 (1987).
20. J. Voogd, Philips Techn. Tijdschr. **5** 87 (1940).
21. J.C. de Vos, Physica **20** 690 (1954).
22. W.L. Wiese and G.A. Martin, *"Wavelengths and transition probabilities for atoms and atomic ions"*, part 2: *"Transition probabilities"*, U.S. Government Printing Office, Washington (1980).
23. F.H.A.G. Fey, D.A. Benoy, M.E.H. van Dongen and J.A.M. van der Mullen, Spectrochim. Acta **50** 51 (1995).

3

On the electron densities and temperatures in plasmas produced by the "Torche à Injection Axiale"

J. Jonkers, J.M. de Regt, J.A.M. van der Mullen, H.P.C. Vos, F.P.J. de Groote and E.A.H. Timmermans, published in Spectrochim. Acta. B **51** 1385 (1996).

The electron temperature and the electron density of plasmas created by the "Torche à Injection Axiale" (TIA) are determined using Thomson scattering. In the plasma with helium as main gas, temperatures around 25000 K and densities between 0.64 and 5.1 × 10^{20} m^{-3} are found. In an argon plasma the electron temperature is lower and the electron density is higher: 17000 K and around 10^{21} m^{-3} respectively. From these results it can be established that the ionisation rates of both plasmas are much larger than the recombination rates, which means that the plasmas are far from Saha equilibrium. However, deviations from a Maxwell electron energy distribution function, as reported for the "Microwave Plasma Torch" (MPT), are not found in the TIA. The excitation and ionisation power of the latter torch appears to be stronger than that of the MPT.

1. Introduction

The "Torche à Injection Axiale" (TIA), i.e. torch with axial (gas) injection, was developed by the group of Moisan in 1993 [1]. This microwave driven torch can create argon and helium plasmas with powers up to 2 kW without any external cooling.

In a previous chapter [2] we presented the atomic state distribution function (ASDF) of argon and helium plasmas created by the TIA. The densities of the excited states were obtained by absolute line intensity measurements and the ground state density by applying the ideal gas law. It was found that the ASDF of both plasmas does not obey the Saha equation, which was explained by assuming that both plasmas are strongly ionising. Therefore it is not possible to determine the electron temperature with this method: the measured excitation temperature is much lower than the electron temperature. Also the electron densities, which are obtained by extrapolating the ASDF towards the ionisation limit, are too low [2]. Since the electron temperature T_e and density n_e are important parameters for a thorough understanding of the processes taking place in the TIA, we performed Thomson scattering measurements. Using the determined values of n_e and T_e, the Saha values of the ground state density can be computed and compared with the actual density as obtained from the ideal gas law. From this comparison it can be concluded that the Saha balance of ionisation and recombination for the ground state is far from equilibrium: the number of ionisation processes exceeds the number of recombination processes. Since the ionisation process is mainly stepwise of character [3,4], this departure from equilibrium propagates through the atomic system and is especially present in the lower (and detectable) part of the atomic system. Therefore we may state that deviation from Saha equilibrium, as found with these Thomson experiments, supports the interpretation of the non-equilibrium ASDF as given in our previous study [2].

Two different kind of plasmas created by the TIA are investigated: a helium and an argon plasma. The results will be compared with similar measurements performed by Huang *et al.* [5] on an other microwave driven torch: the "Microwave Plasma Torch" (MPT) [6,7].

2. Experimental Setup

The TIA structure is depicted in Figure 1. It consists of a coaxial structure perpendicular to a rectangular waveguide (in our case a WR-340, i.e. inner dimensions 86.1×42.9 mm^2). One end of the waveguide is connected to a magnetron and the other end is shortened by a moveable plunger [1].

The gas (either argon or helium) flows through the inner conductor of the coaxial structure and the plasma is created just above the nozzle. Note that no discharge tube is used; the plasma just expands in the open air. The plasma has the shape of a needle: it is approximately 2 mm in diameter and 15 to 50 mm long depending on the gas and the applied power. The radius of the nozzle is 0.9 mm.

The used Thomson scattering setup is treated thoroughly in an other paper [8], so we will only discuss its most important features. A pulsed (10 Hz), frequency doubled Nd:YAG laser at 532 nm is applied to produce an intense light beam. Some photons are scattered by the free electrons (Thomson scattering), by the bound electrons (Rayleigh scattering) or by the molecules (Raman scattering) present in the plasma. The width of the Thomson scattering profile is related to the electron temperature and its area is proportional to the electron density. A part of the photons scattered under 90° is collected by two positive lenses and focused (1:1 image) on the entrance slit of the monochromator, cf. Figure 2. The detection volume is determined by this entrance slit (0.5 mm high and 0.3 mm wide) and the diameter of the laser beam (1.5 mm). Note that it is not possible to investigate the plasma as a function of radius, since the diameter of the laser beam is only slightly smaller than the diameter of the plasma.

Using a grating with 2000 lines/mm the spectrum of the scattered light is imaged on an intensified linear photodiode array (LPA). In order to suppress the light emitted by the plasma, the intensifier is synchronised with the shots of the laser.

Due to the high neutral density the Rayleigh scattering signal is very intense and superimposed on the centre of the Thomson signal. To prevent disturbing of the Thomson

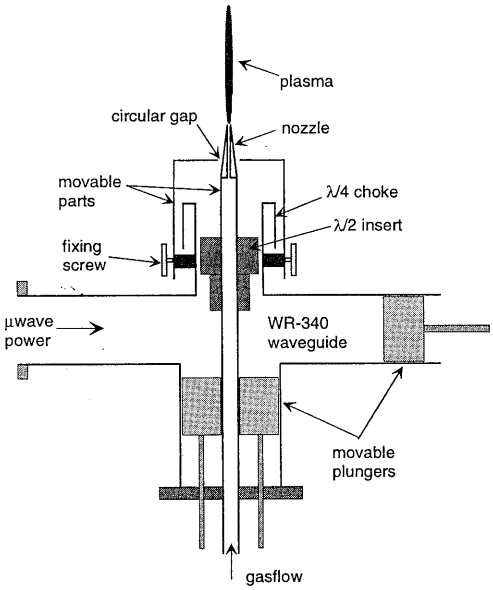

***Figure 1**: The TIA-structure as proposed by Moisan et al. [1] (not on scale).*

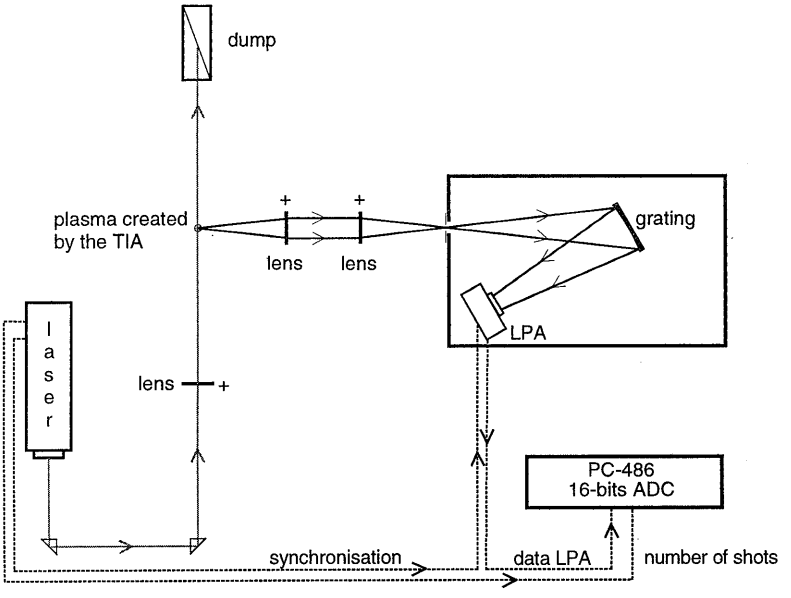

***Figure 2**: The Thomson scattering setup [8].*

scattering profile by blooming of the LPA the central pixels are physically darkened. Two typical examples of measured profiles are depicted in Figure 3.
The electron temperature and density are obtained by fitting a function through the obtained Thomson profile. If the Electron Energy Distribution Function (EEDF) obeys a Maxwell distribution and if every detected Thomson photon is scattered by one (and only one) electron

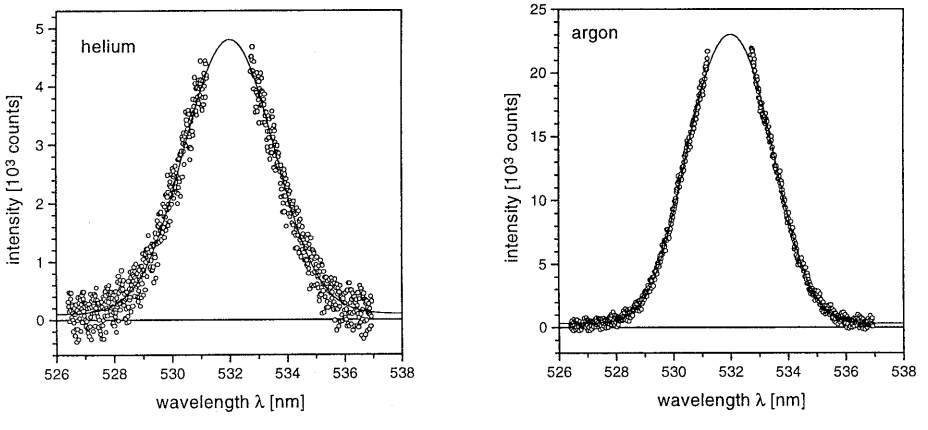

***Figure 3**: Two typical Thomson scattering profiles obtained from plasmas generated by the TIA. These measurements are performed at 1 mm above the nozzle (AN), using the settings listed in section 3. The solid curves are the fits to determine the electron temperature and density. The absence of the signal around the central wavelength is due to the fact that the central pixels are blocked to prevent blooming caused by the intense Rayleigh signal.*

this function would be Gaussian. However, due to the high electron density collective scattering has to be taken into account, as is extensively discussed by Evans and Katzenstein [9]. In this case a modified Gaussian is more appropriate, which is also used by Huang *et al.* [10]. Studying our data carefully, it was found that apart from this modified Gauss function an offset is needed to get a proper fit. The origin of this background can be a limited resolving power of the grating and/or (Rayleigh) photons which are scattered at the inside of the monochromator and not dispersed by the gratings. Therefore the modified Gauss function must have an offset for a proper fitting procedure. In Figure 3 these fits are represented by solid curves. In both cases the offset is around 150 counts.
The setup is calibrated using the Raman scattering signal of nitrogen. During this procedure the plasma is switched off and its main gas is replaced by nitrogen [8].

3. Results

3.1 Helium

A helium plasma is created using 300 W input power and a flow of 5.0 slm. The length of this plasma is about 10 mm. The turbulent upper 3 mm is not investigated in this paper. In Figure 4a the electron temperature is depicted as a function of the height above the nozzle (AN), i.e. the axial position. The temperature is more or less stable around 25000 K and drops to 19100 K at 5 mm AN. The accuracy of the fits is approximately ± 300 K. As expected the measured electron temperatures are much higher than the excitation temperatures found in our previous study [2]: $T \leq 11900 \pm 300$ K.
The electron density as a function of height is presented in Figure 4b. It appears that n_e decreases from (5.1 ± 0.8) at 1 mm to $(0.64 \pm 0.10) \times 10^{20}$ m^{-3} at 5 mm AN. The inaccuracy of 15% is mainly due to the calibration [8]. The electron density tends to decrease with the height above the nozzle, which was also found in our previous study [2]. However, the electron densities obtained by Thomson scattering are higher than those determined by extrapolating the ASDF towards the ionisation limit: $n_e = (2.9 \pm 0.9) \times 10^{20}$ m^{-3} at 0.3 mm AN. As stated in the introduction this difference is due to the strong non-equilibrium character of this plasma, which results in an underestimation of the electron density.

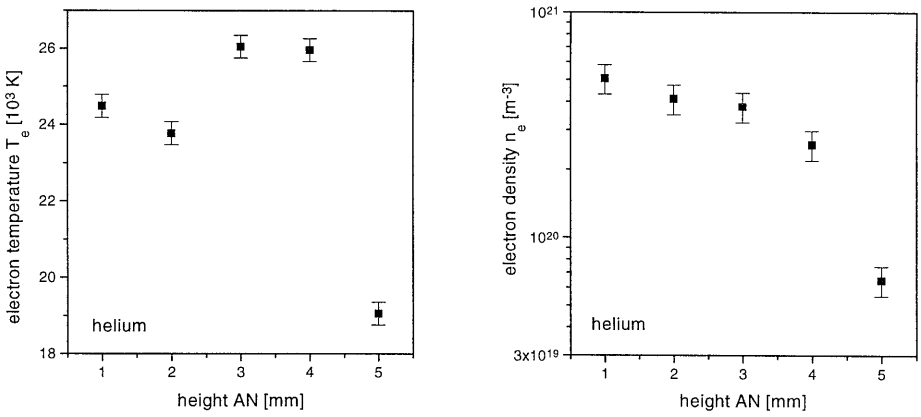

***Figure 4**: The electron temperature and density in the helium plasma.*

Rodero *et al.* [11] used the Stark broadening of H_β to determine the electron density in this helium plasma. Under similar conditions (3.0 slm, 300 W) they found a slightly lower electron density: $(3.8 \pm 0.2) \times 10^{20}$ m^{-3} just above the nozzle.

3.2 Argon

An argon plasma is created using 330 W input power and a flow of 2.0 slm. This results in a slightly longer plasma (15 mm) than the helium plasma described before. The measured electron temperatures are depicted in Figure 5a. The electron temperature remains stable around 17000 K, except for a strange dip between 5 and 6 mm AN. On the other hand the electron density decreases from (22 ± 3) to $(3.5 \pm 0.5) \times 10^{20}$ m^{-3}, as can be seen in Figure 5b. Again, the electron temperature and density obtained by Thomson scattering are much higher than those resulting from absolute line intensity measurements, which in our previous study [2] were found to be: $T \leq 8700 \pm 300$ K and $n_e = (18 \pm 4) \times 10^{20}$ m^{-3} at 1 mm AN.

4. Discussion

4.1 Ionisation and Recombination

Using the measured electron temperature and density, it is possible to calculate the Saha value of the ground state density n_1^S:

$$\frac{n_1^S}{g_1} = \frac{n_e n_+}{2g_+}\left(\frac{h}{\sqrt{2\pi m_e kT_e}}\right)^3 exp\left(\frac{I_1}{kT_e}\right) \qquad (1)$$

The ionic ground state density is represented by n_+, and g_1 and g_+ are the statistical weights of the atomic and ionic ground states respectively. The ionisation energy of the atomic ground state is represented by I_1. The other symbols have their usual meaning. Assuming no multiple ionised particles ($n_e = n_+$) this yields typically $n_1^S = 5 \times 10^{18}$ m^{-3} for the helium plasma ($T_e = 25000$ K and $n_e = 4 \times 10^{20}$ m^{-3}).

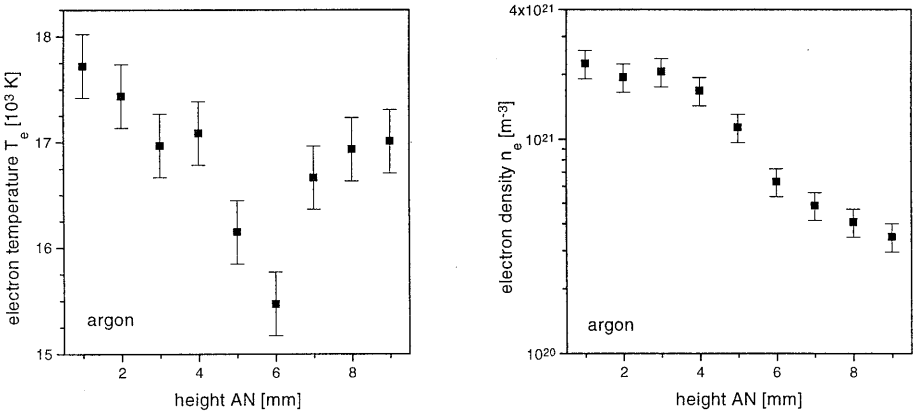

***Figure 5**: The electron temperature and density in the argon plasma obtained by Thomson scattering.*

The actual ground state density n_1 can be computed using the ideal gas law

$$n_1 = \frac{p}{kT_g} \tag{2}$$

Neglecting the electron and ion pressure is justified since the atoms in the ground state are by far the most dominant species. For atmospheric pressure and a gas temperature $T_g \approx T_{rot} = 3000$ K [12,13] the ground state density is approximately 2×10^{24} m^{-3}, which is 4×10^5 times higher than the density according to Saha. As discussed in many previous studies [2,3,4,14,15,16], overpopulation of a level with respect to Saha implies that the number of ionisation processes from that level exceeds the number of three particle recombination processes to that level. So the overpopulation of the ground state in the helium plasma indicates an ionising plasma: the plasma is continuously creating new ions and free electrons. This does not necessarily imply that the electron density will increase as a function of time: in steady state the production of free electrons is balanced by diffusion and/or flow, as will be discussed more quantitatively in a next paper [17]. Also the argon plasma is strongly ionising: following the same procedure the ground state is found to be 10^6 times overpopulated with respect to Saha ($T_e = 17000$ K and $n_e = 10 \times 10^{20}$ m^{-3}).
Due to the huge overpopulation of the ground state, the excitation rate from this state to the first excited state is larger than in case of Saha equilibrium. Consequently, the first excited state is overpopulated with respect to Saha. Again, this induces a larger excitation from the first to the second excited state, leading to an overpopulation of this state, etc. Therefore, due to the stepwise ionisation flow, resulting from the overpopulation of the ground state, the complete lower part of the ASDF deviates from Saha equilibrium [2,3,4,14,15,16].
In general all atmospheric plasmas with a radius of a few millimetres (like for instance the TIA, the MPT [7] and the high pressure surfatron [18]) will have a large gradient in the electron density. This creates large losses of free electrons due to diffusion, which have to be compensated by ionisation. Therefore, it can be stated that in steady state (the detectable part of) the ASDF in the active zone of "small" plasmas will deviate from Saha equilibrium. In these cases it will be very difficult to determine the electron temperature and density by measuring absolute line intensities[a].
If we compare the results of both plasmas we can conclude that in the helium plasma T_e is higher and n_e lower than in the argon plasma. The bottle-neck in the ionisation process is the relatively large step from the ground state to the first excited state. Since the energy of the first excited state is higher for helium than for argon the helium plasma needs a higher electron temperature to maintain itself[a].

4.2 Departures from Equilibrium

In our previous paper [2], it was already concluded that the excitation temperature of the excited states (T_{exc}) is lower than the excitation temperature between the ground and the second excited state (T_{13}). Both temperatures are lower than the electron temperature, but much higher than the gas temperature:

$$T_e > T_{13} > T_{exc} > T_g \tag{3}$$

[a] This will be discussed in a more general way in chapter 6.

Therefore it can be stated that the plasmas produced by the TIA are not in Local Thermal Equilibrium (LTE) [3,19].
As discussed in previous papers [2,3,4,16] the overpopulation of the ground state with respect to Saha propagates through the atomic system and gradually decreases, supporting the stepwise ionisation flow. For levels close to the continuum the rates of ionisation and recombination are very high, so that the Saha balance is not disturbed much. The net ionisation flow is relatively small, so that these levels are in partial Local Saha Equilibrium (pLSE) [2,3,4,16]. Therefore, approaching the continuum the slope in the ASDF will tend to the value corresponding to the electron temperature. That is why the excitation temperatures are not constant.
This is in contrast with the "theory of quantum statistical modelling", where a Fermi-Dirac distribution is used to describe the ASDF [20,21]. In this case one "thermodynamic" temperature is yielded, which is erroneously declared as *the* temperature for all particles in the detection volume [21]. Fermi-Dirac statistics is a consequence from the Pauli principle, which forbids two electrons to occupy exactly the same quantum state [22]. However, in a plasma the average distance between two (excited) atoms is too large for any significant overlap between the wave functions of the electrons in the excited states. Therefore, the distribution of the electrons over the excited states is not restricted by the Pauli principle and Fermi-Dirac statistics is irrelevant; the classical approach (using Boltzmann-Saha statistics) is more appropriate. The observation that in laboratory plasmas (of small dimensions) deviations from the Saha-Boltzmann distribution are present is because the outward transport of particles generates deviations from equilibrium [2,3,4,16]. Of course, outward transport of particles will not impose an other equilibrium distribution.
Also the statement that "all species in a given volume region must share the same thermodynamic temperature when the system is either at equilibrium or in a stationary state" [21] is not true. As discussed at the beginning of this section, the electron temperature is much higher than the gas temperature. This is a direct consequence from the facts that

- only the electrons are heated by the electromagnetic field
- the heat transfer from electrons to heavy particles is inefficient due to the large mass difference [3].

Also in other plasmas it is found that the electron temperature is higher than the gas temperature, for instance in the MPT [5], in the ICP [23,24,25] and in fluorescent lamps [26,27].

4.3 TIA versus MPT

The MPT is a smaller microwave torch with an open top, which was developed by Jin *et al.* [6,7]. It has a similar coaxial structure as the TIA, but the microwave power is fed by a coaxial cable instead of by a waveguide. Inside the inner conductor of the coaxial structure a smaller tube is placed, so that there are two independent gas flows. At low power (typically 100 W and lower) the plasmas produced by the MPT have a comparable shape as those produced by the TIA. When more microwave power is used the shape of the MPT plasma becomes like the flame of a candle [5].
In Table 1 the results presented in this paper are compared with the results for the MPT obtained by Huang *et al.* They applied Thomson scattering, using more or less similar conditions: 350 W power and a total gas flow of 2.0 slm argon or 4.0 slm helium [5].

		helium		argon	
		T_e [10^3 K]	n_e [10^{20} m^{-3}]	T_e [10^3 K]	n_e [10^{20} m^{-3}]
TIA		19.1 .. 26.0	0.64 .. 5.1	17.0	3.5 .. 22
MPT	350 W	16.7 .. 20.0	0.65 .. 1.2	13.0	0.4 .. 10
	100 W	21.5	0.6		

***Table 1**: A comparison between the values of the electron temperature and density in the TIA (this study) and in the MPT [5]. It should be realised that the shape of the MPT plasma at 100 W is different from the shape at 350 W.*

The electron temperatures and densities of the TIA are higher than those of the MPT. This indicates that the TIA is a more effective source for excitation and ionisation of analytes. Moreover, the TIA can easily work at a power of 2 kW [1] whereas the power of the MPT is limited by the coaxial cable.
The fact that the TIA is a better source for excitation and ionisation does not necessarily imply that its detection limits of introduced analytes are better. At the same value of the input flow and length of the plasma the residence time in the MPT is longer than in the TIA, since the total area of the cross section of the "nozzle" of the MPT is five times larger (2.5 mm^2 and 12 mm^2 for the TIA and MPT respectively).

4.4 The Shape of the EEDF

Huang *et al.* [5] investigated the shape of the Electron Energy Distribution Function (EEDF) of plasmas created by the MPT. In their case a Gaussian can be used to fit through the Thomson scattering signal, since the contribution of collective scattering is very small (due to a lower electron density and a larger scattering angle [9,10]). By plotting the logarithm of the intensity of the Thomson signal versus the square of the shift in wavelength, the Gaussian is

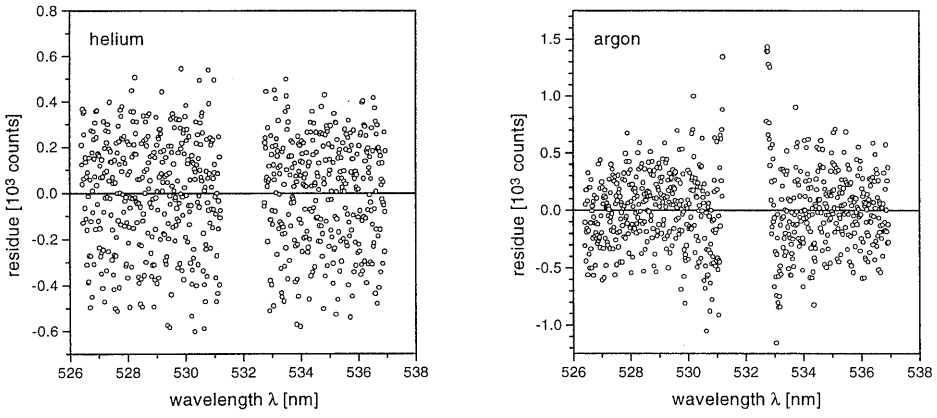

***Figure 6**: The residues of the fits depicted in Figure 3. They are randomly distributed around zero; no systematic deviations are found within the accuracy of the measurement.*

transformed into a straight line. Deviations from this line can be attributed to deviations from the Maxwellian distribution. It was established that above $\Delta\lambda^2 > 13$ nm^2 the intensity of the Thomson scattering signal was systematically higher than expected from the extrapolation of the straight line. Therefore, they concluded that the electrons with high kinetic energy (large $\Delta\lambda^2$) are overpopulated with respect to a Maxwellian distribution [5].
However, in order to trace systematic deviations of a fitted function it is better to study the residues of the fit. In Figure 6 the residues of the fits of the profiles of Figure 3 are shown. In both cases they seem to be randomly distributed around zero. Therefore, it has to be concluded that no systematic deviations can be found within the accuracy of the measurement and that the EEDF in the TIA obeys a Maxwellian distribution[b].
Note that without the correction for the offset we would also find an overpopulation of the high energy tail of the EEDF and that Huang *et al.* did not correct for an offset while fitting their Thomson scattering profiles.

5. Conclusions

- These measurements confirm the statement of our previous article [2] that the plasmas produced by the TIA are far from equilibrium. The high electron temperatures (typical 17000 K for argon and 25000 K for helium) give rise to a large ionisation rate. Since the ionisation rate exceeds the recombination rate by far, large deviations from Saha equilibrium are created.
- However, using this advanced setup and data handling procedures no deviations from Maxwellian equilibrium are found.
- Compared to the MPT the excitation and ionisation power of the TIA is much larger.

References

1. M. Moisan, G. Sauvé, Z. Zakrzewski and J. Hubert, Plasma Sources, Sci. and Techn. **3** 584 (1994).
2. Chapter 2: J. Jonkers, H.P.C. Vos, J.A.M. van der Mullen and E.A.H. Timmermans, Spectrochim. Acta B **51** 457 (1996).
3. J.A.M. van der Mullen, Phys. Rep. **191** 109 (1990).
4. T. Fujimoto, J. Phys. Soc. Jap. **47** 273 (1979).
5. M. Huang, D.S. Hanselman, Q. Jin and G.M. Hieftje, Spectrochim. Acta B **45** 1339 (1990).
6. Q. Jin, G. Yang, A. Yu, J. Liu, H. Zang and Y. Ben, Pittsburgh Conference Abstracts #1171 (1985).
7. Q. Jin, C. Zhu, M.W. Borer and G.M. Hieftje, Spectrochim. Acta B **46** 417 (1991).
8. J.M. de Regt, R.A.H. Engeln, F.P.J. de Groote, J.A.M. van der Mullen and D.C. Schram, Rev. of Sci. Instrum. **66** 3228 (1995).
9. D.E. Evans and J. Katzenstein, Rep. Prog. Phys. **32** 207 (1969).
10. M. Huang, P.Y. Yang, D.S. Hanselman, C.A. Monnig and G.M. Hieftje, Spectrochim. Acta B **45** 511 (1990)

[b] In chapter 9 indications are found that the EEDF is *under*populated with respect to a Maxwellian distribution.

11. A. Rodero, M.C. Quintero, M.C. García, A. Sola and A. Gamero, Europhysics Conference Abstracts **18E** *ESCAMPIG XII*, 203 (1994).
12. M.C. Quintero, A. Rodero, A. Gamero and A. Sola, Europhysics Conference Abstracts **18E** *ESCAMPIG XII*, 342 (1994).
13. A. Ricard, L. St-Onge, H. Malvos, A. Gicquel, J. Hubert et M. Moisan, J. Phys. III France, **5** 1269 (1995).
14. L.M. Biberman, V.S. Vorob'ev and I.T. Yakubov, Sov. Phys. Usp. **22** 411 (1979).
15. H.W. Drawin and F. Emard, Z. Naturforsch. **28a** 1289 (1973).
16. J.A.M. van der Mullen, Spectrochim. Acta B **45**, 1 (1990).
17. Chapter 5: J. Jonkers, L.J.M. Selen, J.A.M. van der Mullen, E.A.H. Timmermans and D.C. Schram, Plasma Sources, Sci. and Techn **3** 533 (1997).
18. M. Moisan and Z. Zakrzewski, J. Phys. D: Appl. Phys. **24** 1025 (1991).
19. J.A.M. van der Mullen, Spectrochim. Acta B **44** 1067 (1989).
20. A.L. Walker, D.L. Curry and H.B. Fannin, Appl. Spectrosc. **48** 333 (1994).
21. H.B. Fannin, Appl. Spectroc. **44** 1143 (1990).
22. S. Gasiorowicz, *"Quantum Physics"*, John Wiley & Sons (1974).
23. J.M. de Regt, F.P.J. de Groote, J.A.M. van der Mullen and D.C. Schram, Spectrochim. Acta B **51** 1371 (1996).
24. J.A.M. van der Mullen, D.A. Benoy, F.H.A.G. Fey, B. van der Sijde and J. Vlcek, Phys. Rev. E **50** 3925 (1994).
25. M. Huang, D.S. Hanselman, P. Yang and G.M. Hieftje, Spectrochim. Acta B **47** 765 (1992).
26. J.F. Waymouth, *"Electric discharge lamps"*, The M.I.T. Press, Massachusetts (1971).
27. W. Elenbaas, *"Light Sources"*, The MacMillan Press LTD (1972).

4

The excitation temperature in helium plasmas

J. Jonkers and J.A.M. van der Mullen, submitted for publication to the Journal of Quantitative Spectroscopy and Radiation Transfer.

Measuring excitation temperatures is a widely used way to characterise plasmas. In this paper we show that in most (atmospheric) helium plasmas this temperature is hardly related to any plasma quantity. It will appear that due to the strong non-equilibrium character of these plasmas the excitation temperature is lower than the electron temperature. The reason for the fact that in particular helium plasmas are far from equilibrium is the easy ambipolar diffusion of helium ions. Together with the relatively high electron temperature (necessary to sustain a helium plasma) this results in an excitation temperature, which strongly depends on the ionisation energies of the levels used to determine this temperature, rather than on the electron temperature. Since due to the specific atomic structure of helium only a limited amount of excited levels can be observed, always more or less the same excitation temperature is found.

1. Introduction

Although the most commonly used laboratory plasma gas is argon, there are some specific applications in which helium is necessary. One good example is the well known He-Ne laser. An other important application is the spectrochemical analysis [1,2,3,4]. Especially for halogen containing species helium plasmas are successful, since the excitation potentials of these halogens are so high that they can not be excited in argon plasmas. Several plasma sources are in use for this kind of application, which have a broad range in operating conditions, like pressure (from roughly 1 mbar to 1 atmosphere), applied power (from a few Watts to 1 kW) and operation frequency of the electromagnetic (EM) field (from DC to 10 GHz). In order to obtain some information about these plasmas the simplest way seems to determine the excitation temperature T_{exc} using the 2λ-method, in which the Boltzmann relation is applied to the ratio of the densities of two excited levels. This ratio is determined from relative measurements of two spectral lines and the corresponding transition probabilities [5,6]. A similar but more elaborate approach is the so-called Boltzmann plot method where the logarithm of the densities of excited states per statistical weight is plotted versus the excitation or the ionisation energy. In the case these points form a straight line, an excitation temperature can be related to the slope of this line [7,8].

The excitation temperature has been and still is the object of many papers. The reasons for this are that this "characteristic" temperature is relatively easy to determine and that it equals the electron temperature T_e *in case of equilibrium.*

One would expect that the two most specific features of helium plasmas, namely

1. helium is the lightest noble gas and
2. it has the highest ionisation potential,

would lead to a demand that the temperature of the plasma should be higher than in case of argon [9]. However, for the excitation temperatures the contrary seems to be the case: in helium T_{exc} is always found to be around 3500 K [4,10,11,12,13,14], which is much lower than in argon (4800 to 20000 K, see for instance [6,14,15,16]). The solution to this paradox can be found in the fact that the specific features of helium given above cause that these plasmas strongly deviate from equilibrium, with the consequence that the excitation temperature is almost independent of the electron temperature.

The electron temperature has to be much higher than 4000 K, a fact that can easily be deduced from the fact that helium line emission is observable. The energy gap between the ground state and the first excited level is relatively large (19.81 eV), so that for an electron temperature of 4000 K and a density of the ground state of 2.4×10^{25} m^{-3} (i.e. at atmospheric pressure and a gas temperature of 300 K) the density of the first excited level would be around 8 m^{-3}. It is clearly that this density is far too low to be measurable in laboratory plasmas.
The aim of this paper is to investigate the influence of the plasma state on the shape of the Atomic State Distribution Function (ASDF) of the main plasma gas and thus on the excitation temperature. Although we mainly refer to atmospheric helium plasmas, most of the theory is also applicable to other plasmas. In section 2 a qualitative study of the ASDF is presented. It will be established here that the phenomenon of the relatively low excitation temperature is related to the fact that (in particular) helium plasmas are very far from equilibrium. In section 3 it is shown that for such plasmas, the excitation temperature is only weakly related to the electron temperature and almost entirely depends on the ionisation energies of the levels in question.

2. The Atomic State Distribution Function

For the determination of the excitation temperature usually a Boltzmann plot is constructed in which the logarithm of the density per statistical weight η_p of excited level p is plotted versus the excitation energy E_p or the ionisation energy I_p. The value of T_{exc} is deduced from the slope of the plot via [5,6,7,8]:

$$\frac{1}{k_B T_{exc}} = -\frac{\partial}{\partial E} ln\,\eta = \frac{\partial}{\partial I} ln\,\eta \tag{1}$$

This temperature determination is based on the fact that *in equilibrium* the states are populated according to Boltzmann's law:

$$\frac{\eta_q^B}{\eta_p^B} = exp\left(\frac{E_p - E_q}{k_B T_e}\right) = exp\left(\frac{I_q - I_p}{k_B T_e}\right) \tag{2}$$

where the superscripts B denote that the populations of both states are in (Boltzmann) equilibrium with each other. Thus if equilibrium is present in the sense that the ASDF obeys the Boltzmann relation, the excitation temperature equals the electron temperature.
However, laboratory plasmas are often out of equilibrium and it can be shown [9] that especially helium plasmas exhibit strong deviations even in those situations where a comparable argon plasma is close to equilibrium. In order to study the effect of equilibrium departures on the ASDF we group the various elementary processes of population and depopulation in three types of balances:

1. The *Planck balance* of (spontaneous and stimulated) emission and absorption:

$$A_p \overset{P}{\longleftrightarrow} A_q + h\upsilon \quad \text{and} \quad A_p + h\upsilon \overset{P}{\longrightarrow} A_q + h\upsilon + h\upsilon \tag{3}$$

   These processes play a minor role for the higher excited states (which are relevant in the determination of the excitation temperature), provided that the electron density is sufficiently high [17,18].
2. The *Boltzmann balance* describes the exchange of internal energy of atoms with the kinetic

energy of free electrons in inelastic collisions. It consists of a forward (excitation) and a corresponding backward reaction (deexcitation):

$$A_p + e \overset{B}{\longleftrightarrow} A_q + e \tag{4}$$

In case this balance equilibrates for two given levels (i.e. the forward and reverse reaction rates are equal) and the energy distribution of the free electrons is Maxwellian, the ratio of the populations of these levels obeys the Boltzmann relation (2).

3. The *Saha balance* governs the production and destruction of free electrons:

$$A_p + e \overset{S}{\longleftrightarrow} A_1^+ + e + e \tag{5}$$

which links the ASDF (of the atom) to the ion ground state density. In the case that such a balance equilibrates, it is found that the state density η_p of level p can be described by the Saha formula:

$$\eta_p^S = \frac{n_e n_+}{2g_+}\left(\frac{h}{\sqrt{2\pi m_e k_B T_e}}\right)^3 exp\left(\frac{I_p}{k_B T_e}\right) \tag{6}$$

If the Saha balance equilibrates for all the levels, that is if the whole ASDF obeys the Saha formula, the plasma is said to be in Local Saha Equilibrium (LSE). In this case, in which the production of free electrons equals the destruction by (three particle) recombination, other loss mechanisms for the free electrons (like diffusion for instance) are negligible. If the Saha balance is only in equilibrium for a part of the atomic system, these levels are said to be in partial Local Saha Equilibrium (pLSE) [6,8,18,19][a]. These states are also interrelated to each other via the Boltzmann formula and the excitation temperature determined from the relative population of these levels, equals the electron temperature.

In case of (complete) LSE the rates of collisional ionisation and three particle recombination are equal to each other. However, since laboratory plasmas have finite dimensions, free electrons and ions can diffuse out of the plasma, so that net production is necessary to sustain the plasma. Therefore, almost all laboratory plasmas at moderate or lower power densities are not in LSE. In particular for helium plasmas this will be the case since the helium ions are relatively light and therefore diffuse easily [9]. This means that in a steady state new charged particles have to be created continuously, so that the Saha balances (5) can not be in equilibrium, since the number of reactions to the right (ionisation) has to be larger than that to the left (recombination). In order to create this net ionisation, the actual elementary occupation η_p of an excited level p has to be higher than its (Saha) equilibrium value η_p^S, cf. Figure 1.
It is customary to relate the actual density of a level p to its Saha density via the dimensionless quantity

---

[a] In the literature the term "partial Local Thermal Equilibrium" or "pLTE" is often used to denote that a part of the atomic system is populated according to Saha. This is somewhat misleading since "Local Thermal Equilibrium" refers to the situation in which for each relevant plasma location the heavy particles, the free electrons and the densities of the excited states are described by one temperature. However, the fact that a part of the ASDF obeys Saha does not necessarily mean that the electron temperature equals the gas temperature.

$$b_p = \frac{\eta_p}{\eta_p^S} = \frac{n_p}{n_p^S} \tag{7}$$

If this parameter is larger than unity, the ionisation from this level is larger than the three particle recombination to this level. For an ionising plasma the atomic states have to be over-populated:

$$b_p = \frac{\eta_p}{\eta_p^S} > 1 \tag{8}$$

Since the ionisation flow is mainly stepwise in character[b] [18,20], a chain of disturbed Boltzmann balances is needed to generate an ionisation flow, which is accompanied by the following chain of inequalities:

$$b_1 > b_2 > b_3 > \ldots > 1 \tag{9}$$

Each level has to be more overpopulated than its adjacent higher level, so that the number of excitations ($p \rightarrow p+1$) is larger than the number of corresponding deexcitations ($p \leftarrow p+1$). Due to the decreasing overpopulation the slope of the actual distribution is much steeper than the slope of the Saha (or Boltzmann) distribution, see Figure 1. This means that the measured excitation temperature is smaller than the actual electron temperature, cf. equation (1).
The monotonic decrease of b_p as a function of principal quantum number p predicts that b_p approaches unity for $p \rightarrow \infty$. That is, approaching the continuum we will eventually meet with levels for which the number of ionising and recombining processes is much larger than the net ionisation flow through that part of the system. This can be understood by realising that the population production/destruction per state due to recombination/ionisation increases with p^4 whereas the step flow decreases with p^{-1} [18]. Therefore, above a certain value for p the population is (nearly) according to Saha. This part of the atomic system is said to be in partial Local Saha Equilibrium [6,8,18,19].
In case of argon plasmas with moderate or large electron densities the part of the ASDF which is in pLSE extends towards observable levels so that the electron temperature can be obtained from the excitation temperature. Recently this fact was used to deduce accurate transition probabilities of highly excited argon states [21]. Using these it is possible to measure the electron temperature (and density) in, for instance, Inductively Coupled Plasmas (ICPs) operating at and around atmospheric pressure [15,16]. These plasmas, for which the gradient lengths are approximately 1 mm, are characterised by an electron density of order 10^{21} m^{-3} and an electron temperature of 0.75 eV. This together with a ground state density of around 10^{24} m^{-3} results in a relatively low overpopulation of the ground state ($b_1 < 10^2$). However, when the pressure becomes lower or the dimensions of the plasma smaller, the effect of diffusion becomes more important. This means that the deviation from equilibrium as expressed by b_1 increases, since more free electrons have to be created to sustain the plasma and that the pLSE part of the atomic system shifts to the undetectable high atomic levels [9,14].

---

[b] This is not valid in case of low electron densities and/or low in the atomic system, since in these cases radiation is important and the excited states are in so-called Corona Balance (CB). However, in CB there is also a chain of disturbed Boltzmann balances, so that the overpopulation decreases also with increasing quantum number [18].

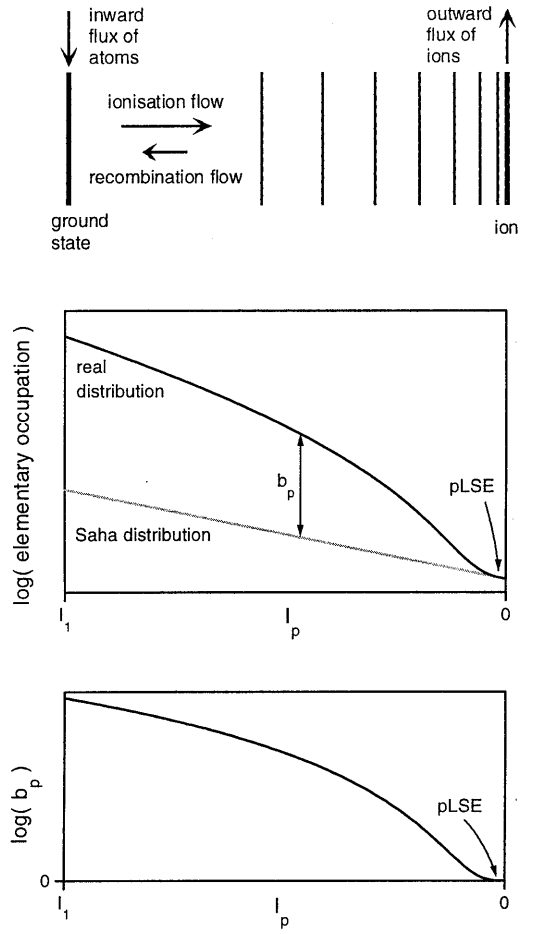

***Figure 1**: The ASDF of an ionising plasma [14,18]. In steady state the outward flux of ions and free electrons towards the boundaries of the plasma is balanced by an ionisation flow through the atomic system. Due to the drain of charged particles the lower atomic states are overpopulated with respect to Saha. This overpopulation propagates through the atomic system, but decreases with decreasing ionisation potential.*

If argon is replaced by helium as the main plasma gas this effect becomes stronger because helium is much lighter so that the diffusion is larger. Therefore it is much more difficult to observe the pLSE part of the ASDF even at atmospheric pressure [9]. Before discussing the specific results for helium, we present a general and more quantitative description for the upper part of the ASDF.

It is possible to determine analytically the shape of a large part of the ASDF using scaling laws for the transition rates [18]. In that part of the excitation space where

1. radiation processes can be neglected,
2. the probability of excitation is larger than that of deexcitation and

3. the atomic energy scheme is hydrogenic

it is found that the levels are mainly populated via a step-wise excitation flow. This simplification makes an analytical solution possible. In practice conditions 1 to 3 are fulfilled provided that the states are not too low in the excitation space. The part of the atomic system for which the first two criteria hold is said to be in Excitation Saturation Balance (ESB) [18,20]. In ESB the densities of the levels can be found by solving a continuity equation in the excitation space:

$$J(p-1,p)-J(p,p+1)=S(p)-R(p) \tag{10}$$

Here J(p,p+1) represents the step-wise excitation flow from p to p+1 and S(p) and R(p) are the ionisation from and the three-particle recombination to level p respectively. In the case where the third condition also holds, the hydrogenic excitation and ionisation/recombination rates can be substituted, which yields an overpopulation of the form [18]

$$b_p = 1+\beta I_p^3 \tag{11}$$

which is confirmed by experiments [22,23,24] as well as numerical calculations [20,25]. This agrees with the qualitative result of the previous section that the overpopulation decreases monotonically with decreasing energy, since the second term of equation (11) approaches zero for $I_p \rightarrow 0$. If we combine this analytical expression for the b factor with the Saha equation (6) we obtain the actual shape of the ASDF:

$$\eta_p = \left(1+\beta I_p^3\right)\eta_p^S \propto \left(1+\beta I_p^3\right) exp\left(\frac{I_p}{k_B T_e}\right) \tag{12}$$

in which the last expression yields the dependence on the ionisation energy. The excitation temperature which would be measured can be determined by applying equation (1), which is the relation between the shape of the ASDF and T_{exc}:

$$\frac{1}{k_B T_{exc}} = \frac{\partial}{\partial I} ln\,\eta = \frac{1}{k_B T_e} + \frac{3\beta I_p^2}{1+\beta I_p^3} \tag{13}$$

This equation shows that apart from the electron temperature the excitation temperature is also effected by the local ionisation potential of that part of the atomic system from which T_{exc} is deduced. This influence is larger for higher electron temperatures and higher β values. We will show that for the helium plasmas under study the impact of the ionisation energy on the excitation temperature is so large that the influence of the electron temperature vanishes almost completely.

3. Specific results for helium

Atmospheric helium plasmas are characterised by a low electron density and a high electron temperature [9]. This is directly related to two important characteristics of the helium atom: it is very light and its ionisation potential is very high. Under these circumstances (high T_e, low n_e) the Saha density of the ground state is much lower than its actual density. For example, for an electron temperature of 2 eV and an electron density of 1×10^{20} m^{-3} the equilibrium density of the ground state equals 6.4×10^{17} m^{-3}, whereas the actual density is around 7.3×10^{24} m^{-3} (at atmospheric pressure and a gas temperature of 1000 K). This huge overpopulation of the

pqn	^3S	^1S	^3P	^1P	^3D, ^1D	L > 2
1	--	24.580	--	--	--	--
2	4.766	3.970	3.622	3.368	--	--
3	1.868	1.666	1.579	1.499	1.512	--
4	0.992	0.913	0.879	0.844	0.850	0.849
5	0.615	0.575	0.558	0.541	0.544	0.543
6	0.418	0.395	0.386	0.376	0.377	0.377
7	0.302	0.288	0.282	0.276	0.277	0.277

***Table 1**: The lower part of the atomic system of helium [26]. The first column gives the principal quantum number (pqn) and the other columns the ionisation potential in eV.*

ground state of more than six orders of magnitude propagates through the atomic system. It can be shown [9] that also a considerable part of the excited levels (being in ESB) is far from equilibrium, i.e. that the non-equilibrium parameter β is much larger than unity

$$\beta >> 1 \tag{14}$$

so that equation (13) reduces to

$$\frac{1}{k_B T_{exc}} \approx \frac{1}{k_B T_e} + \frac{3}{I_p} \tag{15}$$

It should be noted that the excitation temperature does not depend on the exact overpopulation anymore, since the densities of the regarded levels are completely determined by the step-wise ionisation flow. This means that the population rate of a certain level as well as its depopulation rate scale with β. Therefore a change of the overpopulation will not effect the ratio of the densities (i.e. the excitation temperature).

When determining the excitation temperature in helium plasmas only a limited number of levels can be taken into account, due to the structure of the helium atom, see Table 1. The densities of the first excited levels can not be obtained by passive emission spectroscopy, since they are metastable (2^3S and 2^1S) or radiate in the far UV or in the far IR (2^3P and 2^1P) [26]. So the lowest excited state from which radiation can be measured is 3^3S with an ionisation potential of 1.868 eV. Higher in the atomic scheme the population of the excited states decreases, cf. equation (12). Since also the transition probability A_{pq} for optical transitions decreases as well [18,27]

$$A_{pq} \propto I_p^{2.25} \tag{16}$$

the yield of photons emitted by a certain state declines very rapidly with decreasing ionisation energy. For this reason measurements of absolute state densities are normally restricted up to level 5D, so that the typical average ionisation energy $\langle I_p \rangle$ of the measured levels is around 1.0 eV, see Table 2. This means that the second term is the dominant term of the right hand side of equation (15), since the typical electron temperature in atmospheric helium plasmas is around 2 eV [9]. Therefore we conclude that the excitation temperature merely depends on the

ref.	measured levels		$\langle I_p \rangle$	reported T_{exc}	theoretical T_{exc}	
	lowest	highest	[eV]	[K]	T_e = 1.5 eV	T_e = 2 eV
[10]	3^1P	5^3D	1.02	3100 .. 3500	3220	3380
[11]	3^3P	5^1D	1.06	2990 .. 3300	3320	3490
[12]	3^3S	4^1D	1.36	3000 .. 3400	4040	4280
[13]	3^3P	6^3P	0.98	3200 ± 220	3120	3260
[14]	3^3S	4^1D	1.36	3800 ± 200	4040	4280

***Table 2**: A few of the reported excitation temperatures in various helium plasmas together with the range of atomic states from which they are obtained. The last two columns give the prediction according to equation (15), depending on the average ionisation energy $\langle I_p \rangle$ and an assumed electron temperature T_e.*

ionisation energy of the levels taken into account and not on the electron temperature.
In Table 2 the predicted T_{exc} is compared with the experimentally obtained values. Both temperatures are more or less the same, although the predicted values depend slightly on the electron temperature. For this reason it might be tempting to use equation (15) for obtaining T_e out of T_{exc}:

$$\frac{1}{k_B T_e} \approx \frac{1}{k_B T_{exc}} - \frac{3}{\langle I_p \rangle} \tag{18}$$

However, in this case a small uncertainty in the excitation temperature leads to a large inaccuracy in T_e, since the difference in the two terms at the right hand side of (18) is relatively small. Moreover, it is not straightforward to determine the characteristic $\langle I_p \rangle$ from the ionisation energies of the levels taken into account.
The theory discussed in this section can also be applied to other elements. However, since helium plasmas combine large deviations from equilibrium with a relatively high electron temperature, they form the most striking example.

4. Conclusions

If the excitation temperature in helium is determined, only a limited amount of excited states can be taken into account. The population of these states is normally far from equilibrium, since high diffusion losses of helium ions cause a large ionisation flow through the atomic system. Owing to this the excitation temperature is lower than the electron temperature. Moreover, due to the limited range in ionisation energy of the observable levels and due to the high electron temperature (necessary to sustain the helium plasma) the excitation temperature is only dependent on the characteristic ionisation energy of the levels taken into account and not on the electron temperature.

References

1. C.A. Bache and D.J. Lisk, Anal. Chem. **37** 1477 (1965).
2. R.S. Braman and A. Dynako, Anal. Chem. **40** 95 (1968).
3. B.D. Quimby and J.J. Sulivan, Anal. Chem. **62** 1027 and 1034 (1990).
4. J. Hubert, S. Bordeleau, K.C. Tran, S. Michaud, B. Milette, R. Sing, J. Jalbert, D. Boudreau, M. Moisan and J. Margot, Fresenius J. Anal. Chem. **355** 494 (1996).
5. H.R. Griem, *"Plasma spectroscopy"*, McGraw-Hill Inc., New York (1964).
6. P. Fauchais, J.F. Coudert and M. Vardelle, *"Diagnostics in thermal plasmas"*, p349 in *"Plasma diagnostics"*, ed. by O. Auciello and D.L. Flamm, Academic Press, New York (1989), see also J.F. Waymouth *"Plasma diagnostics in electric discharge light sources"*, ibid. p47
7. P.W.J.M. Boumans, *"Inductively coupled plasma emission spectroscopy"*, part 2: *"Applications and fundamentals"*, John Wiley & Sons, New York (1987).
8. W.L. Wiese, Spectrochim. Acta B **46** 831 (1991).
9. Chapter 6: J. Jonkers, J.A.M. van der Mullen and D.C. Schram, *"On the differences between ionising helium and argon plasmas at atmospheric pressure"*, submitted to Phys. Rev. E.
10. K. Tanabe, H. Haraguchi and K. Fuwa, Spectrochim. Acta B **38** 49 (1983).
11. R.E. Sturgeon, S.N. Willie and V.T. Luong, Spectrochim. Acta B **46** 1021 (1991).
12. M.C. Quintero, A. Rodero, M.C. García and A. Sola, Appl. Spectrosc. **51** 778 (1997).
13. W.E. Wenthwoth, Y. Qin, S. Wiedeman, S.D. Stearns and J. Madabushi, Appl. Spectrosc. **49** 1282 (1995).
14. Chapter 2: J. Jonkers, H.P.C. Vos, J.A.M. van der Mullen and E.A.H. Timmermans, Spectrochim. Acta B **51** 457 (1996).
15. J.M. de Regt, R.D. Tas, J.A.M. van der Mullen and D.C. Schram, J. Phys. D: Appl. Phys. **29** 1489 (1996).
16. J.M. de Regt, F.P.J. de Groote, J.A.M. van der Mullen and D.C. Schram, Spectrochim. Acta B **51** 1371 (1996).
17. H. Griem, Phys. Rev. **131** 1170 (1963).
18. J.A.M. van der Mullen, Phys. Rep. **191** 109 (1990).
19. T. Fujimoto and R.W.P. McWhirter, Phys. Rev. A **42** 6588 (1990).
20. T. Fujimoto, J. Phys. Soc. Jap. **47** 265 (1979).
21. J.M. de Regt, R.D. Tas, J.A.M. van der Mullen, B. van der Sijde and D.C. Schram, J. Quant. Spectrosc. Radiat. Transfer **56** 67 (1996).
22. W. Kohsiek, J. Quant. Spectrosc. Radiat. Transf. **16** 1079 and **17** 651 (1976).
23. L. Vriens, J. Appl. Phys. **49** 3814 (1978).
24. J.A.M. van der Mullen, B. van der Sijde and D.C. Schram, Phys. Lett. A **79** 51 (1980).
25. J. Vlcek, J. Phys. D: Appl. Phys. **22** 623 (1989).
26. W.L. Wiese, M.W. Smith and B.M. Glennon, *"Atomic transition probabilities"*, volume I: *"Hydrogen through neon"*, NSRDS-NBS 4, National Buro of Standards, Washington DC (1966).
27. H.A. Bethe and E.E. Salpeter, *"Quantum mechanics of one and two electron atoms"*, Academic Press (1957).

5

Steep plasma gradients studied with spatially resolved Thomson scattering measurements

J. Jonkers, L.J.M. Selen, J.A.M. van der Mullen, E.A.H. Timmermans and D.C. Schram, published in Plasma Sources, Sci. and Techn. **6** 533 (1997).

Plasmas created by the microwave torch "Torche à Injection Axiale" (TIA), which are around 2 mm in diameter and 15 mm long, are investigated. In these plasmas large gradients are present so that the edge is supposed to play an important role. Using global Thomson scattering measurements, in which global refers to the fact that the size of the laser beam is approximately equal to the diameter of the plasma, the electron densities and temperatures were determined. However, these results lead to discrepancies in the particle balance: the production of free electrons is much larger than the classical losses due to recombination, convection and diffusion. Radially resolved Thomson scattering measurements show the plasma has a hollow structure. Although this enhances the losses due to diffusion, still a large discrepancy remains between production and destruction of free electrons in the argon plasmas. Probably some molecular processes are significant as well. A good candidate is the charge transfer between argon ions and nitrogen molecules, since mixing with the surrounding air has a large impact on the plasma.

1. Introduction

One of the most essential differences between laboratory and celestial plasmas, i.e. the difference in size, leads to the fact that laboratory plasmas have much steeper gradients and thus much larger related fluxes. This results in the presence of larger departure from equilibrium. Departures which are larger the smaller the plasma.

Besides the deviation from Local Thermal Equilibrium (LTE), as manifest in the inequality between the electron temperature T_e and the gas temperature T_g, most laboratory plasmas have an imbalance between electronic ionisation and the corresponding backward process of three particle recombination. The latter will effect the Atomic State Distribution Function (ASDF) in such a way that its slope is not constant, but changes as a function of the excitation energy [1,2,3]. This means that the excitation temperature T_{exc}, which is related to the slope of the ASDF, is not clearly defined and can attain values which are largely different from those of T_e and T_g. On the other hand the excitation temperature is relatively easy to determine and is widely used as a characteristic temperature for a plasma. However, for small plasmas there is no unique T_{exc}, so that the characterisation of these plasmas is often associated with the presence of a large variety in temperatures, as is for instance shown in the paper of Snyder *et al.* [4].

A typical example of a small plasma with a large temperature variation is a plasma produced by the "Torche à Injection Axiale" (TIA). This torch with axial gas injection is driven with typically 1 to 2 kW microwave power [5]. The typical dimensions of the plasma are 1 mm in radial and 15 mm in axial direction. The plasmas produced by the TIA expand in the open air. The various temperatures found in the literature [3,6,7,8,9], as given in Table 1, clearly show that there are large discrepancies and that the meaning of the various temperatures is still under discussion.

In the past we studied argon and helium plasmas produced by the TIA. In [3] absolute measurements of the densities of the excited states are presented. It was found that the deduced T_{exc} values depend on the excitation energy of the levels taken into account[a]. In argon

[a] A more extensive treatment of the excitation temperature is given in chapter 4.

	ref.	argon [K]	helium [K]
T_g	[6]	3000	2500
	[7,8]	-	3000
T_{exc}	[3]	4860, 8700	3800, 11400
	[7]	-	13000
	[8]	-	12500
T_e	[9]	17000	25000

***Table 1**: Various reported temperatures for the Torche à Injection Axiale.*

excitation temperatures between 4860 and 8700 K were obtained and in helium between 3800 and 11400 K. In the same paper it is concluded that apparently the ASDF is far from Saha-Boltzmann equilibrium, so that it is impossible to determine the electron temperature from emission spectroscopy and that the actual electron temperature has to be higher than the presented excitation temperatures.
This was confirmed by our second paper on the TIA [9] in which the electron temperature was obtained using Thomson scattering experiments. The found temperatures (typically 17000 K for argon and 25000 K for helium) are indeed higher than all other temperatures reported before. In spite of this large discrepancy it was not possible to find any indication for a deviation of the Electron Energy Distribution Function (EEDF) from a Maxwellian shape [9], as is claimed to be found by Huang *et al.* [10] for a similar torch. We therefore concluded that the electron temperature is well-defined and that it can be found by Thomson scattering and not (easily) via the variable slope of the ASDF[b].
The Thomson experiments in [9] were performed with a laser beam of around 1.5 mm in diameter, so that almost the whole plasma was radially imbedded in the beam. We will refer to these measurements as global Thomson measurements. It is the aim of this study to verify in how far the high T_e values as found by global Thomson scattering are consistent with the ionisation as deduced from the electron particle balance. To obtain information about the diffusion, which is to be expected a dominant term in the particle balance, spatially resolved information is needed. Therefore Thomson experiments have been performed with a much smaller beam; a technique to which we refer to as the local Thomson scattering method.
The TIA is an ideal plasma for the study on the relationship between the plasma interior and the (sharp) boundaries. The radius of the plasma is very small, so that the effect of steep gradients is surely present. On the other hand the plasma is large enough that, after considerable effort, it can still be subjected to a spatially resolved study. Insights obtained in this investigation might contribute to a better understanding of other plasmas as well. For instance, it is known that although in atmospheric cascaded arcs LTE is present in the main channel (due to the high electron density), deviations from LTE are found in the neighbourhood of the cathode [11,12]. An other example is the edge of an atmospheric

[b] Possible deviations from a Maxwellian EEDF are discussed in chapter 9.

Inductively Coupled Plasma (ICP), where (partly) due to entrainment of air [13], the gradient lengths are small and the fluxes high. In all these cases we essentially meet the same phenomenon: boundaries with steep gradients which influence the properties of a considerable plasma part.

In this paper the particle balance of the TIA plasmas is discussed in section 2. By balancing the production and destruction of the free electrons, the electron temperature can be estimated [14]. It will turn out that the electron temperature, as found by the global Thomson scattering measurements [9], leads to a much too large production compared to the losses due to diffusion, if the radius of the plasma is taken as the gradient length of the radial electron density profile. This demands more precise spatially resolved measurements which are presented in section 3. The resulting gradient is indeed much steeper than deduced from global considerations, but not steep enough to explain the high electron temperatures in the argon plasma. It is shown that if the air, in which the plasma normally expands, is replaced by argon, the plasma is significantly different (section 4). The entrainment of air in the outer regions of the plasma appears to have a strong influence on the plasma as a whole.

2. The particle balance

If a plasma is in steady state, the ionisation, i.e. the production of ions and free electrons, equals the destruction by recombination and outward transport. This is represented by the particle balance for charged particles:

$$n_e n_1 S_{CR} - n_e n_+ \alpha_{CR} = \vec{\nabla} \cdot \left(n_e \vec{w}_p \right) - \vec{\nabla} \cdot \left(D_a \vec{\nabla} n_e \right) \qquad (1)$$

In which n_e, n_+ and n_1 refer to the electron, ion and atom ground state densities respectively. The terms on the right hand side of equation (1) equal the outward transport due to convection

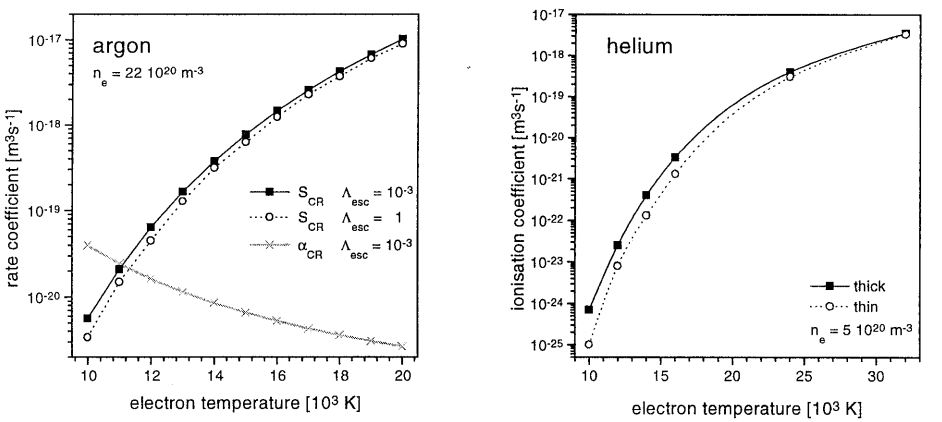

***Figure 1**: The ionisation coefficient as a function of the electron temperature for argon [15] and helium [16]. In the case of argon the ionisation coefficient is given for two different escape factors for resonance radiation: $\Lambda_{esc} = 1$ (i.e. optically open) and $\Lambda_{esc} = 10^{-3}$ (a more realistic one). The crosses represent the recombination coefficient. For helium the solid squares refer to a plasma which is optically thick for resonance radiation and the open circles to a completely optically thin plasma.*

and ambipolar diffusion (mainly in radial direction) respectively and will be discussed below. The left hand side represents the local net production. The ionisation (S_{CR}) and recombination (α_{CR}) coefficients can be calculated using a Collisional Radiative (CR) model [1,15,16]. Here we will use the CR model by Benoy *et al.* for argon [15]. Although this paper is focused on argon plasmas, we will make the same estimation for a helium plasma, operating at the same conditions. For this we use the model of Drawin and Emard [16]. In Figure 1 the ionisation coefficients for helium and argon are depicted versus the electron temperature. Due to the very high electron temperature (see Table 1) recombination of atomic ions can be neglected.
The losses of charged particles due to convection, i.e. the first term at the right hand side of equation (1), can be estimated by

$$\vec{\nabla}\cdot\left(n_e\vec{w}_p\right)\approx\frac{n_e}{h_p}w_p \tag{2}$$

in which h_p is the scale length in the direction of the flow (for which 1 cm is taken) and w_p the flow velocity of the plasma (approximately 100 ms^{-1}). The other transport term, i.e. the flux due to diffusion, can be written as

$$\left|\vec{\nabla}\cdot\left(D_a\vec{\nabla}n_e\right)\right|\approx\frac{n_e}{\Lambda^2}D_a \tag{3}$$

in which Λ is the gradient length of the electron density profile, which we assume to be equal to the radius of the plasma (1 mm). An expression for the diffusion coefficient D_a can be found in reference 17:

$$D_a=\frac{3k_B}{8n_1M\Omega\left(T_g\right)}\left(T_g+T_e\right) \tag{4}$$

with M the atomic mass. For argon the ion-atom collision integral Ω is given by [17]

$$\Omega^{Ar}\left(T_g\right)=\left(3.03+6.82\times10^{-4}T_g-3.70\times10^{-8}T_g^2+9.15\times10^{-13}T_g^3\right)\times10^{-16}\ [m^3s^{-1}] \tag{5}$$

and for helium by[c]

$$\Omega^{He}\left(T_g\right)=\left(1.72+8.26\times10^{-4}T_g-5.10\times10^{-8}T_g^2\right)\times10^{-16}\ [m^3s^{-1}] \tag{6}$$

For the gas temperature 3000 K is taken, see Table 1, so that the density of the ground state equals 2.4×10^{24} m^{-3}. Using these approximations and the T_e values as determined by global Thomson scattering measurements (cf. reference 9 or Table 1), the terms of the particle balance can be estimated. It should be noted that the exact value of the electron density is not important, since the dominant terms of equation (1) scale with n_e. The radial distribution of the electron density however, influences the electron temperature via the diffusion term. The magnitudes of each term of the particle balance divided by the electron density are listed in Table 2.

[c] The collision integral which is used in this paper is not correct, but should be multiplied by 2, cf. chapter 6.

	argon [s^{-1}]	helium [s^{-1}]
ionisation	6×10^6	1×10^6
recombination	1×10^1	6
convection	1×10^4	1×10^4
diffusion	1×10^3	2×10^4

***Table 2**: Typical rates of the separate terms of the particle balance, using T_e and n_e as determined by global Thomson scattering measurements (17000 K and 22 × 10^{20} m^{-3} for argon and 25000 K and 5 × 10^{20} m^{-3} for helium [9]). The diffusion loss rates are obtained using a radial gradient length of 1 mm.*

A comparison of the ionisation with the three loss terms shows that the production outranges the destruction by roughly two orders. This might be due to a too high electron temperature. However, if for the helium plasma the temperatures are taken which are found by passive emission spectroscopy (around 12500 K) [3,7,8], the ionisation frequency becomes 1×10^2 s^{-1}, which is even too small to balance the losses due to convection (1×10^4 s^{-1}, see Table 2). Therefore an electron temperature much higher than 12500 K is needed to sustain the plasma. Although one could argue that T_e could be somewhere in between the values as determined by the passive and active (Thomson) techniques, we assume in the following that the electron temperature obtained by global Thomson scattering is correct. In this case the apparent imbalance as indicated by Table 2 can have two reasons:

- the effective ionisation is smaller for the given T_e values or
- the loss terms is larger in reality.

First we investigate the effective ionisation. The ionisation coefficient depends on the escape factor of resonance radiation. A higher escape factor will disfavour the stepwise excitation and therefore decrease the ionisation. The escape factor depends on the spectral line profile which is partly determined by Van der Waals or pressure broadening [18]. Besides broadening, this process can cause a shift in the wavelength and therefore it strongly effects the escape factor. The Van der Waals interaction is due to the interaction between atoms, so that it depends on the atom density. In small plasmas, as produced by the TIA, large gradients in the gas temperature (and therefore in the atom density) are probably present, so that the Van der Waals line shift can increase the escape factor drastically, which results in a lower ionisation rate.

In Figure 1a the ionisation coefficient in argon is depicted for two escape factors of the resonance radiation: 10^{-3} (squares) and 1 (circles). It can be seen that the influence of the escape factor is limited, especially at the high electron temperatures present in the TIA plasmas. This is also the case for helium, as can be seen in Figure 1b. The basic reason for this insensitivity of radiation escape is the relatively high electron density (in the order of 10^{21} m^{-3}, see [9] or next section) due to which the population of the excited states is determined by (inelastic electron) collisions rather than radiative processes [1].

Therefore we assume that the ionisation coefficients are correct, so that the loss terms have to be underestimated. The actual losses can be higher due to:

1. formation and destruction of molecular rare gas ions,
2. mixing with the surrounding air or
3. a smaller gradient length.

ad 1: formation and destruction of molecular rare gas ions
Due to the formation of rare gas molecular ions

$$Ar^+ + Ar + Ar \rightarrow Ar_2^+ + Ar \tag{7}$$

followed by their destruction via dissociative recombination

$$Ar_2^+ + e \rightarrow Ar + Ar(4p) \tag{8}$$

charged particles are lost. Normally, the formation of the molecular ion is the limiting process. This frequency is around 1×10^6 s^{-1} in the argon plasma for a neutral density equal to 2.4×10^{24} m^{-3} [19]. However, the argon atom in the 4p state, which is produced by the second reaction, is easily ionised again, since (radiative) decay to the ground state is not likely (see above). Moreover, the formation of molecular ions is also accompanied by its inverse process, so that the resulting ion loss rate of this channel is much smaller than the ionisation rate (6×10^6 s^{-1}). Therefore, we conclude that the formation and destruction of molecular argon ions play a minor role in the particle balance of these plasmas[d].

ad 2: mixing with the surrounding air
Extra destruction channels for free electrons are created if the surrounding air is mixed with the plasma. For instance, for argon and nitrogen a possible mechanism is charge transfer

$$Ar^+ + N_2 \rightarrow Ar + N_2^+ \tag{9}$$

followed by dissociative recombination

$$N_2^+ + e \rightarrow N + N \tag{10}$$

The charge transfer reaction is resonant since the ionisation energies of argon and molecular nitrogen are almost equal (15.76 and 15.58 eV respectively). The second reaction is fast due to the attractive Coulomb interaction between the positively charged molecule and the electron. The possible presence of nitrogen is supported by the fact that in the plasma the First Negative system of N_2^+ and many atomic nitrogen lines can be observed [6,7]. At low power levels (< 1 kW) also the Second Positive system of N_2 is strongly present. Moreover, a significant entrainment of air into an ICP, which is also expanding in the open air, was measured by de Regt and co-workers [13].
The rate coefficient of the charge transfer reaction is about 4×10^{-16} m^3s^{-1} [20], so that if 1% of the heavy particles in the plasma are nitrogen molecules this destruction channel is more than fast enough to balance the ionisation. The significance of such kind of mechanisms is investigated by controlling the environment in which the plasma expands (see section 4).

ad 3: a smaller gradient length
Another possible explanation for the large discrepancy between the ion production and the destruction rates might be that the actual radial gradient length is smaller than the value of 1 mm, which is used for estimating the diffusion losses in Table 2. An indication of the gradient

[d] A more extensive treatment of the role of molecular rare gas ions is given in chapter 7.

length is obtained by the skin effect. The penetration of the microwaves into the plasma is limited, since they are absorbed by the free electrons. As can be found in e.g. Jackson [21] the skin depth is given by:

$$\delta = \sqrt{\frac{1}{\pi \mu_0 \sigma f}} \tag{11}$$

For an argon plasma at our conditions the conductivity σ is approximately $10^4\ \Omega^{-1}m^{-1}$ [22], so that due to the high frequency of the microwaves (f = 2.45 GHz) the skin depth is only 0.1 mm. If we assume that the gradient length of the electron density equals the skin depth in stead of the (global) plasma radius, the diffusion losses will increase by two orders, cf. equation (3). As can be concluded from Table 2 this is sufficient to satisfy the particle balance for the helium plasma, but not enough for the argon plasma. However, this is only an estimation of the gradient length. The actual gradient length has to be obtained from the radial distribution of the electron density, which requires a spatially resolved measurement technique.

3. Experimental determination of the gradient length

For the measurements of the radial gradient length, the same setup is used as for the previously reported global Thomson scattering measurements [9,23]. The main difference is that now the laser beam is focused at the position of the plasma, in order to obtain a good spatial resolution. In the past [23] the focus of the laser beam was situated behind the plasma to avoid the possibility that stray light from the ablation of dust particles is detected during the calibration procedure. To avoid interference with this signal a dust free chamber is constructed surrounding the plasma, for the measurements presented now.
In Figure 2 the radially resolved electron density and temperature profiles are depicted. These measurements are taken at 2 mm above the nozzle (AN) using 1.0 kW input power and 3.0

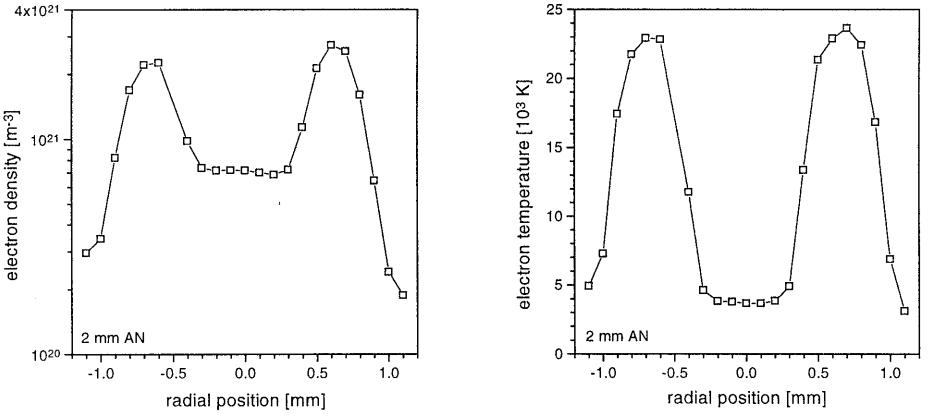

***Figure 2**: The radial electron density and temperature profiles in an argon plasma at 2 mm above the nozzle (1.0 kW and 3.0 slm), obtained by local Thomson scattering. The density profile seems to have a donut like shape. The steep outer gradients increase the losses due to diffusion.*

slm argon. Due to the construction of the TIA the reflected power can be tuned easily to a negligible level (< 2%) [5]. Every point in Figure 2 is obtained using 2500 laser shots with approximately 0.26 J per shot.

Both the density and the temperature profile appear to have a hollow structure. Owing to this the measured radial gradient length is approximately 0.2 mm[e]. As is discussed at the end of section 2 a gradient length of 0.1 mm is not enough to balance the ionisation in the argon plasma. Therefore it has to be concluded that the gradient length might be even smaller or that molecular recombination channels are also important.

It appears to be very difficult to perform the same measurements for the helium plasma with this setup. Due to the lower electron density the area of the Thomson scattering profile is lower and due to the higher electron temperature the profile is also more broadened. Both effects lead to a much lower number of photons per wavelength interval compared to the argon plasma. If we assume that the gradient length in helium is the same as in argon, the actual diffusion losses are 25 times higher than was estimated in Table 2, so that they become of the same order as the ionisation.

As can be seen in Figure 2 the maxima of the electron density and temperature are situated at r = ±0.7 mm, which is closer to the centre than the edges of the nozzle (at r = ±0.9 mm). In Figure 3 measurements at different axial positions are depicted. The larger the distance to the nozzle, the more the maxima of n_e and T_e are shifted towards the centre of the plasma. At 10 mm AN the plasma is located at the centre. The reason for the hollow shape close to the nozzle is probably the skin effect. During the time the free electrons need to diffuse to the center, they are also transported downstream by the flow of the plasma. Meanwhile the free electrons at the outside are destroyed most likely by the entrained nitrogen molecules (see next section).

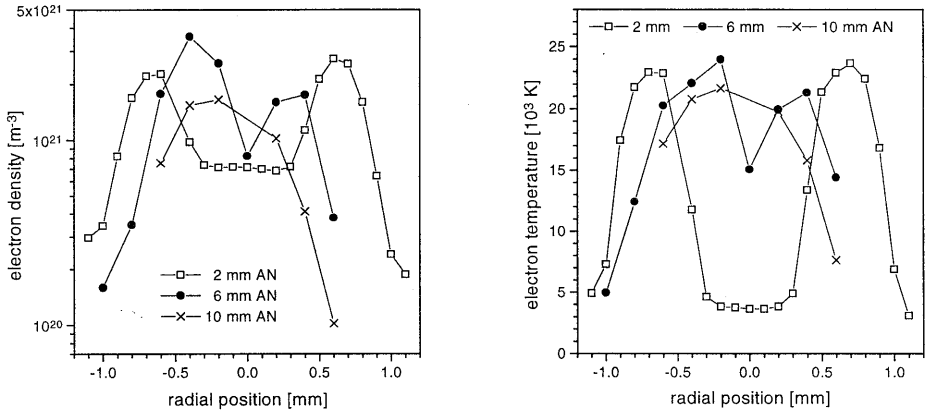

***Figure 3**: The dependence of the radial profiles on the height above the nozzle (AN). Close to the nozzle both the electron density and temperature appear to have a donut-like shape. This donut narrows downstream and at 10 mm AN it becomes more like a candle flame.*

[e] A quantitative study in chapter 9 shows that the gradient length in Figure 2 is actually 0.07 mm.

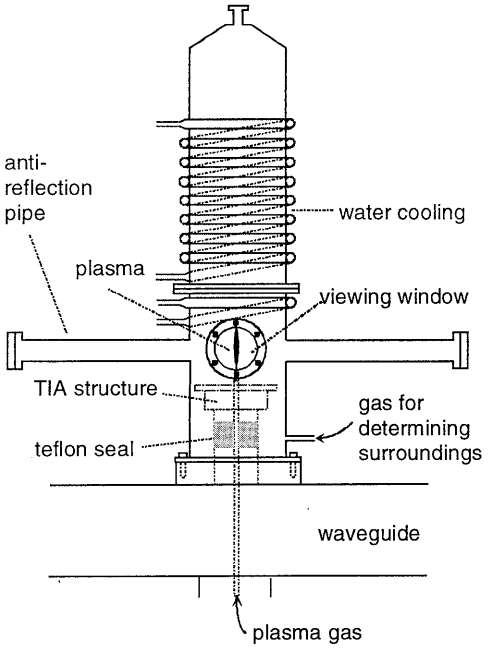

Figure 4: The setup for the determination of the influence of the surrounding atmosphere on the plasma.

More downstream the plasma flame becomes very turbulent, so that measurements of the electron temperature and density are difficult, since the Thomson scattering signal is much weaker (due to the lower electron density) and moreover it is disturbed by rotational Raman scattering. This means that for this region mixing with the surrounding air can certainly not be neglected.

4. The influence of the surrounding atmosphere

As stated in section 2 mixing with the surrounding atmosphere can have a strong influence on the plasma. In case of the TIA this is investigated by placing a special vessel on top of the rectangular waveguide structure, see Figure 4. The vessel is flushed with either argon or air (3 slm). The plasma (argon) gas flow is 1.8 slm and the applied microwave power 0.6 kW.
Using the same high resolution Thomson scattering setup, the electron density and temperature are measured as a function of the radius at 5 mm above the nozzle. The results are depicted in Figure 5. The plasma which is sustained in an air atmosphere is more or less the same as the one expanding in the open air (i.e. without the metal vessel). There are some slight differences which are probably due to the facts that the microwave power is lower and that the metal vessel has some small influences on the shape of the EM-field and on the flowing pattern of the gas. However, in case the air is replaced by argon, the plasma radius becomes much larger and the electron temperature slightly lower. This confirms that mixing with the surrounding gas is an important mechanism. To determine the quantitative effect of the air entrainment on the particle balance measurements of the molecular nitrogen density are necessary. In the past this was done in our lab using vibrational Raman scattering on an atmospheric ICP [13]. However, in that case a laser beam with a large diameter was used, which is not suitable in case of the TIA.

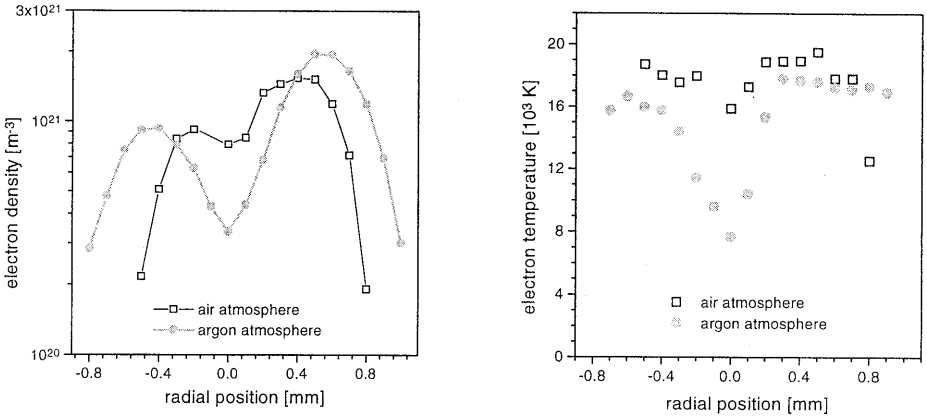

***Figure 5**: The influence of the surrounding atmosphere on the plasma. In an argon atmosphere the plasma is larger, allowing a lower electron temperature. These measurements are taken at 5 mm AN.*

5. Conclusions

Due to the small dimensions of the plasmas created by the TIA high electron temperatures are necessary to sustain these plasmas. However, temperatures, obtained by Thomson scattering using a laser beam whose diameter is of the same magnitude as the plasma, are higher than those which are needed to compensate for the estimated classical losses due to diffusion, flow and recombination. For a thorough understanding of the plasma radially resolved measurements of the electron density proved to be necessary. These measurements show that the plasma has a donut-like shape close to the nozzle, which means that the diffusion losses based on a global consideration are underestimated. For helium the corrected diffusion seems to balance the production more or less. However, in argon the losses due to diffusion are not large enough, which indicates that other mechanisms play a significant role as well. This is probably charge transfer between argon ions and nitrogen molecules and subsequent dissociative recombination of the molecular ion, since the surrounding air influences the plasma.

References

1. J.A.M. van der Mullen, Phys. Rep. **191** 109 (1990).
2. Chapter 4: J. Jonkers and J.A.M. van der Mullen, *"The meaning of the helium excitation temperature"*, submitted to J. Quant. Spectrosc. Radiat. Transf.
3. Chapter 2: J. Jonkers, H.P.C. Vos, J.A.M. van der Mullen and E.A.H. Timmermans, Spectrochim. Acta B **51** 457 (1996).
4. S.C. Snyder, L.D. Reynolds, J.R. Fincke, G.D. Lassahn, J.D. Grandy and T.E. Repetti, Phys. Rev. E **50** 519 (1994).
5. M. Moisan, G. Sauvé, Z. Zakrzewski and J. Hubert, Plasma Sources, Sci. and Techn. **3** 584 (1994).

6. A. Ricard, L. St-Onge, H. Malvos, A. Gicquel, J. Hubert et M. Moisan, J. Phys. III France **5** 1269 (1995).
7. A. Rodero, M.C. García, M.C. Quintero, A. Sola and A. Gamero, J. Phys. D: Appl. Phys **29** 681 (1996).
8. A. Rodero, M.C. Quintero, A. Sola and A. Gamero, Spectrochim. Acta B **51** 467 (1996).
9. Chapter 3: J. Jonkers, J.M. de Regt, J.A.M. van der Mullen, H.P.C. Vos, F.P.J. de Groote and E.A.H. Timmermans, Spectrochim. Acta B **51** 1385 (1996).
10. M. Huang, D.S. Hanselman, Q. Jin and G.M. Hieftje, Spectrocim. Acta B **45** 1339 (1990).
11. G.N. Haddad and A.J.D. Farmer, J. Phys. D: Appl. Phys. **17** 1189 (1984).
12. S. Megy, J.-M. Baronnet and E.A. Ershov-Pavlov, J. Phys. D: Appl. Phys. **28** 344 (1995).
13. J.M. de Regt, F.P.J. de Groote, J.A.M. van der Mullen and D.C. Schram, Spectrochim. Acta B **51** 1527 (1996).
14. M.A. Lieberman and A.J. Lichtenberg, *"Principles of plasma discharges and materials processing"*, John Wiley & Sons (1994).
15. D.A. Benoy, J.A.M. van der Mullen and D.C. Schram, J. Quant. Spectrosc. Radiat. Transfer **46** 195 (1991).
16. H.W. Drawin and F. Emard, Z. Physik **243** 326 (1971).
17. Chapter 6: J. Jonkers, J.A.M. van der Mullen and D.C. Schram, *"On the differences between atmospheric helium and argon plasmas"*, submitted to Phys. Rev. E.
18. A.C.G. Mitchell and M.W. Zemansky, *"Resonance radiation and excited atoms"*, Cambridge University Press, London (1961).
19. D.C. Schram, J.A.M. van der Mullen, J.M. de Regt, D.A. Benoy, F.H.A.G. Fey, F.P.J. de Groote and J. Jonkers, J. of Anal. At. Spectrom. **11** 623 (1996).
20. D. Smith and N.G. Adams, Phys. Rev. A **23** 2327 (1981).
21. J.D. Jackson, *"Classical electrodynamics"*, John Wiley Inc., New York (1975).
22. J. Aubreton, C. Bonnefoi et J.M. Mexmain, Rev. Phys. Appl. **21** 365 (1986).
23. J.M. de Regt, R.A.H. Engeln, F.P.J. de Groote, J.A.M. van der Mullen and D.C. Schram, Rev. of Sci. Instrum. **66** 3228 (1995).

6

On the differences between ionising helium and argon plasmas at atmospheric pressure

J. Jonkers, J.A.M. van der Mullen and D.C. Schram,
submitted for publication to Physical Review E.

In this paper the electron density and temperature of atmospheric helium and argon plasmas which are operated at the same experimental conditions are compared. The conditions are chosen such that both plasmas are ionising. It is found that a helium plasma has a higher electron temperature and a lower electron density than an equi-operational argon plasma, i.e. an argon plasma which is operated at the same external conditions. The main reasons for these are the higher excitation potential of the first excited state and the lower mass of helium, respectively. Due to these differences in electron density and temperature the densities of the helium ground and excited states are much larger than their corresponding Saha equilibrium values for a wide range of conditions. The consequence of this is that the spectroscopic methods which are used to determine the electron density and temperature have a very limited validity region in case of helium. For argon the deviations are much smaller so that these methods can be applied.

1. Introduction

The fact that the application field of plasma technology is increasingly expanding is for an important part based on the tremendous chemical freedom offered by the fourth state of matter. There is virtually no limitation on the chemical properties of mixtures of atoms and molecules which can be brought into the plasma state. Combined with the variability in the state of equilibrium departure there is a nearly unlimited freedom in composing mixtures of molecules, atoms, radicals and ions. However, it is well known that different mixtures demand for different operational conditions. For instance, molecular species ask for a larger input power than atomic gases to get comparable properties of the electron gas, the most important plasma constituent. To state it differently: the plasma parameters n_e and T_e (electron density n_e and temperature T_e) strongly depend on the chemical composition of the gas.

To study the effect of the chemical composition on the plasma parameters n_e and T_e we should compare plasmas operated at the same conditions with each other. We therefore introduce the concept of equi-operational plasmas which are plasmas subjected to the same external controllable conditions such as pressure, power and volume but with different (initial) chemical composition. This concept is an important tool to achieve a classification theory of the chemical dependence of the interrelation of external parameters on the one hand and plasma parameters on the other hand.

However, it is the enormous variety of plasmas which makes this classification theory a challenge which can only be tackled in a step by step approach.

A first step is that we confine ourselves in this study to atomic plasmas, i.e. noble gas plasmas and more specifically to pure argon and helium plasmas. This choice is based on the fact that argon is the most popular plasma working gas whereas helium is the lightest atomic gas. The intercomparison of equi-operational argon and helium plasmas shows that being composed of light and thus mobile particles enhances the outward transport and therefore pushes the plasma further out of equilibrium.

A second step is that laws have to be selected from which relations between external parameters on one hand and plasma parameters on the other hand can be deduced. For this we

take simplified forms of the electron particle balance and the electron energy balance.
A third step is selecting the most appropriate set of external controllable parameters. From the electron particle and energy balance it is found that

- the characteristic size Λ,
- the power density ε and
- the pressure p

form the most suitable set.
Of all possible characteristic sizes the gradient length of the electron density profile Λ_n appears the most useful. Therefore, we generalise the concept of *wall stabilised* plasmas where the wall determines the size of the discharge and thus the ambipolar diffusion length [1,2,3]. To incorporate in the classification theory plasmas which are operated in the open air (for which the size is not fixed by the presence of a wall but by the combination of the shape of the electromagnetic field and the gas flows), we have to generalise this idea of wall stabilisation and denote this general type of plasmas (including the wall stabilised) as being *size stabilised.*
The power density ε can be deduced from the dissipated power P and the volume V. The power is in many cases easy to control externally but the determination of the volume is less straightforward. In most cases it can be related to the gradient length Λ_n of the electron density profile and the length of the active zone.
The pressure p, which is rather simple to control, has an important impact on the plasma in the sense that it determines the density of the atom ground state n_1, via Dalton's law $p = n_1 k_B T$. It therefore has an important *obstructing* impact on the ambipolar diffusion but also a *stimulating* role on the ionisation rate. The higher the ground state density the more ionisation processes per unit of volume and time can be realised at the same electron temperature. The pressure is thus important for the particle balance but also for the energy balance. We will confine ourselves to those plasmas in which the partial pressure of the electrons and ions can be neglected so that Dalton's law reduces to $n_1 = p/k_B T_g$. Although the pressure has an important impact on the plasma properties we will restrict ourselves in this study to atmospheric pressures for which the gas temperature T_g, being usually different from the electron temperature T_e, is taken as a parameter. Extrapolation to lower or higher pressures is expected to be straightforward. In fact the low pressure variant was already studied for instance by Ferreira [2] and by Lieberman [3].
With the steps mentioned before we arrive at the aim of this study namely the intercomparison between atmospheric helium and argon plasmas with respect to the relation between the external parameters Λ and ε on one hand and the plasma parameters n_e and T_e on the other hand. The gas temperature is chosen. We confine ourselves to ionising plasmas so that three particle recombination can be neglected which means a small gradient length (between 0.05 and 2 mm) and moderate power densities (between 3×10^7 and 3×10^{11} Wm^{-3}).
But there is more. If, for a given set of external parameters Λ and ε, the plasma quantities n_e and T_e are known we can determine in what extent the ground state density n_1 deviates from n_1^S, i.e. the value as predicted by the equilibrium state of the Saha balance of ionisation and three particle recombination. The parameter $b_1 = n_1 / n_1^S$ can be used to determine the validity region of operation conditions for which our theory on size stabilised plasmas is valid. It is found that the b_1 value in helium plasmas is usually four to five orders of magnitude larger than that of equi-operational argon plasmas.

Apart from the overpopulation of the ground state density with respect to Saha, it can also be quantified how the local production of charged particles, which is necessary to compensate for the diffusion losses, leads to an excitation flow through the atomic system and thus how the overpopulation b_1 propagates through the system. This allows us to determine directly from the external parameters which part of the atom system deviates from Saha and where the lower boundary of partial Local Saha Equilibrium (pLSE) starts. This prediction of the pLSE boundary is important, since it provides a direct way to test whether the widely used spectroscopic way of determining the electron temperature and density from the measured densities of excited states [4,5,6] is allowed or not. It is found that this spectroscopic method can be applied to most of the atmospheric argon plasmas discussed in this paper, but seldom to helium plasmas.

2. Particle balance

Due to the finite dimensions of laboratory plasmas, charged particles are lost by diffusion. Therefore, in order to sustain the discharge a net production of free electrons is necessary. From the fact that in steady state the diffusion losses are exactly balanced by the production due to ionisation the electron temperature can be obtained. This can be expressed by a simplified particle balance for the electrons:

$$n_e \frac{p}{k_B T_g} S_{CRM} = -\nabla(D_a \nabla n_e) \qquad (1)$$

Here the left hand side represents the production due to ionisation and the right hand side the losses due to diffusion. The losses due to convection and volume recombination are neglected (see section 4). The quotient at the left hand side ($p/k_B T_g$) is the atom density n_1 according to Dalton's law. The electron and ion pressures can be neglected since they are less than 1% of the total pressure for the operation conditions under study, cf. section 3.
The ionisation coefficient S_{CRM} can be calculated using Collisional Radiative Models (CRM). In this study we use the model of Drawin and Emard [7] for helium and of Benoy *et al.* [8] for argon (cf. Figure 1). It is found that a variation of the electron density of one order of magnitude only creates a deviation in S_{CRM} of less than 3%. Therefore, we will neglect this n_e dependence. The ionisation coefficients can be represented by the following fits:

$$S_{CRM}^{He} = 3.15 \times 10^{-15} \sqrt{\hat{T}_e}\, exp\left(\frac{-19.38}{\hat{T}_e}\right) \quad [m^3 s^{-1}] \qquad (2)$$

and

$$S_{CRM}^{Ar} = 7.34 \times 10^{-15} \sqrt{\hat{T}_e}\, exp\left(\frac{-12.06}{\hat{T}_e}\right) \quad [m^3 s^{-1}] \qquad (3)$$

in which $\hat{T}_e$ is the electron temperature in eV. These equations represent the results of the models within 10% for the temperature ranges as used in Figure 1.
Note that the constants in the exponents of the fits are close to the energy gap between the ground and the first excited state (19.8 and 11.6 eV respectively). This is related to the fact that the bottle-neck in the ionisation process is formed by the step from the ground to the first excited state. The rate for this transition mainly depends on the energy gap ΔI_{12} and the

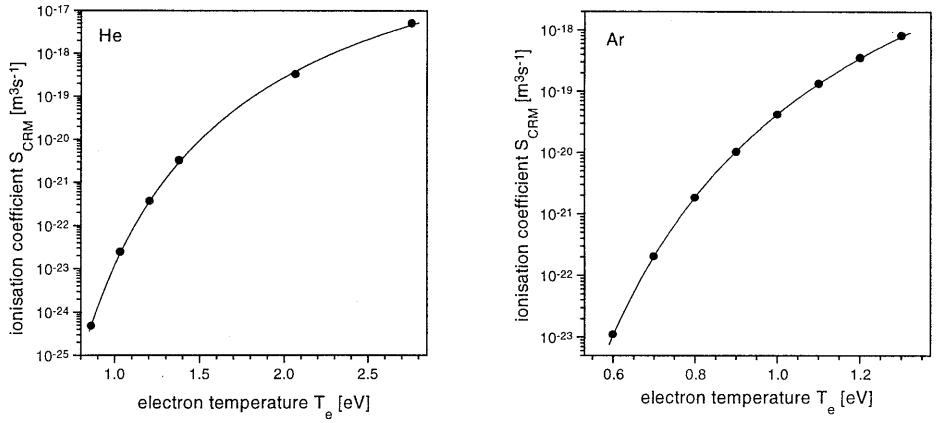

***Figure 1**: The ionisation coefficients of helium [7] and argon [8] and their fits, cf. equations (2) and (3). The small dependency of S_{CRM} on the electron density is neglected.*

electron temperature [3,9]:

$$k(1,2) \propto \frac{\sqrt{k_B T_e}}{\Delta I_{12}^2} exp\left(-\frac{\Delta I_{12}}{k_B T_e}\right) \tag{4}$$

Also the pre-exponential factors of equations (2) and (3) scale within 15% with ΔI_{12}^{-2}.
The right hand side of equation (1) can be simplified to the expression

$$-\nabla\left(D_a \nabla n_e\right) \approx \frac{D_a}{\Lambda_n^2} n_e = \nu_{diff} n_e \tag{5}$$

in which ν_{diff} is the frequency with which the electrons are diffusing out of the plasma and Λ_n the gradient length of the ion (or electron) density profile. The ambipolar diffusion coefficient D_a equals [3,10]:

$$D_a = D_i\left(1 + \frac{T_e}{T_g}\right) \tag{6}$$

Here the ion diffusion coefficient D_i is taken equal to

$$D_i = \frac{3k_B^2 T_g^2}{8pM\Omega\left(T_g\right)} \tag{7}$$

which is found using the first Chapman-Enskog approximation[a] of the binary diffusion coefficient [10,11]. This coefficient is inversely proportional to the atom mass M and the ion-atom collision integral[b] Ω [10,11]:

---

[a] The higher order corrections are small and are usually ignored [11].

[b] A better name for this integral would be ion-atom collision rate coefficient, since its dimension is $m^3 s^{-1}$.

$$\Omega(T_g) = \sqrt{\frac{k_B T_g}{\pi M}} \int_0^\infty \sigma_D\left(\sqrt{\frac{4k_B T_g}{M}}\gamma\right)\gamma^5 \exp(-\gamma^2)d\gamma \quad (8)$$

in which

$$\gamma = v\sqrt{\frac{M}{4k_B T_g}} \quad (9)$$

is the dimensionless initial relative velocity [10,11]. Dalgarno [12] has shown that the diffusion cross section $\sigma_D(v)$ is, in good approximation, equal to twice the cross section for momentum transfer between ions and atoms, in case the diffusion of ions in their parent gas is studied. Using this fact Devoto calculated the integral of equation (8) for argon [13]. Fitting the product of these integral values and $(k_B T_g/\pi M)^{1/2}$ results in the following analytical expression:

$$\Omega^{Ar}(T_g) = (3.03 + 6.82\times10^{-4}T_g - 3.70\times10^{-8}T_g^2 + 9.15\times10^{-13}T_g^3)\times10^{-16} \quad [m^3s^{-1}] \quad (10)$$

with the gas temperature T_g in Kelvin. For the range $3000\ K < T_g < 15000\ K$ the original calculations by Devoto are reproduced within 1%.
For helium the cross section for charge transfer is tabulated by Barnet [14]. We used a double exponential decay to fit these data in order to calculate the collision integral. For the range $1000\ K < T_g < 6000\ K$ this results in the following analytical approximation:

$$\Omega^{He}(T_g) = (3.43 + 1.65\times10^{-3}T_g - 1.02\times10^{-7}T_g^2)\times10^{-16} \quad [m^3s^{-1}] \quad (11)$$

The accuracy is determined by that of the tabulated cross sections (within 20% [14]).
Using the data on the ionisation and diffusion coefficients the particle balance (1) can be solved, yielding the electron temperature as function of the gradient length with the gas temperature as a free parameter. Note that the electron density cancels out in the particle balance (1) in case the simplification of equation (5) is used. The results are depicted in Figure 2, from which it can be seen that the shorter the gradient length the higher the electron temperature. The reason for this dependency is that a shorter gradient length enhances the diffusion losses, cf. equation (5), so that a higher T_e value is needed for the enlarged

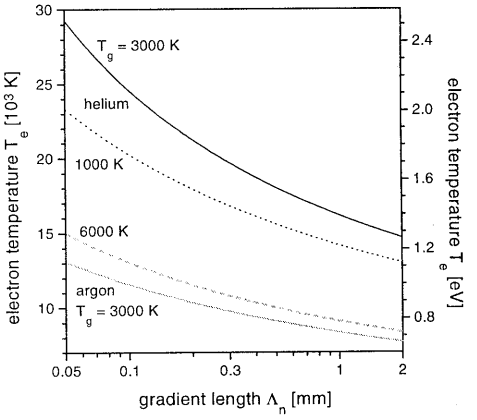

***Figure 2**: The electron temperature in helium and argon plasmas as estimated from the particle balance (black and grey lines respectively). For each plasma the result is given for two typical gas temperatures. As the gradient length decreases the diffusion losses increase, so that a higher electron temperature is needed to sustain the plasma.*

production of charged particles. The same figure also shows that at a higher gas temperature a higher electron temperature is needed to sustain the plasma. This is because a higher gas temperature reduces the production (the atom density is lower) and facilitates the diffusion, see equation (1) and (7) respectively.
It appears that for equi-operational plasmas the electron temperature in argon is always much lower than in helium. The ratio T_e^{He}/T_e^{Ar} ranges roughly from 1.9 to 2.3 for Λ_n from 2 to 0.05 mm. This difference is mainly caused by the fact that argon ions are easier to produce, due to the smaller energy gap ΔI_{12} between the atom ground state and the first excited state. The fact that the temperature does not exactly scale with this energy gap ($\Delta I_{12}^{He} / \Delta I_{12}^{Ar} \approx 1.7$) is caused by the differences in diffusion and the pre-exponential factor in equation (4).

3. Energy balance

The value of the electron density can be obtained from the simplified power balance of the free electrons, which expresses that the input power density ε equals the power per unit of volume which is lost by the free electrons in inelastic and elastic collisions:

$$\varepsilon = n_e \frac{p}{k_B T_g} S_{CR} I_1 + n_e \left[n_+ \langle \sigma_{ei}^m v_e \rangle + \frac{p}{k_B T_g} \langle \sigma_{ea}^m v_e \rangle \right] \frac{2m_e}{M} \frac{3}{2} k_B (T_e - T_g) \qquad (12)$$

Here $\langle \sigma^m_{ei} v_e \rangle$ and $\langle \sigma^m_{ea} v_e \rangle$ represent the electron-ion and the electron-atom collision rate coefficients for momentum transfer averaged over the (Maxwellian) Electron Energy Distribution Function (EEDF). The first one can be found in for instance [15]:

$$\langle \sigma_{ei}^m v_e \rangle = \frac{4\sqrt{2\pi}}{3} \left(\frac{e^2}{4\pi\varepsilon_0 m_e} \right)^2 \left(\frac{m_e}{k_B T_e} \right)^{3/2} ln\,\Lambda_{Coul} \approx 2.91 \times 10^{-12} \frac{ln\,\Lambda_{Coul}}{\hat{T}_e^{3/2}} \quad [m^3 s^{-1}] \qquad (13)$$

in which

$$ln\,\Lambda_{Coul} \approx ln\left(1550 \sqrt{\frac{\hat{T}_e^3}{\hat{n}_e}} \right) \qquad (14)$$

is the Coulomb logarithm [10,15], with $\hat{n}_e$ the electron density in 10^{20} m^{-3}. For helium the electron-atom collision rate coefficient $\langle \sigma^m_{ea} v_e \rangle$ is obtained after fitting the cross sections given by McEachran and Stauffer [16] and integrating over the Maxwellian EEDF. The result can be reproduced within 2% for the range $1.0 < \hat{T}_e < 3.4$ eV using:

$$\langle \sigma_{ea}^m v_e \rangle^{He} = \left(2.21 + 2.59 \hat{T}_e - 0.344 \hat{T}_e^2 \right) \times 10^{-14} \quad [m^3 s^{-1}] \qquad (15)$$

A similar procedure leads for argon (using the experimental data of Rees *et al.* [17]) to

$$\langle \sigma_{ea}^m v_e \rangle^{Ar} = \left(0.084 + 0.537 \hat{T}_e + 1.192 \hat{T}_e^2 \right) \times 10^{-14} \quad [m^3 s^{-1}] \qquad (16)$$

for $0.5 < \hat{T}_e < 2.5$ eV.
For the inelastic losses only those related to the production of new ions is taken into account, as can be seen in the first term at the right hand side of equation (12). One should realise that this is the left hand side of the particle balance (1) multiplied by the ionisation potential of the atom in question. Note that the energy required to heat the cold electrons which are produced

in the ionisation process (5/2 $k_B T_e$) is neglected. Also the energy losses due to radiation can be omitted in the energy balance. For argon an estimation of this term can be obtained using the results of Janssen *et al.* [18] who used a Collisional Radiative Model to calculate the losses due to line radiation, which they assumed to be dominant. For the minimum and maximum electron temperature as found in Figure 2, the radiation losses are given by [18]:

$$\varepsilon_{rad}^{Ar} \approx \begin{cases} 1\times10^{-36} n_e^2 & \text{for } T_e = 8000 \text{ K} \\ 7\times10^{-17} n_1 & \text{for } T_e = 16000 \text{ K} \end{cases} \quad [\text{Wm}^{-3}] \tag{17}$$

for the relevant n_e and n_1 values. This is (much) smaller than the power densities under study (see below), except for the very small plasmas (with T_e = 15000 K, see Figure 2) for which it is found that the radiation losses are comparable to the lowest power densities, cf. Figure 3. In helium plasmas the radiation losses are in general lower than in argon plasmas, due to the lower electron density.

If we assume that the ion density equals the electron density, which is justified in this study of noble gases, solving equation (12) yields n_e as function of the power density for given electron and gas temperatures. In the previous section the electron temperature was determined as a function of the gradient length. Using this result it is possible to express the electron density in the macroscopic parameters ε and Λ_n with the gas temperature as free parameter. The results are given in Figure 3. For small gradient lengths the losses of free electrons due to diffusion are relatively high, so that almost all the power is used in the production of charged particles. The elastic energy losses can be neglected which results in an electron density proportional to the power density:

$$n_e \approx \frac{\varepsilon}{I_1} \frac{k_B T_g}{p S_{CR}} = \frac{\varepsilon}{I_1 \nu_{diff}} \tag{18}$$

The diffusion loss frequency of the free electrons in the plasma ν_{diff} is related to the ionisation via the particle balance (1). This frequency is roughly proportional to Λ_n^{-2}, cf. equation (5)[c], so that for small gradient lengths the electron density scales with the square of the gradient length. For increasing gas temperature and/or decreasing ion mass the charged particles can diffuse easier out of the plasma, so that the residence time decreases and a higher power density is needed to retain the same electron density.

For large gradient lengths the influence of the diffusion decreases and the elastic collisions become the main loss process. For helium this results in an electron density which is proportional to the product of power density and gas temperature:

$$n_e \approx \frac{M}{3m_e} \frac{k_B T_g}{p} \frac{\varepsilon}{\langle \sigma_{ea}^m v_e \rangle k_B (T_e - T_g)} \tag{19}$$

The electron-ion collisions are negligible because of the high electron temperature and the relatively low electron density. Both disfavour the electron-ion (e-i) collisions with respect to the electron-atom collisions (e-a). For larger gradient lengths the discharge can be sustained using reduced power densities (cf. Figure 3), since due to the lower electron temperature, the collision rate coefficient $\langle \sigma^m_{ea} v_e \rangle$ and the temperature difference (T_e - T_g) decrease, so that less

[c] For smaller gradient lengths also the electron temperature increases slightly (cf. section 2), so that the diffusion loss frequency increases a little bit faster than Λ_n^{-2}.

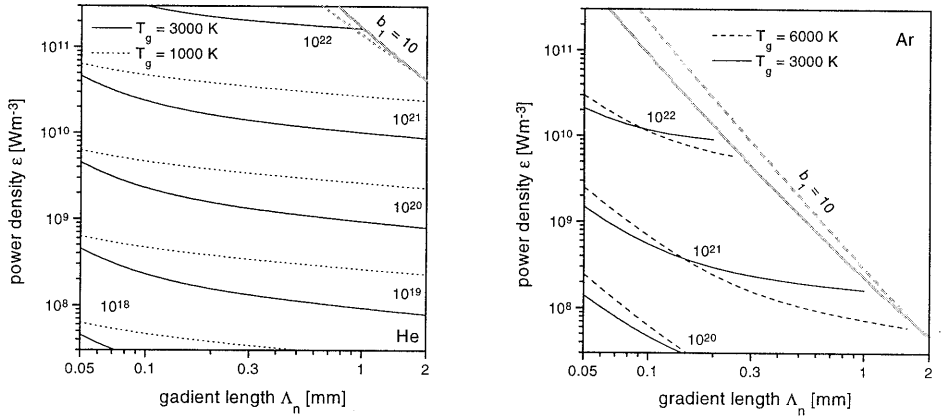

***Figure 3**: The electron density (in m^{-3}) in helium and argon plasmas as obtained from the simplified energy balance for different power densities and gradient lengths of the electron density profile. Only contours are plotted for which $b_l \geq 10$, since for $b_l < 10$ the plasma is not strongly ionising anymore and some of the used simplifications lose their validity (see next section).*

power is transferred to the heavy particles.

For argon it appears that when the elastic losses are dominant, the electron-atom and the electron-ion collisions are of the same order of magnitude. This has two reasons:

1. As is discussed in the previous section the electron temperature in an argon plasma is lower than that of an equi-operational helium plasma. This means that the rate coefficient for e-a collisions is smaller and that of the e-i collisions larger.
2. In an elastic collision of a free electron with an argon atom or ion less kinetic energy is transferred than in a collision with a helium atom (or ion), so that the electron density (and thus ion density) in argon can be higher at the same power density, which favours the relevance importance of the e-i collisions.

At higher power density the ion density is larger and so are the losses due to Coulomb collisions. In case the e-i collisions are the dominant loss process, the electron density is proportional to $\varepsilon^{1/2}$. However, the role of the e-a collisions can not be neglected at these power densities so that the electron density scales with:

$$n_e \propto \varepsilon^{\alpha} \tag{20}$$

with α somewhere between 0.5 and 1.

For larger plasma dimensions the electron temperature is lower. Since the elastic electron-atom losses depend stronger on T_e than the electron-ion losses, a smaller power density is needed to sustain a larger discharge at the same electron density.

4. The b_1 parameter

Using the results of the previous sections it is possible to determine whether the plasma is close to or far from equilibrium. For this we use the b_1 parameter:

$$b_1 = \frac{n_1}{n_1^S} \tag{21}$$

which is the relative population of the ground state with respect to the density according to Saha:

$$n_1^S = \frac{g_1}{2g_+} n_e n_+ \left(\frac{h}{\sqrt{2\pi m_e k_B T_e}} \right)^3 exp\left(\frac{I_1}{k_B T_e} \right) \tag{22}$$

The Saha density would be the ground state density if the ionisation from the ground state is in equilibrium with the corresponding reverse process of three particle recombination. In equation (22) g_1 and g_+ refer to the statistical weight of the atom and ion ground states, respectively. According to this definition b_1 is larger than unity if the ionisation from the ground state is larger than the three particle recombination to the ground state. However, in the class of plasmas under study, b_1 can also be used to judge whether the *total* ionisation is larger than the *total* recombination, since

$$\frac{n_e n_1 S_{CRM}}{n_e n_+ \alpha_{CRM}} = \frac{b_1 n_1^S S_{CRM}}{n_+ \alpha_{CRM}} \approx b_1 \tag{23}$$

with α_{CRM} the recombination coefficient. Thus a plasma (part) is ionising if b_1 is larger than unity. As we will see in the next section the larger b_1 is, the stronger the densities of the excited states deviate from their equilibrium values.
The approximation used in the second step of (23), i.e.

$$n_e n_1^S S_{CRM} \approx n_e n_+ \alpha_{CRM} \tag{24}$$

is only valid for relatively high electron densities (as in the plasmas under study), because for high n_e the influence of radiative decay processes can be neglected. This approximation is therefore related to the statement in section 2 that the ionisation coefficient S_{CRM} does not depend significantly on the electron density.
The b_1 parameter can also be used to obtain the validity region of the size-stabilised plasmas. In the determination of the electron temperature (cf. section 2) it was assumed that the diffusion outweighs the recombination as loss process of the charged particles, so that the latter can be neglected. Also in the energy balance the energy gain due to the recombination processes is omitted. These simplifications are justified as long as the local production of charged particles is much larger than the local destruction via recombination. In this paper we assume that this the case if $b_1 > 10$.[d] The plasmas which are close to equilibrium ($0.1 < b_1 < 10$) are discussed in other papers of our group [19,20].
The relative population of the ground state $b_1 = n_1/n_1^S$ can easily be calculated using the results of the previous section. The Saha density n_1^S is determined by the electron density and temperature and can therefore be expressed in the operation conditions, via the particle and

[d] In the next chapter an alternative way of volume recombination is discussed: the formation and destruction of molecular rare gas ions.

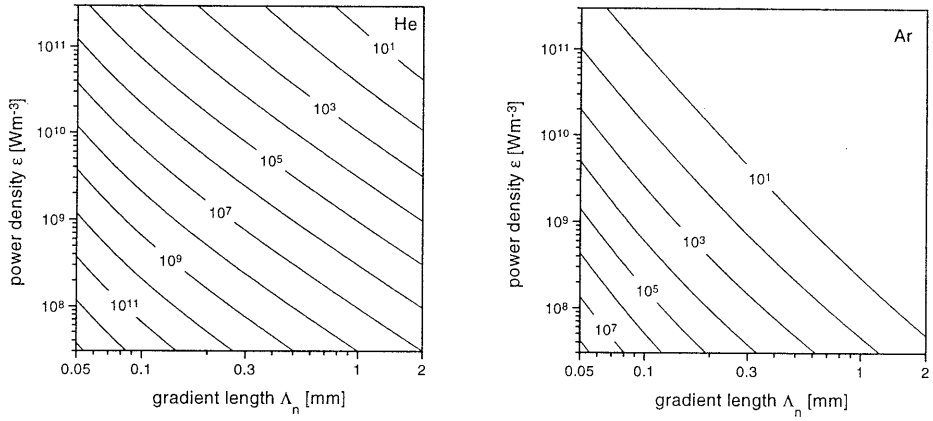

***Figure 4**: Iso-contour plots of the overpopulation of the ground state b_1 for helium and argon respectively, both for a gas temperature of 3000 K. For $b_1 < 10$ the diffusion dominance in the particle balance loses its strength. Note that the close to equilibrium regime (i.e. $b_1 < 10$) of external parameters is much larger for argon than for helium.*

energy balances. The actual density n_1 can be obtained from the gas temperature and the pressure using Dalton's law. The electron and ion pressures can be neglected, since they are less than 1% of the total pressure.

The calculated b_1 values are depicted in Figure 4 for helium and argon. In both cases the b_1 factor is lower for larger gradient lengths and for higher power densities. This is because for the corresponding lower electron temperatures and higher electron densities the Saha density of the ground state is higher, so that the plasma is closer to ionisation/recombination equilibrium. It can also be seen in Figure 4 that a helium plasma deviates stronger from equilibrium than an equi-operational argon plasma. This is based on the fact that in helium both I_1/T_e and n_e are lower, which result in a lower Saha density n_1^S.

5. The upper part of the ASDF

The population densities of the excited states are of special interest. They determine the line radiation of the plasma and are consequently in many cases used in spectroscopic methods to determine the plasma parameters T_e and n_e. In the interpretation of these methods it is assumed that the radiating levels are in partial Local Saha Equilibrium (pLSE), i.e. they are populated according to Saha's formula (22). This is a tempting assumption because the rates corresponding to the Saha balance of ionisation and recombination

$$A_p + e \xleftarrow{\text{Saha}} A_1^+ + e + e \tag{25}$$

are indeed high, especially for those levels close to the continuum, so that the balances of this type are not easily to disturb. However, the class of plasma under study is characterised by moderate to large overpopulations of the ground state with respect to Saha ($b_1 > 10$), so that the Saha balance will not be in equilibrium for the ground state. This deviation is not only limited to the ground state, but propagates through the atomic system, since the Boltzmann

balances of excitation and deexcitation

$$A_p + e \xleftarrow{\text{Boltzmann}} A_q + e \tag{26}$$

are disturbed as well. Thus the overpopulation of the ground state induces an excitation flow through the atomic system effecting the equilibrium state of excited states as well [9,21,22].
This section deals with the consequences of this flow for the higher excited (and still measurable) states. In principle this can be investigated using Collisional Radiative models for which the plasma parameters n_e, T_e and n_1 are input parameters. However, it is more elegant to determine a direct relation between the externally controllable parameters and the equilibrium departure of the excited states. For this we make use of the fact that an analytical description exists for a large part of the Atomic Sate Distribution Function (ASDF) [9,21,23,24,25]. This so-called Excitation Saturation Balance (ESB) dominates a large part of the excitation space for the plasmas under study. Since (most of) the ionisation flow passes through ESB, it is possible to calculate the overpopulation of the excited states. Due to the analytical structure of the non-equilibrium state of the ASDF, the dependency on Λ and ε can be simplified.
The levels for which

1. the atomic energy scheme is hydrogenic,
2. radiation processes can be neglected and
3. the probability on excitation is larger than that on deexcitation

are in ESB. In the class of plasmas under study the second condition is the most restricting one, which means that the lower boundary of ESB is determined by the Griem criterion [9,26]:

$$I_{CR} < R\left(\frac{n_e}{9\times 10^{23}}\right)^{2/9} \tag{27}$$

For the lowest electron density in helium (10^{18} m^{-3}) the upper 0.65 eV of the atomic scheme (i.e. with principal quantum number $p > 4.6$) is in ESB. For argon the lowest electron density is roughly one order of magnitude higher so that the states for which $I_p < 1.1$ eV (or $p > 3.6$) holds, fulfil the Griem criterion. For higher electron densities more states are in Excitation Saturation Balance, up to around $n_e \approx 5 \times 10^{21}$ m^{-3} when all the excited states are in ESB.
The population of the levels in ESB can be described by [9,21,22,23,24,25]

$$n_p = \left(1+\beta I_p^3\right) n_p^S \propto \left(1+\beta I_p^3\right) exp\left(\frac{I_p}{k_B T_e}\right) \tag{28}$$

in which the last expression denotes the functional dependence on the ionisation potential I_p. The ESB parameter β depends on the flow through the upper part of the ASDF and can be expressed in the external parameters Λ and ε. In doing so we will assume that most of the ionisation takes place from the states in ESB, as is shown by the CRM calculations of Fujimoto [21].
In ESB the population and depopulation of a level are dominantly due to step-wise excitation and deexcitation and to ionisation and recombination [9,21]. Since we assume that the complete ionisation flow passes the lower boundary of ESB, this means that for this lowest ESB level p_{CR} the following continuity equation holds:

$$\frac{D_a}{\Lambda_n^2} n_e = n_e \frac{p}{k_B T_g} S_{CRM}$$
$$\approx n_e n_{pCR} k(p_{CR}, p_{CR}+1) - n_e n_{pCR+1} k(p_{CR}+1, p_{CR}) + n_e n_{pCR} S(p_{CR}) - n_e^2 n_+ R(p_{CR}) \quad (29)$$

in which k(p,q) represents the electron induced transition rate from $p \rightarrow q$ and S(p) and R(p) the ionisation rate from and the (three particle) recombination rate to level p, respectively. The first two members of equation (29) represent the flow of electrons in real space and excitation space, respectively, as discussed in section 2. The last term is the net flow through the top of the atomic system. Together with the principle of detailed balancing and (28), equation (29) can be rewritten as

$$\frac{D_a}{\Lambda_n^2} = \beta I_{CR}^3 n_{p_{CR}}^S \left[k(p_{CR}, p_{CR}+1)\left(1 - \frac{I_{p_{CR}+1}^3}{I_{p_{CR}}^3}\right) + S(p_{CR}) \right] \quad (30)$$

Thus the ESB parameter β can be expressed[e] in the electron temperature and density or in the operation conditions p, Λ_n and ε, provided that k and S are known as function of the temperature and the principal quantum number. For this we use the semi-empirical rates as given by Vriens and Smeets [27]. The results are depicted in Figure 5. It can be seen that smaller plasma dimensions and lower power densities lead to stronger overpopulations with respect to Saha equilibrium. For low electron densities (i.e. low ε) this is because the population according to Saha is low, so that a higher overpopulation is needed to carry the same ionisation flow. For smaller plasma dimensions (or lighter ions) the losses due to diffusion are higher. This results in a lower electron density and in a larger ionisation flow through the atomic system. Since at smaller dimensions also the electron temperature is higher, the stepwise excitation and ionisation rates increases too, so that it is not immediately clear whether an increase in T_e increases or decreases the deviations from Saha. Since the

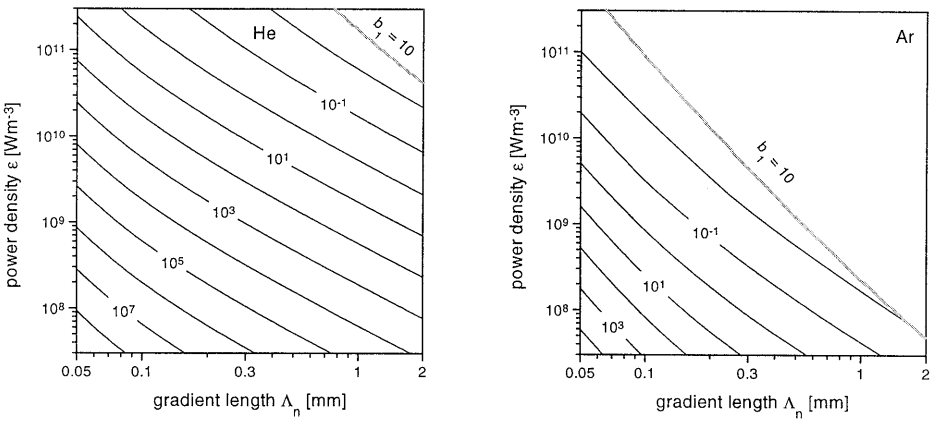

***Figure 5**: The ESB parameter β (in eV^{-3}) for helium and argon respectively (at T_g = 3000 K).*

[e] For $n_e > 6 \times 10^{21}$ m^{-3} all the excited states of helium are in ESB and for the lower ESB boundary p = 1.73 is taken. For argon these numbers are 4×10^{21} m^{-3} and 1.82, respectively.

excitation rates are dependent on the Boltzmann factor [9,27]:

$$k(p,q) \propto exp\left(\frac{-\Delta I_{pq}}{k_B T_e}\right) \tag{31}$$

the rate of the transition with the largest energy gap increases faster with the electron temperature than the other rates. This means that for increasing T_e the left hand side of equation (30), i.e. the excitation from the atom ground state to the first excited state, increases faster than the rates between the square brackets at the right hand side. Since also the Saha density $n_p^>$ decreases (due to the increasing T_e and thus decreasing n_e) this means that the overpopulation as expressed by β is an increasing function of T_e and thus a decreasing function of Λ_n.

Now the ESB parameter β is known, it is possible to determine which states are in pLSE, i.e. for which states the overpopulation is negligible. As an arbitrary criterion we choose that this is the case for an overpopulation less than 20%, since this is more or less the accuracy with which the densities of the excited states can be determined [28]. This boundary condition can be written as

$$I_{pLSE} = \sqrt[3]{\frac{0.2}{\beta}} \tag{32}$$

Note that this condition is only valid for those states which satisfy the Griem criterion (27), i.e. $I_{pLSE} < I_{CR}$. In practice this appears always to be the case for the plasma under study.

Using the results of Figure 5 the lower limit of pLSE (that is the largest value for I_p) can be calculated, which is depicted in Figure 6. The pLSE part of the atomic system is larger for larger plasmas, higher power densities and heavier gases. This can be understood by realising that under these circumstances diffusion plays a smaller role, so that the necessary excitation flow through the atomic system is also smaller and consequently the ASDF is closer to

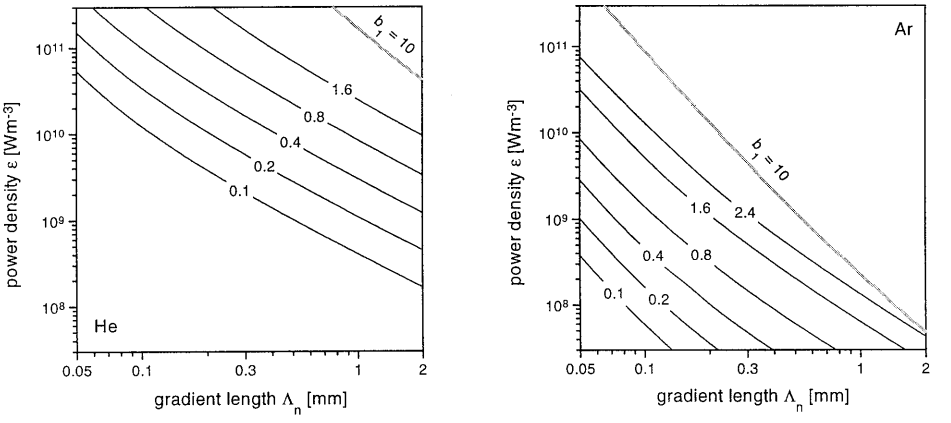

***Figure 6**: The boundary for the ionisation energy (in eV) of the levels which are in pLSE, according to equation (32) in helium and in argon respectively. It can be seen that for given external parameters, pLSE is reached in a much larger part of the ASDF for argon than for helium.*

equilibrium.
Since by far most helium plasmas are operated at relatively low power densities the spectroscopic methods can not be used to determine the electron temperature and density. The fact that the observed excited states are not in pLSE but in ESB, is the reason that the spectroscopic methods always yield temperatures around 3500 K [22]. For argon these methods are found to be valid in a wide range of conditions.

6. Conclusions

The electron temperature in a strongly ionising helium plasma at atmospheric pressure is 1.9 to 2.3 times higher than in an argon plasma operated at the same conditions. This difference is mainly caused by the fact that the first excited state of helium has a higher excitation potential than that of argon.
The fact that helium is ten times lighter results in a lower electron density than in an equi-operational argon plasma. For small plasma dimensions this is because the charged particles can diffuse easier out of the plasma and for large dimensions because of the better heat transfer from the free electrons to the heavy particles.
Both characteristics of helium (the high excitation potential of the first excited state and the low mass) cause that a helium plasma deviates stronger from equilibrium than a comparable argon plasma. This is also manifest in the densities of the excited states, which are, in case of helium, strongly overpopulated with respect to the Saha equilibrium distribution and close to equilibrium in case of argon. Due to this it is possible to determine the electron density and temperature by spectroscopic methods in most argon plasmas, but they fail to diagnose helium plasmas correctly.

References

1. Y. P. Raizer, *"Gas discharge physics"*, Springer-Verlag, Berlin (1991).
2. C.M. Ferreira, M. Moisan and Z. Zakrzewski, *"Physical principles of microwave plasma generation"*, p11 in *"Microwave induced plasmas"*, ed. by M. Moisan and J. Pelletier, Elsevier, Amsterdam (1992).
3. M.A. Lieberman and A.J. Lichtenberg, *"Principles of plasma discharges and materials processing"*, John Wiley & Sons (1994).
4. H.R. Griem, *"Plasma spectroscopy"*, McGraw-Hill Inc., New York (1964).
5. P.W.J.M. Boumans, *"Inductively coupled plasma emission spectroscopy, part 2: applications and fundamentals"*, John Wiley & Sons, New York (1987).
6. W.L. Wiese, Spectrochim. Acta B **46** 831 (1991).
7. H.W. Drawin and F. Emard, Z. Physik **243** 326 (1971).
8. D.A. Benoy, J.A.M. van der Mullen and D.C. Schram, J. Quant. Spectrosc. Radiat. Transfer **46** 195 (1991).
9. J.A.M. van der Mullen, Phys. Rep. **191** 109 (1990).
10. E.W. McDaniel, *"Collision phenomena in ionized gases"*, John Wiley & Sons (1964).
11. J.O. Hirschfelder, C.F. Curtis and R.B. Bird, *"Molecular theory of gases and liquids"*, John Wiley & Sons (1966).
12. A. Dalgarno, Phil. Trans. Roy. Soc. (London) A **250** 426 (1958).
13. R.S. Devoto, Phys. Fluids **16** 616 (1973).

14. C.F. Barnett, *"Atomic data for fusion"*, volume 1: *"Collisions of H, H_2, He and Li atoms and ions with atoms and molecules"*, Controlled Fusion Atomic Data Centre (1990).
15. M. Mitchner and C.H. Kruger, *"Partially ionized gases"*, Wiley & sons, New York (1973).
16. R.P. McEachran and A.D. Stauffer, J. Phys. B: At. Mol. Phys. **16** 255 (1983).
17. J.A. Rees, H.B. Milloy, R.W. Crompton and A.G. Robertson, Austr. Journ. of Phys. **30** 61 (1977).
18. G.M. Janssen, J. van Dijk, D.A. Benoy, M.A. Tas, J.A.M. van der Mullen and D.C. Schram, in preparation.
19. D.C. Schram, J.C.M. de Haas, J.A.M. van der Mullen and M.C.M. van de Sanden, Plasma Chem. Plasma Proc. **16** 19S (1996).
20. D.C. Schram, J.A.M. van der Mullen, J.M. de Regt, D.A. Benoy, F.H.A.G. Fey, F.P.J. de Groote and J. Jonkers, J. of Anal. At. Spectrom. **11** 623 (1996).
21. T. Fujimoto, J. Phys. Soc. Jap. **47** 273 (1979).
22. Chapter 4: J. Jonkers and J.A.M. van der Mullen, *"On the excitation temperature in helium plasmas"*, submitted to J. Quant. Spectrosc. Radiat. Transf.
23. W. Kohsiek, J. Quant. Spectrosc. Radiat. Transf. **16** 1079 (1976).
24. L. Vriens, J. Appl. Phys. **49** 3814 (1978).
25. J.A.M. van der Mullen, B. van der Sijde and D.C. Schram, Phys. Lett. A **79** 51 (1980).
26. H. Griem, Phys. Rev. **131** 1170 (1963).
27. L. Vriens and A.H.M. Smeets, Phys. Rev. A **22** 940 (1980).
28. J.M. de Regt, R.D. Tas, J.A.M. van der Mullen, B. van der Sijde and D.C. Schram, J. Quant. Spectrosc. Radiat. Transf. **56** 67 (1996).

7

The role of rare gas molecular ions in plasmas operated at atmospheric pressure

J. Jonkers, J.A.M. van der Mullen and D.C. Schram.

Molecular Rare gas Ions (MRI) are of interest, since they may offer a fast volume recombination channel in rare gas plasmas, via Dissociative Recombination (DR). In this paper the concentration of MRI is calculated by balancing the most important processes for formation and destruction of these ions. It will be shown that the effective loss frequency of charged particles in the plasma due to DR of MRI is not determined by the formation of these ions, but by the dissociative recombination process itself. Also the consequences for the particle and energy balances of atmospheric "size-stabilised" helium and argon plasmas are discussed, as well as the influence on the lower boundary for pLSE.

1. Introduction

In the previous chapter [1] atmospheric size-stabilised helium and argon plasmas are compared with each other. In these plasmas diffusion is assumed to be the dominant loss process of charged particles and volume recombination is neglected. It was shown [1] that for relatively small plasmas at not too high power densities the three particle recombination

$$Ar^+ + e + e \longrightarrow Ar + e \tag{1}$$

can indeed be neglected. For these conditions diffusion losses prevail and it turns out to be possible to obtain the electron temperature T_e and density n_e as function of the characteristic size Λ, the power density ε and the pressure p. Also the population densities of the highly excited states can be calculated, which offers a powerful tool to determine directly the position of the lower boundary of pLSE (partial Local Saha Equilibrium) as a function of the operation parameters Λ, ε and p [1]. This can be used to test the validity of the experimental spectroscopic methods used for characterisation of these plasmas.

However, the fact that three particle (atomic) recombination (1) can be neglected, does not necessarily imply that volume recombination in the plasma is absent: molecular recombination channels may still play an important role. This can be either via the formation of molecular rare gas ions Rg_2^+ via Atom Assisted Association (AAA)[a]

$$Rg^+ + Rg + Rg \xrightarrow{AAA} Rg_2^+ + Rg \tag{2}$$

or the Charge Transfer (CT) with a foreign molecule such as N_2:

$$Rg^+ + N_2 \xrightarrow{CT} Rg + N_2^+ \tag{3}$$

both followed by Dissociative Recombination (DR):

$$X_2^+ + e \xrightarrow{DR} X + X^* \tag{4}$$

in which X^* denotes a (possibly) excited atom. In the literature it is often assumed that the last

[a] The processes in which an electron or an ion acts as third particle can be neglected due to the relatively low density of charged particles in the plasmas under study, see appendix.

reaction is much faster than the AAA and CT reactions so that the effective recombination rate as offered by the molecular channels is determined by the formation process (2) [2,3,4]. The reason for this assumption is the Coulomb character of the interaction between the molecular ion and the free electron. However, as we shall see below, this simplification is not justified in most cases.

The charge exchange with a foreign molecule can not be expressed in a general way, since it depends on the concentration of these molecules, which is, for instance, determined by the entrainment of the surrounding air or by the deliberate introduction of molecules into the plasma. Here we will discuss the influence of the Molecular Rare gas Ions (MRI) only. In particular for plasmas at atmospheric pressure this channel is expected to be important, since the high atom density facilitates the formation of MRI in the three particle reaction (2).

One important point of attention is the internal energy of the atoms produced in the DR reaction. In the case that one of the atoms produced in reaction (4) is (relatively highly) excited, this atom is very likely to be ionised again[b], so that the molecular rare gas channel does not have a strong influence on the particle balance. It is usually assumed that by far the most important DR channel of Ar_2^+ ions leads to an argon atom in the 4p state and one in the 3p ground state [2,3,4,5,6]. Recently evidence was found that also a significant amount of excited atoms in the 4s state are produced [7]. Moreover, an "undetermined non-negligible fraction" [8] of the dissociation events would yield two rare gas atoms in the ground state. These new results were obtained using a time of flight technique, which makes it possible to measure the kinetic energy of the dissociation products directly. An important drawback of this work is that the dissociation recombination events took place inside a plasma, so that the different escape probabilities of the various products make it impossible to obtaine any quantitative information on the branching ratio.

The two channels leading to Ar(3p) + Ar(3p) and to Ar(4s) + Ar(3p) are of extreme importance. The first one is a direct contribution to the number of (volume) recombination processes, whereas the latter produces a 4s atom with a large kinetic energy (around 1.5 eV). If this atom is in a radiative 4s state the escape of the (resonant) radiation is rather large, due to the high kinetic energy. This enhances the recombination as well. Here it is assumed that the fraction of the DR recombination events in which directly or indirectly two ground state atoms ar produced equals $\chi = 0.05$.

This chapter is devoted to the impact of the formation and destruction of MRI on the particle and energy balances of atmospheric plasmas. In section 2 the density of these ions is calculated using a particle balance in which all the relevant processes are incorporated. The consequences of the MRI channel for the particle and energy balances of the electrons are discussed in sections 3 and 4. Section 5 deals with the influence of MRI on the pLSE boundary.

It should be realised that the exact value of χ is not known. As is shown in section 3 to 5, the choice of the branching ratio χ mainly influences the particle balance and thus the electron temperature of the plasma. The energy balance and the pLSE condition do not depend strongly on χ.

---

[b] Re-ionisation is more likely than decay to the ground state, due to the high electron density and temperature in the plasma and due to the fact that most of the resonance radiation, created by radiative decay towards the ground state, is re-absorbed.

2. Density of the molecular rare gas ion

In order to determine the rate of the dissociative recombination reaction the concentration of the molecular rare gas ion has to be known. This can be obtained from the particle balance of the molecular ions. Besides AAA (2) and DR (4), also Dissociation by Atom Impact (DAI, the inverse reaction of the AAA)

$$Rg_2^+ + Rg \xrightarrow{DAI} Rg^+ + Rg + Rg \tag{5}$$

and Dissociation by Electron Impact (DEI):

$$Rg_2^+ + e \xrightarrow{DEI} Rg^+ + Rg + e \tag{6}$$

have to be included. The rate coefficients of the various reactions are given below. An overview is given in Figure 1 and Table 1. The inverse process of DEI, Electron Assisted Association (EAA)

$$Rg^+ + Rg + e \xrightarrow{EAA} Rg_2^+ + e \tag{7}$$

can be neglected, as well as the association process in which an ion acts as third particle, both due to the low electron density. This is discussed in the appendix where it is also shown that the inverse process of DR, Associative Ionisation (AI)

$$Rg^* + Rg \xrightarrow{AI} Rg_2^+ + e \tag{8}$$

is only important for plasmas which are far from equilibrium, so that the densities of the highly excited atoms Rg* is high with respect to the electron density. However, it turns out that for these conditions more than 90% of the ions are molecules, even in case this reaction is omitted.

If we assume that the reactions are so fast that the diffusion can be neglected, the particle balance can be written as:

$$k_{AAA} n_1^2 n_+ = k_{DAI} n_1 n_{MRI} + k_{DEI} n_e n_{MRI} + k_{DR} n_e n_{MRI} \tag{9}$$

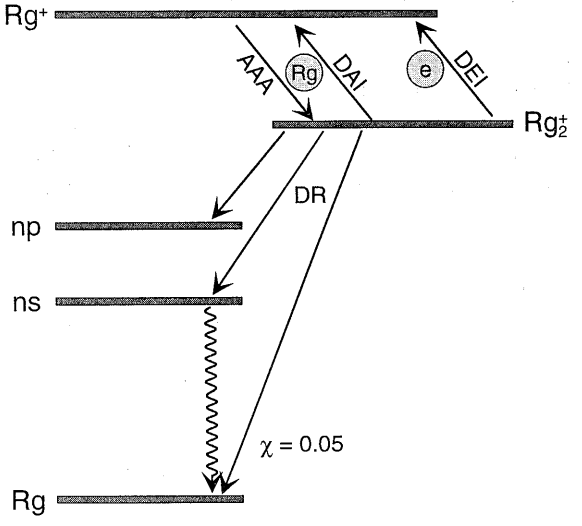

Figure 1: A schematic of the formation and destruction processes of Rg_2^+ which are taken into account in this paper. An explanation of the abbreviations is given in Table 1.

	process		rate coefficients	
	name	reaction	helium	argon
AAA	atom assisted association	$Rg^+ + Rg + Rg \rightarrow Rg_2^+ + Rg$	(12)	(13)
DR	dissociative recombination	$Rg_2^+ + e \rightarrow Rg + Rg^*$	(14)	(15)
DAI	dissociation by atom impact	$Rg_2^+ + Rg \rightarrow Rg^+ + Rg + Rg$	(25)	(26)
DEI	dissociation by electron impact	$Rg_2^+ + e \rightarrow Rg^+ + Rg + e$	(16) & (18)	(17) & (18)

***Table 1**: An overview of the reactions and rates which are used in this paper to calculate the concentrations of the molecular rare gas ions. The last two columns refer to equation given below.*

which together with charge neutrality

$$n_+ + n_{MRI} = n_e \tag{10}$$

leads to

$$n_{MRI} = \frac{k_{AAA} n_I^2 n_e}{k_{AAA} n_I^2 + k_{DAI} n_i + k_{DEI} n_e + k_{DR} n_e} \tag{11}$$

The rate coefficient of the association reaction for helium is given by [9]

$$k_{AAA}^{He} = 4.3 \times 10^{-42} T_h^{-0.6} \quad [m^6 s^{-1}] \tag{12}$$

For argon we assume the same temperature dependence, which results in [2,10]

$$k_{AAA}^{Ar} = 6.1 \times 10^{-42} T_h^{-0.6} \quad [m^6 s^{-1}] \tag{13}$$

For the dissociative recombination of He_2^+ we take the rate as proposed by Collins and Lee [11]:

$$k_{DR}^{He} = 5.0 \times 10^{-15} \hat{T}_e^{-0.5} \quad [m^3 s^{-1}] \tag{14}$$

and the DR rate for argon the expressions as given by Mehr and Biondi [12] is used:

$$k_{DR}^{Ar} = 7.35 \times 10^{-14} \hat{T}_e^{-0.67} \quad [m^3 s^{-1}] \tag{15}$$

Note that the symbol ^ is used to denote that a quantity is expressed in eV, whereas the symbols without ^ are given in SI units.

In contrast to the large number of papers on dissociative recombination (DR), the dissociation by electron impact (DEI) of MRI is hardly studied in literature [13,14,15]. The cross sections for excitation to a predissociation state were calculated by Marchenko [13]. The rate is obtained after averaging over a Maxwellian EEDF. For helium the results are given by

$$k_{DEI}^{He,300K}\left(\hat{T}_e\right) = 1.06 \times 10^{-13} \frac{1}{\hat{T}_e^3} exp\left(-\frac{9.97}{\hat{T}_e}\right) \quad [m^3 s^{-1}] \tag{16}$$

which is valid in the electron temperature range $1.6 < \hat{T}_e < 3.5$ eV. The relatively high energy in the exponent of this rate (9.97 eV) is due to the high excitation energy to the

predissociation state [13]. For argon this energy is much lower and thus the corresponding reaction faster. Averaging the cross sections as given by Marchenko [13] results in:

$$k_{DEI}^{Ar,300K}\left(\hat{T}_e\right) = 1.11\times10^{-12}\, exp\left(-\frac{2.94}{\hat{T}_e}\right) \quad [m^3s^{-1}] \tag{17}$$

for the range $0.25 < \hat{T}_e < 2.2$ eV. The fits reproduce the calculated rates in the corresponding temperature intervals within 10%. The superscript 300K refers to the fact that the cross sections are determined for a vibrational temperature of T_{vib} = 300 K (room temperature) [13]. It is expected that for a given electron temperature the dissociation rate increases with the vibrational (or gas) temperature. This is related to the fact that for higher vibrationally excited states the energy gap ΔE between the classical outer turning point and the anti-bonding curve becomes smaller [13], as shown in Figure 2. Moreover, this energy gap is also decreased by the typical rotational energy ($\approx k_B T_h$). In total the typical dissociation energy is reduced by approximately $3k_BT_h$, see Figure 2, so that we assume that the influence of the gas temperature on the DEI rate coefficient can be described in first order approximation by replacing the exponents of equations (16) and (17) by

$$exp\left(-\frac{\Delta\hat{E}}{\hat{T}_e}\right) \longrightarrow exp\left[-\frac{\Delta\hat{E}-3\left(\hat{T}_h-0.026\right)}{\hat{T}_e}\right] \tag{18}$$

in which the constant 0.026 (eV) stems from the typical energy associated with 300 K.
For helium it is found that the DEI rate is at least ten times smaller than that of the dissociative recombination (for the conditions under study: $\hat{T}_e < 2.5$ eV and $T_h \leq 3000$ K) due to the relatively high threshold energy. However, for argon both rates are of about the same order of magnitude, cf. Figure 3. Experiments have shown that DEI and DR of Ar_2^+ [14] (and of Xe_2^+ [15]) have the same rate at $\hat{T}_e \approx 1$ eV and T_h = 300 K, which is more or less in accordance with the expressions given above.
The rate coefficient of the dissociation by atom impact (DAI) can be calculated by applying the principle of detailed balancing on DAI (5) and its inverse reaction, AAA (2):

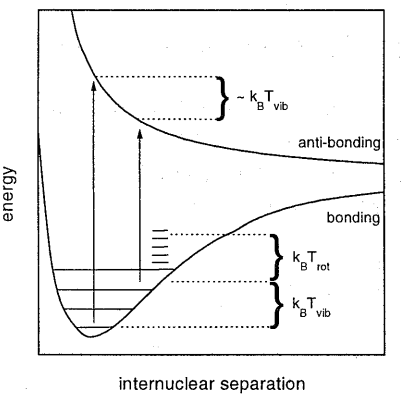

***Figure 2**: The dissociation of a rare gas molecular ion by electron impact is due to excitation to an anti-bonding state. For the vibrationally excited states the threshold energy is smaller, so that these states can dissociate more easily. This is not only due to a larger excitation energy (the sum of vibrational and rotational excitation), but also due to the fact that the classical right turning point is situated at larger inter-nuclear distance, where the corresponding anti-bonding potential is lower.*

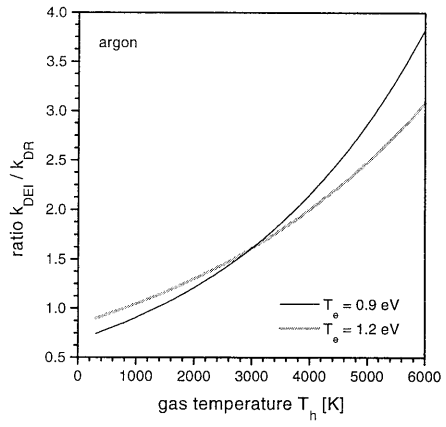

***Figure 3**: The ratio of the rates for dissociation by electron impact (DEI) and dissociative recombination (DR) of the argon molecular ion as a function of the gas temperature for two different electron temperatures. For helium this ratio is much more constant and around 0.02 (for $\hat{T}_e$ = 1.7 eV).*

$$k_{DAI} n_1 n_{MRI}^{eq} = k_{AAA} n_1^2 n_+ \tag{19}$$

in which n_{MRI}^{eq} denotes the density of molecular rare gas ions in the case that their formation by association (2) is in equilibrium with their destruction by atom impact (5). This density can be obtained from a modified Saha equation:

$$n_{MRI}^{eq} = n_+ n_1 \frac{Q_{MRI}}{g_1 g_+} \left(\frac{h}{\sqrt{2\pi\mu k_B T_h}} \right)^3 exp\left(\frac{E_{diss}}{k_B T_h} \right) \tag{20}$$

Here μ represents the reduced mass of the rare gas atom-ion system. The dissociation energy of the molecular ions E_{diss} equals around 2.4 eV for helium [16,17,18,19] and 1.3 eV for argon [16,20,21,22]. The quotient of the partition function and the statistical weights can be written as [23]

$$\frac{Q_{MRI}}{g_1 g_+} = Q_{rot} Q_{vib} \tag{21}$$

The partition function of the vibrational states equals

$$Q_{vib} = \sum_{v<v_{max}} exp\left(-v \frac{\hat{E}_{vib}}{\hat{T}_h} \right) \quad \text{with} \quad v_{max} = \frac{E_{diss}}{E_{vib}} \tag{22}$$

in which the vibrational energy spacing $\hat{E}_{vib}$ equals 0.211 eV for helium [19] and 0.03 eV for argon [22].
The partition function of the rotational states can be approximated by [23]

$$Q_{rot} = \sum_J (2J+1) exp\left[-J(J+1) \frac{\hat{E}_{rot}}{\hat{T}_h} \right] \approx \frac{\hat{T}_h}{\hat{E}_{rot}} \tag{23}$$

The rotational energy constant $\hat{E}_{rot}$ equals 3.3×10^{-5} eV for argon [22]. For helium it is calculated using

$$E_{rot} = \frac{\hbar^2}{2\mu r_b^2} \tag{24}$$

in which r_b is the equilibrium internuclear spacing. Substituting r_b = 1.08 Å [19] results in $\hat{E}_{rot}$ = 8.94×10^{-4} eV.

With equations (20) to (23) the equilibrium density of the molecular rare gas ion can be calculated and after substitution of this value into (19), the rate coefficient for dissociation by atom impact is obtained. The results can be reproduced using the following fits

$$k_{DAI}^{He} = \frac{2.66 \times 10^{-15}}{\hat{T}_h^{0.67}} exp\left(-\frac{2.421}{\hat{T}_h}\right) \quad [m^3 s^{-1}] \tag{25}$$

for the gas temperature range $0.02 \leq \hat{T}_h \leq 0.3$ eV and

$$k_{DAI}^{Ar} = \frac{5.22 \times 10^{-16}}{\hat{T}_h} exp\left(-\frac{1.304}{\hat{T}_h}\right) \quad [m^3 s^{-1}] \tag{26}$$

for $0.03 \leq \hat{T}_h \leq 0.6$ eV. Both fits are better than 10% in their temperature intervals.

Now all the rates are known (cf. Table 1), the densities of molecular rare gas ions can be calculated using equation (11). The molecular fractions of the total number of ions in helium and argon are depicted in Figure 4, each for one typical electron temperature [1]. For low electron densities the dissociative recombination and the destruction by electron impact are not important so that the balance of association and dissociation by atom impact

$$Rg^+ + Rg + Rg \xleftrightarrow{AAA/DAI} Rg_2^+ + Rg \tag{27}$$

is in equilibrium and the density of molecular ions is given by equation (20). This is the grey line in Figure 4. In case the electron induced destruction processes are important the density of

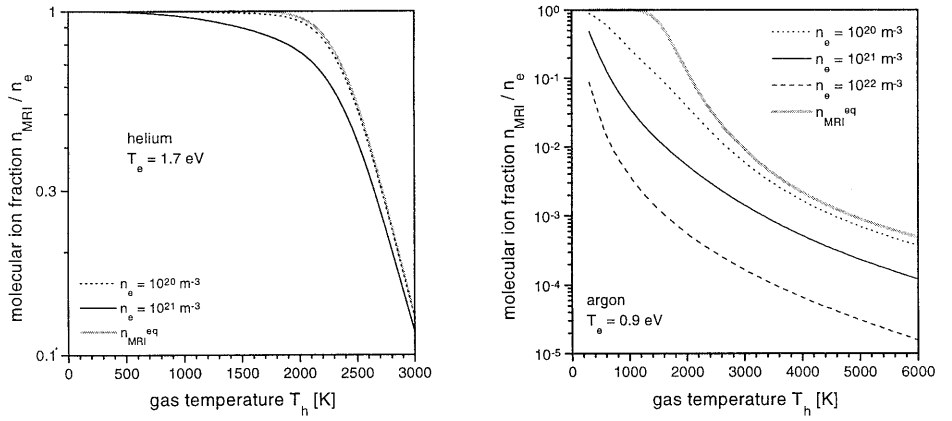

***Figure 4**: The relative amount of molecular rare gas ions as a function of the gas temperature at atmospheric pressure (1.0×10^5 Pa) and for typical values of the electron temperature (1.7 eV for helium and 0.9 eV for argon [1]). The fraction in case the balance of association and dissociation via atom impact is in equilibrium (i.e. the electron induced destruction can be neglected) is depicted as the grey line. Note the difference in the range of the Y-axis.*

MRI is lower than the equilibrium density.
It can be seen from Figure 4 that the number of helium molecular ions exceeds that of atomic ions if the gas temperature is lower than 2500 K. This is a rather sharp boundary on which the electron density has not a large influence. For argon this boundary is situated between 300 and 1600 K, depending on the value of n_e. The reason for the fact that the fraction of helium molecular ions is higher than that of argon can mainly be traced back to the difference in dissociation energy (2.4 versus 1.3 eV), which is only partially compensated by the larger partition function of Ar_2^+.
Experimental evidence for the presence of Ar_2^+ in atmospheric plasmas can be found in the fields of laser technology [24] and of inductively coupled plasma mass spectrometry (ICP-MS), where this molecular ion interferes with the detection of elements like bromine and selenium [25].

3. Consequences for the electron particle balance

The electron temperature in an atomic size-stabilised plasma can be obtained from the particle balance of the electrons. In the previous chapter it is assumed that diffusion is the dominant loss process of the charged particles, so that the particle balance of the free electrons reads

$$n_e n_1 S_{CRM} = -\nabla\left(D_a \nabla n_e\right) \tag{28}$$

The left hand side represents the production due to ionisation and the right hand side the losses due to diffusion. Expressions for the ionisation S_{CRM} and ambipolar diffusion coefficients D_a are given in [1]. Using equation (28), the electron temperature can be found easily since S_{CRM} is strongly and D_a only weakly dependent on T_e.
However, as stated in the introduction, the presence of molecular ions influences the particle balance, since the molecules offer an extra loss channel of charged particles. Using the results of section 2 the effective loss frequency due to the MRI channel can be calculated

$$\nu_{MRI} = n_{MRI} k_{DR} \chi \tag{29}$$

in which the branching ratio χ is used. It accounts for the fact that only those dissociative recombination events have to be included which yield two atoms in the ground state (possibly via a radiative 4s state). This is because in case one excited atom remains, the chance on re-ionisation is large, in which has no effect on the level of the particle balance. The two atoms in the ground state can be produced either directly in the dissociative reaction or via radiative decay of a fast excited atom created in the DR reaction. The escape of the resonant photon, which is emitted in the latter process, is large because of the relative high kinetic energy of the atoms produced by dissociative recombination.
In order to determine the influence of dissociative recombination on the particle balance, the branching ratio χ has to be known. Unfortunately, it appeared not to be possible to measure it up to now, see section 1. Therefore, we assume that it equals 5% for both argon and helium[c].
The results for atmospheric plasmas are presented in Figure 5. It can be seen that the effective loss frequency of the MRI channel increases with increasing electron density. This is due to the fact that at relatively low electron densities the AAA/DAI balance is in or close to

[c] Note that no evidence has been reported that also the dissociative recombination of He_2^+ can produce directly two atoms in the ground state.

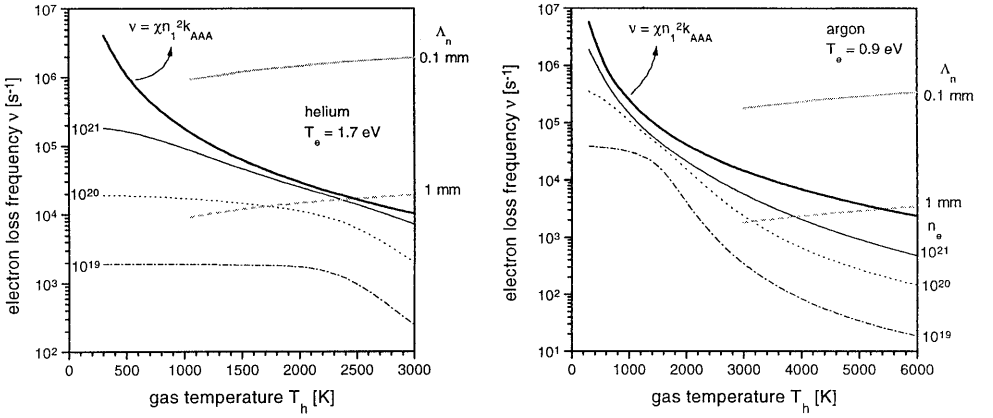

***Figure 5**: The loss frequency of the free electrons due to dissociative recombination of the molecular ions for various electron densities (black lines). It is assumed that 5% of the DR events yields two atoms in the ground state and in the other 95% one of the atoms is excited and will be re-ionised. For comparison also the conventional loss frequency calculated from the atom assisted association (AAA) reaction (2) [2,3,4] is depicted (thick black line), as well as the loss frequency due to diffusion of atomic ions for two different gradient lengths of the electron density profile Λ_n = 0.1 and 1 mm (grey lines). Especially for large cold atmospheric plasmas the losses due to MRI are dominant.*

equilibrium and the molecular ion density scales with n_e if T_e and T_h are kept constant (see also equation (11) and Figure 4). This holds for all the conditions depicted in Figure 5. The volume loss frequency of charged particles, as obtained in this paper, is smaller than the frequency related to the formation of the molecular ions (the thick black line), which is normally taken as the limiting process [2,3,4].

In Figure 5 also the diffusion loss frequency is depicted using the expressions given in [1]. For small plasmas with relatively high gas temperatures the losses due to diffusion are larger than those due to DR, so that the impact of the MRI channel on the particle balance is limited. For relatively large plasmas ($\Lambda_n \approx 1$ mm) with high electron density and low gas temperature, the losses due to DR have to be included in the electron particle balance:

$$n_e n_1 S_{CRM} = -\nabla\left(D_a \nabla n_e\right) + n_e n_{MRI} k_{DR} \chi \qquad (30)$$

Apart from the extra term in the particle balance, the presence of MRI also influences the diffusion, since the diffusion coefficient of the molecular ions is higher than that of the atomic ions[d]. This difference is around 50% for helium and 20% for argon [16,26,27]. In particular for atmospheric helium plasmas the molecular ion is the most abundant in a wide range of conditions (as can be seen in Figure 4). However, this will only affect the electron temperature

[d] Molecular ions diffuse easier in spite of the larger mass, since the effect of resonant charge transfer with the neutral atoms is not present. For atomic ions this is the dominant process which determines the diffusion coefficient [27].

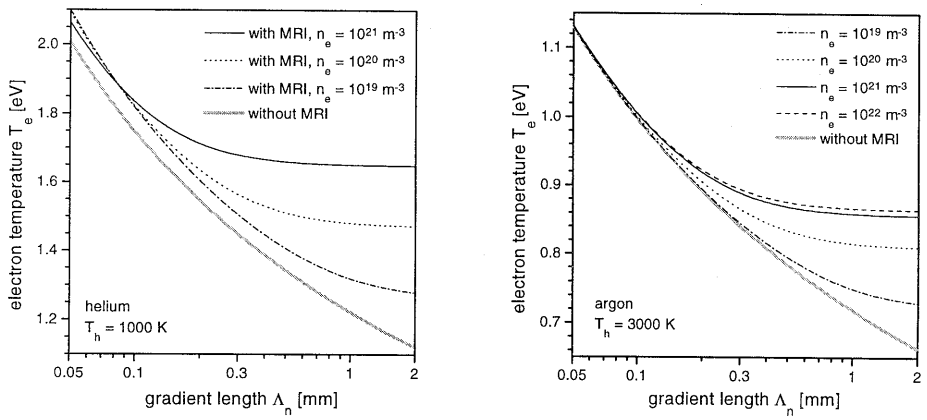

***Figure 6**: The electron temperature as function of the gradient length of the electron density profile Λ_n. For small gradient lengths the diffusion losses dominate, so that the higher diffusion coefficient of He_2^+ leads to a slightly higher T_e.*

slightly, since T_e is mainly determined by the energy gap between the ground and the first excited state [1].

Solving the electron particle balance (30) yields the electron temperature necessary to sustain the plasma as function of the characteristic size of the plasma and with the electron density and the gas temperature as parameters, see Figure 6. This is in analogy with what was done in the previous chapter [1]. It can be seen that indeed only relatively large scale plasmas are affected seriously at the chosen gas temperatures. However, especially for these larger plasmas it can be argued that the difference between T_e and T_h vanishes, so that the example given in Figure 6, where the gas temperature is taken constant and substantially lower than the electron temperature, is not realistic. The choice of more appropriate T_h values for the various operational parameters is beyond the scope of this study.

It should be noted that in this paper only the role of MRI *in* the plasma is discussed. At the edges of the plasma molecular rare gas ions are expected to provide a very efficient recombination channel, since there the gas temperature is relatively low and due to the low electron density re-ionisation is less likely. In this case the branching ratio χ will also be a function of the electron density and temperature.

4. Consequences for the energy balance

In [1] the electron density was obtained by solving the electron energy balance. Including the effects of the molecular rare gas ions this balance reads:

$$\varepsilon = n_e n_1 S_{CRM} I_1 + \varepsilon_{el} + n_e n_{MRI} k_{DR} (1-\chi) E_{re-ion} + n_e n_{MRI} k_{DEI} E_{DEI} \qquad (31)$$

in which ε and ε_{el} are the dissipated power and the power lost in elastic collisions, both per unit of volume [1]. The first term at the right hand side stems from the particle balance and is discussed in the previous section, cf. equation (30). The third term represents power needed for the re-ionisation of the excited atoms which are produced in (1-χ) of the DR reactions. The

		helium [eV]	argon [eV]
ionisation	I_1	24.59	15.76
re-ionisation	$E_{re\text{-}ion}$	4.5	4.0
dissociation	E_{DEI}	10	2.9

Table 2: The energy lost by the electrons in the different inelastic processes.

power lost in the dissociation of the molecular ions by electron impact is given by the last term. The energy needed for each reaction is listed in Table 2.
Using the rates given in [1] and in this paper the electron energy balance (31) can be solved, which yields the electron density as a function of the characteristic size and the power density. The results are presented in Figure 7. For the purely atomic helium plasmas the energy losses in elastic electron-atom collisions were found to be dominant in a wide range of conditions [1]. Due to the relatively low rates for DR and DEI (see section 2) this remains the case, so that the electron density can be approximated by [1]

$$n_e \approx \frac{k_B T_h}{p} \frac{M}{3m_e} \frac{\varepsilon}{\langle \sigma^m_{ea} v_e \rangle k_B (T_e - T_h)} \tag{32}$$

In the previous section it is shown that the presence of MRI leads to (the necessity of) a higher electron temperature. Due to this the rate coefficient for elastic electron-atom collisions $\langle \sigma^m_{ea} v_e \rangle$ increases, so that the electron density is slightly lower at the same power density, cf. Figure 7.

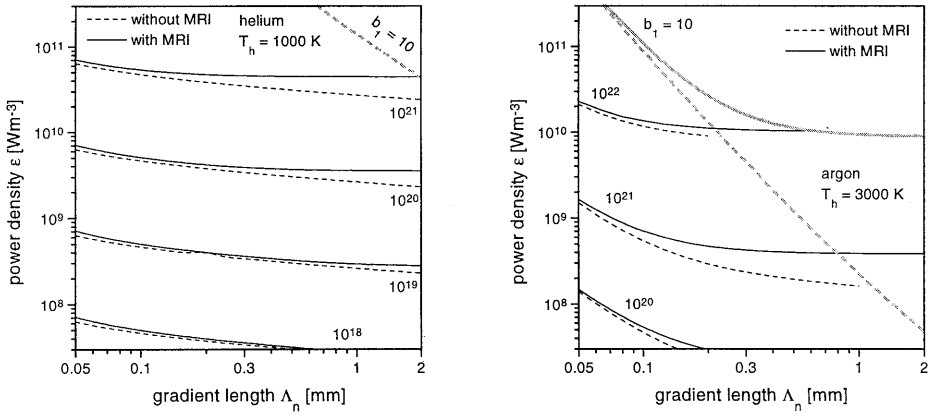

***Figure 7**: The iso-contour lines of the electron density (in m^{-3}) in helium and argon plasmas, including and excluding the effects of molecular rare gas ions. Besides the power lost in dissociation of the MRI and re-ionisation of the excited state after DR, the easier diffusion in case of MRI is taken into account. The grey lines denote the boundary above which also the three particle recombination (1) becomes important [1]. For helium this boundary lies outside the depicted ranges in case the effects of MRI are included.*

For argon the rates of DR and DEI are higher, so that these processes become important. These extra losses of energy demand a higher power density in order to sustain the discharge at the same electron density.

5. Consequences for the lower boundary of pLSE

In [1] the position of the pLSE boundary was determined by comparing the efflux of charged particles out of the plasma with the effective ionisation flow through the atomic system. In contrast to other work, this approach has the advantage that the pLSE boundary can be determined directly from the operational conditions such as pressure, power density and characteristic size.

However, the presence of molecular ions influences the electron temperature and density, cf. Figure 6 and Figure 7, which was not taken into account in our previous study [1]. Moreover, the re-ionisation of the excited atoms produced in the DR reactions, leads to a higher ionisation flow through the top of the atomic system. This increased flow has a strong influence on the lower boundary of pLSE, especially in relatively large plasmas with low gas temperatures. Figure 8 presents the new results. Because in large atomic plasmas the ionisation flow is small, due to the low diffusion losses [1] the extra flow due to DR has a much stronger influence than in small plasmas where the ionisation flow through the atomic system is already high. It should be noted that the number of DR events and thus the extra re-ionisation flow depend strongly on the gas temperature, so that for relatively large plasmas the pLSE boundary also depends on T_h.

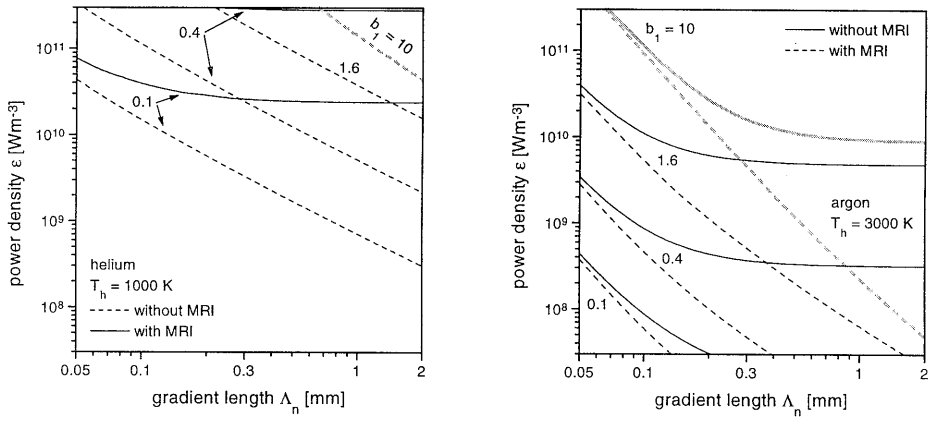

Figure 8: The influence of the molecular rare gas ions on the lower boundary of pLSE (in eV). In the calculations of the solid lines the extra flow through the upper part of the ASDF is included, as well as the more efficient diffusion of the molecular ions. The dashed lines are the calculations of [1]. The grey lines denote the boundary above which also the three particle recombination (1) becomes important [1]. In case the effects of MRI are included for helium this boundary and the 1.6 eV pLSE boundary lie outside the studied ranges.

6. Conclusions

- For all helium and argon plasmas under study the effective loss frequency of the molecular rare gas ion channel is *not* limited by the formation of these ions, but by the dissociative recombination process. Therefore, the effective loss frequency is proportional to the concentration of molecular ions (which increases with the electron density) in a wide range of conditions.
- For $T_h < 2500$ K the molecular ion He_2^+ is the dominant ion in atmospheric helium plasmas. Since these ions diffuse easier than He^+, the electron temperature is slightly higher than expected from a purely atomic approach.
- In relatively large plasmas (i.e. low diffusion losses) with a high electron density the dissociative recombination can be the dominant electron loss process, depending on the electron density, gas temperature and branching ratio of direct and indirect recombination to two atoms in the ground state (which is assumed here to be equal to 5%). A high n_e and a low T_h both lead to higher concentrations of molecular ions and thus to more recombination events. The branching ratio is important, since an excited atom, which can remain after the dissociative recombination, is very likely to be ionised again, so that effectively no charged particles are lost.
- The presence of MRI pushes the lower boundary of pLSE towards lower ionisation potentials (i.e. higher levels). This is mainly caused by the extra flow through the atomic system as a result of the re-ionisation of the excited atoms which remain after most of the dissociative recombination events. The magnitude of this flow and thus the lower boundary of pLSE depend on the gas temperature.
- Here only the role of MRI in the plasma is studied. In the cooler outer regions of the plasma DR probably plays an important role. Moreover, due to the low electron density it is more likely that a dissociative recombination event results in two atoms in the ground state.

Appendix: The rates of other molecular ion formation reactions

Besides Atom Assisted Association (AAA) molecular rare gas ions can also be formed in association reactions with an ion or an electron as third particle. We will refer to the latter two reactions as Ion Assisted and Electron Assisted Association (IAA and EAA, respectively). A third alternative way is the inverse process of DR, which is the Associative Ionisation (AI) or the Hornbeck-Molnar reaction [28] and is given by equation (8). In the discussion above it is assumed that only AAA is important and that the other reactions can be neglected. These will be discussed in this appendix.

Ion Assisted Association (IAA)

According to Beulens [3] the ratio of ion assisted and atom assisted association equals that of the ion-ion and the ion-atom collision rate coefficients (k_{ii} and k_{il}, respectively):

$$\frac{k_{IAA}}{k_{AAA}} = \frac{k_{ii}}{k_{il}} \tag{33}$$

For $n_e = 10^{22}$ m^{-3}, $n_l = 10^{24}$ m^{-3} and $\hat{T}_h = 0.3$ eV Beulens stated that k_{IAA} equals 30% of k_{AAA}. In the plasmas under study the ion density is normally lower (see Figure 7) and the atom density higher, so that the ion assisted association can be neglected.

Electron Assisted Association (EAA)

The rate coefficient for EAA can be obtained via a similar way as was done in section 2 for the rate coefficient of DAI. In case the balance of EAA and DEI

$$Rg^+ + Rg + e \xleftrightarrow{EAA/DEI} Rg_2^+ + e \tag{34}$$

is in equilibrium, the number of processes to the right equals that to the left

$$n_+ n_1 n_e k_{EAA} = n_{MRI}^{EAA/DEI} n_e k_{DEI} \tag{35}$$

in which $n_{MRI}^{EAA/DEI}$ represents the density of the molecular ions in case the EAA/DEI balance (34) is in equilibrium. We assume that this density is given by

$$n_{MRI}^{DEI/EAA} = n_+ n_1 Q_{rot}(T_h) Q_{vib}(T_e) \left(\frac{h}{\sqrt{2\pi\mu k_B T_h}} \right)^3 exp\left(\frac{E_{diss}}{k_B T_e} \right) \tag{36}$$

Substitution of (36), the expressions for the partition functions (22) and (23) and the rate coefficients for DEI, equations (16) to (18), in (35) yields the rate coefficients for EAA, see Figure 9.

The electron assisted association can be neglected in case the following inequality holds for the ionisation degree

$$\alpha = \frac{n_e}{n_1} << \frac{k_{AAA}}{k_{EAA}} = \alpha_{crit} \tag{37}$$

The typical value for k_{AAA} is between 10^{-44} and 10^{-43} m^6s^{-1} for the gas temperatures under study, cf. equations (12) and (13). For helium k_{EAA} is lower than 3×10^{-44} m^6s^{-1}, so that EAA is not significant ($\alpha_{crit}^{He} > 3$). For argon the rate coefficient for electron assisted association is much larger, so that $\alpha_{crit}^{Ar} \approx 10^{-2}$ for electron temperatures around 1 eV, which corresponds to an electron density of 2.4×10^{22} m^{-3} (for T_h = 3000 K). Since this density is only reached at high power densities (see Figure 7), this process is neglected.

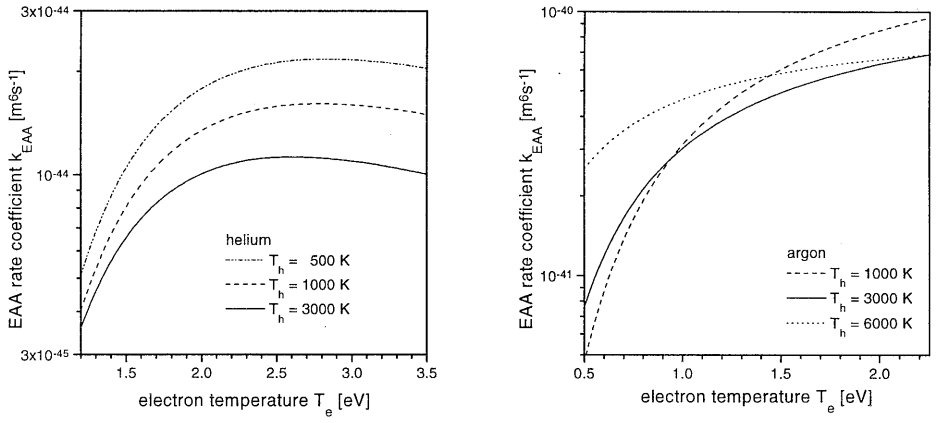

***Figure 9**: The rate coefficients for the formation of molecular ions via electron assisted association (EAA).*

Associative ionisation (AI)
The ratio of the production of MRI due to the AI and AAA reactions is given by

$$\frac{k_{AI}}{k_{AAA}}\frac{n_p n_1}{n_+ n_i^2} = \frac{k_{AI}}{k_{AAA}}\left(1+\beta I_p^3\right)\frac{n_e}{n_1}\frac{g_p}{2g_+}\left(\frac{h}{\sqrt{2\pi m_e k_B T_e}}\right)^3 exp\left(\frac{I_p}{k_B T_e}\right) \tag{38}$$

where the relation

$$\frac{n_p}{g_p} = \left(1+\beta I_p^3\right)\frac{n_e n_+}{2g_+}\left(\frac{h}{\sqrt{2\pi m_e k_B T_e}}\right)^3 exp\left(\frac{I_p}{k_B T_e}\right) \tag{39}$$

is used, which is valid for highly excited states [1,29,30]. The so-called ESB parameter β can be obtained by comparing the losses of charged particles due to diffusion (and MRI) with the ionisation flow through the atomic system [1].
For the process to occur at thermal energies the ionisation potential of the excited atom in the associative ionisation reaction (8) should be around or smaller than the dissociation energy of the molecular ion. Substitution of a typical rate constant for AI $k_{AI} \approx 10^{-16}$ m^3s^{-1} [31,32] and $I_p \approx E_{diss}$ in equation (38) results in

$$\frac{k_{AI}}{k_{AAA}}\frac{n_p}{n_+ n_1} \approx 2\times 10^1 \beta \frac{n_e}{n_1} \tag{40}$$

for typical conditions in the helium and argon plasmas under study ($\hat{T}_e^{He} \approx 1.7$ eV and $\hat{T}_e^{Ar} \approx$ 0.9 eV). This ratio is larger for plasmas which deviate stronger from equilibrium [1]. Especially for helium plasmas the associative ionisation is found to be important for a relatively large range of conditions, but even if this reaction is omitted it is found that He_2^+ is the dominant ion in these plasmas (cf. Figure 4). Therefore, this extra formation reaction will not change drastically the results discussed above.

References

1. J. Jonkers, J.A.M. van der Mullen and D.C. Schram, *"On the differences between atmospheric, strongly ionising helium and argon plasmas"*, submitted for publication to Phys. Rev. E.
2. Y.P. Raizer, *"Gas discharge physics"*, Springer-Verlag, Berlin (1991).
3. J.J. Beulens, *"Surface modification using a cascade arc plasma source"*, Ph.D. Thesis Eindhoven University of Technology (1992).
4. D.C. Schram, J.A.M. van der Mullen, J.M. de Regt, D.A. Benoy, F.H.A.G. Fey, F.P.J. de Groote and J. Jonkers, J. of Anal. At. Spectrom. **11** 623 (1996).
5. L. Frommhold and M.A. Biondi, Phys. Rev. **185** 244 (1969).
6. Y.J. Shiu and M.A. Biondi, Phys. Rev. A **17** 868 (1978).
7. A. Barrios, J.W. Sheldon, K.A. Hardy and J.R. Peterson, Phys. Rev. Lett. **69** 1348 (1992).
8. G.B. Ramos, M. Schlamkowitz, J. Sheldon, K.A. Hardy and J.R. Peterson, Phys. Rev. A **51** 2945 (1995) and ibid. **52** 4556 (1995).
9. H. Böhringer, W. Glebe and F. Arnold, J. Phys. B: At. Mol. Phys. **16** 2619 (1983).
10. J.B. Hasted, *"Physics of atomic collisions"*, Butterworth & Co, London (1972).
11. C.B. Collins and F.W. Lee, J. Chem. Phys. **68** 1391 (1978).

12. F.J. Mehr and M.A. Biondi, Phys. Rev. **176** 322 (1968).
13. V.S. Marchenko, Sov. Phys. JETP **58** 292 (1983).
14. V.A. Ivanov, Opt. Spectrosc. **73** 374 (1992).
15. V.A. Ivanov and A.S. Prikhodjko, J. Phys. B: At. Mol. Opt. Phys. **24** L459 (1991).
16. E.W. McDaniel, *"Collision phenomena in ionized gases"*, John Wiley & Sons (1964).
17. B.K. Gupta and F.A. Matsen, J. Chem. Phys. **47** 4860 (1967).
18. R.S. Mulliken, J. Chem. Phys. **52** 5170 (1970).
19. K.P. Huber and G. Herzberg, *"Molecular spectra and molecular structure: IV. constants of diatomic molecules"*, Van Nostrand Reinhold Company, New York (1979).
20. D.C. Lorents, R.E. Olson and G.M. Conlin, Chem. Phys. Lett. **20** 589 (1973).
21. T.L. Gilbert and A.C. Wahl, J. Chem. Phys. **55** 5247 (1971).
22. J.T. Moseley, R.P. Saxon, B.A. Huber, P.C. Cosby, R. Abouaf and M. Tadjeddine, J. Chem. Phys. **67** 1659 (1977).
23. G. Herzberg, *"Molecular spectra and molecular structure: I. Spectra of diatomic molecules"*, Van Nostrand Reinhold Company, New York (1950).
24. J.W Shon and M.J. Kushner, J. Appl. Phys. **75** 1883 (1994).
25. G. Horlick and Y. Shao, Chapter 12 in *"Inductively Coupled Plasmas in Analytical Atomic Spectrometry"* by A. Montasar and D.W. Golightly (editors), VCH Publishers, New York (1992).
26. H.J. Oskam and V.R. Mittelstadt, Phys. Rev. **132** 1435 (1963).
27. A. Dalgarno, Phil. Trans. Roy. Soc. (London) A **250** 426 (1958).
28. J.A. Hornbeck and J.P. Molnar, Phys. Rev. **84** 621 (1951).
29. T. Fujimoto, J. Phys. Soc. Jap. **47** 273 (1979).
30. J.A.M. van der Mullen, Phys. Rep. **191** 109 (1990).
31. L.L. Alvest, G. Gousset and C.M. Ferreira, J. Phys. D: Appl. Phys. **25** 1713 (1992).
32. M.A. Lieberman and A.J. Lichtenberg, *"Principles of plasma discharges and materials processing"*, John Wiley & Sons (1994).

8

The influence of nitrogen entrainment on argon plasmas created by the "Torche à Injection Axiale"

J. Jonkers, A. Hartgers, L.J.M. Selen, J.A.M. van der Mullen and D.C. Schram

When a plasma is sustained in the open air, nitrogen will diffuse into the plasma. Especially for plasmas sustained by the "Torche à Injection Axiale" this appears to be the case, since this turbulent jet draws gases from the surroundings. In the argon plasma the entrained nitrogen is probably converted into N_2^+ (via charge transfer with argon ions), which is consequently destroyed by dissociative recombination (DR). This mechanism affects the plasma in two ways: 1) it offers an important loss channel for the free electrons and 2) the gas is heated by the kinetic energy of the nitrogen atoms produced in the DR reaction.

1. Introduction

For a wide variety of small scale plasmas it is possible to relate the fundamental plasma properties to the operating conditions, such as: size, power density, pressure and plasma gas, as was shown in chapter 6 [1]. The electron temperature T_e and density n_e can be obtained from the electron particle and energy balance, respectively. The basic assumption of this size-stabilised plasma approach is that diffusion is the only dominant loss process of the electrons and that three particle recombination is only a minor loss channel. In chapter 7 [2] it was shown that also the formation of molecular ions and their destruction via dissociative recombination has a limited influence on these types of plasmas. However, in case a plasma is sustained in the open air, the entrainment of nitrogen (and oxygen) can play an important role. Especially for small plasmas this may be the case, since small dimensions imply large gradients in the concentrations of species and therefore generate a high inward diffusion.

In this paper the entrainment of nitrogen in a relatively small argon plasma is investigated. The plasma under study is created by the "Torche à Injection Axiale", or shortly TIA. This microwave driven plasma torch was developed by the group of Moisan in 1994 [3]. The relatively small dimensions of the plasma flame (1 mm in radial and 15 mm in axial direction) make this plasma well suitable for a study on the influence of steep gradients on the plasma [4].

The most probable way in which the presence of nitrogen molecules can affect an argon plasma is via charge transfer (CT)

$$Ar^+ + N_2 \xrightarrow{CT} Ar + N_2^+ \tag{1}$$

followed by dissociative recombination (DR)

$$N_2^+ + e \xrightarrow{DR} N + N \tag{2}$$

The resulting nitrogen atoms are in one of the three "ground" states and can not be easily re-ionised. As can be seen, the combination of these two reactions offers a loss channel of the ions and the free electrons. Moreover, the two nitrogen atoms which are produced in the DR reaction have a relatively high kinetic energy, so that this reaction can become a significant heat source. The influence of nitrogen entrainment on the electron particle and the heavy particle energy balances is discussed (in sections 5 and 6) after the presentation of spatially resolved measurements of the gas temperatures and of the nitrogen densities, which is given in sections 3 and 4. These results are obtained using Rayleigh and Raman scattering with a focused laser beam. But first we start with a short description of the TIA.

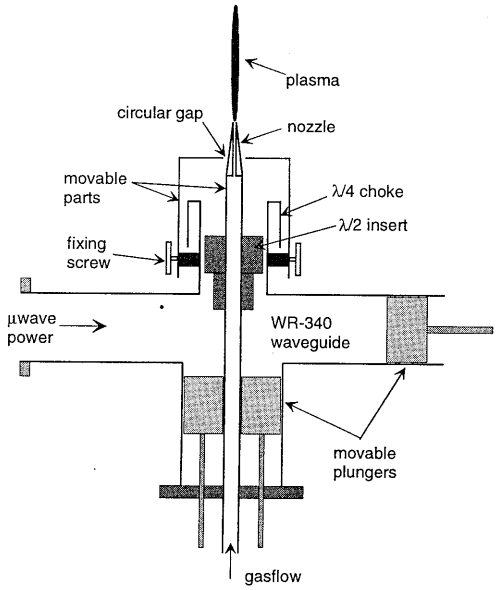

Figure 1: A schematic of the TIA (not on scale) [3,4].

2. The "Torche à Injection Axiale"

The TIA is extensively discussed in ref. [3], so we will repeat here only its most important features which are of relevance for this specific study. The torch is depicted in Figure 1. The main part is a coaxial waveguide which is mounted on a standard WR-340 rectangular waveguide. At the top of the inner conductor of the coaxial part (the nozzle) a plasma is created. The plasma gas is flowing through the inner conductor, which explains the name of this torch: Torche à Injection Axiale, i.e. torch with axial (gas) injection. In this paper argon plasmas are studied which are sustained by 1 kW microwave power coupled into an argon gas flow of 3.0 slm. The diameter of the gas outlet of the nozzle equals 1.75 mm.

3. Rayleigh scattering

Rayleigh scattering is the scattering of photons by bound electrons. One of the advantages of this technique is the possibility of determining the gas temperature inside the plasma as well as in its surroundings, so that Rayleigh scattering is a good technique for the study of the interaction between plasma and environment.

In principle the gas temperature can be obtained from the Doppler broadening of the Rayleigh signal. However, the wavelength resolution of our setup is not good enough to obtain the gas temperature, so that a different procedure is necessary. This procedure was also used by, for instance, Huang *et al.* [5,6], Lapierre *et al.* [7] and de Regt *et al.* [8,9].

The intensity of the Rayleigh signal is proportional to the density of the heavy particles n_h and is thus related to the gas temperature T_h via Dalton's law:

$$p_h = n_h k_B T_h \tag{3}$$

Here p_h is the partial pressure of the heavy particles which is taken equal to 1 atmosphere, since the partial pressure of the electrons can be neglected (see below). The calibration can simply be done by switching off the plasma and performing Rayleigh scattering measurements

in free flowing argon gas. In this case T_h is known (room temperature), so that from the decrease of the Rayleigh signal when the plasma is switched on, the gas temperature in the plasma can be obtained [5,6,7,8,9].

3.1 Experimental

For the measurements basically the same experimental setup is used, as described by de Regt *et al.* [10] and in chapter 3 [11]. It consists of a frequency doubled Nd:YAG laser with a maximum output of 0.45 J per pulse (at 532 nm) and a repetition frequency of 10 Hz. By means of a lens the laser beam is focused at various positions in the plasma to obtain a good spatial resolution [4]. The detection volume is imaged by two lenses onto the entrance slit of a monochromator. During the Rayleigh scattering measurements a diaphragm of 1 cm diameter is placed between the lenses, to reduce the stray light (see below). The detection unit is an intensified Optical Multichannel Analyser (OMA). The intensifier is synchronised with the laser to suppress the light emitted by the plasma. To limit the inaccuracy due to shot-to-shot variations in the laser energy the average signal of 10 measurements of 15 laser shots each is taken. The energy per shot is approximately 0.26 J.

A more serious problem is the scatter of the laser on the nozzle of the TIA and on the several optical components. Since this so-called stray light has the same wavelength as the Rayleigh scattering signal it can not be distinguished by the monochromator. In order to determine the stray light level, measurements are performed on two different gases at room temperature. The Rayleigh signal has not the same intensity for each gas, since the Rayleigh cross sections are different [6,7]. This means that the intensity of the stray light can be obtained by extrapolating the Rayleigh signal to zero cross section, cf. Figure 2. It appears that the stray light at 3 mm Above the Nozzle (AN) is only 2.0% of the Rayleigh signal on argon at room temperature, whereas more downstream it decreases to around 1.2%. However, at higher temperatures the density and thus the Rayleigh scattering signal is lower, so that the relative amount of the stray light is higher (up to 15% of the total signal for the experiments reported here).

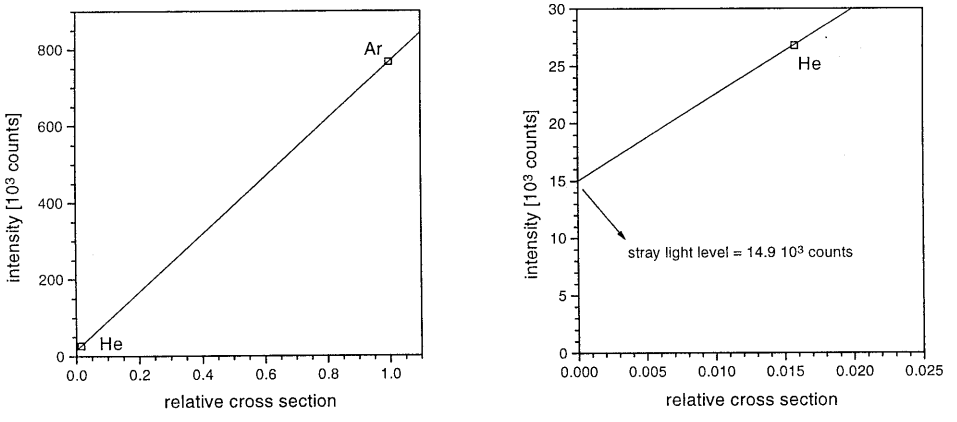

***Figure 2**: A typical example of the determination of the stray light level using the scattering signal on helium and argon (σ_{He} = 0.0158 σ_{Ar}). In this case (3 mm AN) the intensity of the stray light is 14.9 × 10^3 counts, which is about 2.0% of the Rayleigh signal of room temperature argon.*

Although for argon the amount of stray light is acceptable, this is certainly not the case for helium. Owing to the relatively low Rayleigh scattering cross section for helium the contribution of stray light is 36% of the total signal at room temperature. Since at higher gas temperatures this ratio is even worse, the measured temperatures of the helium plasma are far too inaccurate to present here.
Besides the shot-to-shot variations in the laser energy and the stray light, three other sources of errors are contributing to the inaccuracy of the measurements:

1. the electron pressure,
2. the contribution of the Thomson signal and
3. the scattering on other heavy particles than argon.

In equation (3) the partial pressure of the heavy particles is set equal to 1 atmosphere, i.e. the partial pressures of the free electrons and ions are neglected. The resulting error can be estimated using the spatially resolved measurements of the electron density n_e and temperature T_e presented in a previous paper [4]. It is found that n_e is always smaller than 4×10^{21} m^{-3} and T_e smaller than 24000 K, so that the maximum electron pressure is 1.3% of the total pressure. The ion pressure is much lower than this 1.3%, since the gas temperature (and thus the ion temperature) is much lower than the electron temperature (see below).
In the determination of the Rayleigh signal the intensity is integrated over a relatively large wavelength interval (around 1.3 nm), so that also a part of the Thomson signal is included. An upper limit of this second error can be found by comparing the intensity of the total Thomson signal I_{TS} with that of the Rayleigh signal I_{RS}:

$$\frac{I_{TS}}{I_{RS}} = \frac{n_e}{n_{Ar}} \frac{\sigma_{TS}}{\sigma_{Ar}} = 143 \frac{n_e}{n_{Ar}} \tag{4}$$

where σ_{Ar} and σ_{TS} refer to the cross sections for Rayleigh scattering on argon and for Thomson scattering, respectively. This ratio reaches its maximum at 6 mm AN and -0.4 mm radial position, where the electron density equals 3.6×10^{21} m^{-3} [4] and the neutral density 8.6×10^{24} m^{-3} (see below). This would result in a 6% overestimation of the Rayleigh signal and thus in an underestimation of the gas temperature of 6%. However, due to the high electron temperature the typical Full Width at Half Maximum (FWHM) of the TS profile equals 3 nm, so that the actual systematic error is even smaller and can safely be assumed to be below 3%.
The gas temperature is not only measured in the plasma, but also in its environment where N_2 and O_2 are the most abundant species. Since the Rayleigh scattering cross sections of these molecules differ not too much from that of argon ($\sigma_{N2} = 1.12\,\sigma_{Ar}$ and $\sigma_{O2} = 0.915\,\sigma_{Ar}$ [9]), the error in the obtained temperature will be small. In case of pure air (80% N_2 and 20% O_2) the used simplification results in a 8% underestimation of the gas temperature.
Concluding, we can state that the accuracy of the gas temperature is around 3% in the plasma and around 8% in the surroundings of the plasma. This latter error is mainly caused by the different cross sections, so that it is possible to be corrected for (see section 4).

3.2 Results

Measurements are performed at 14 different heights Above the Nozzle (AN) with steps of 2 mm and starting at 3 mm AN. Closer to the nozzle the stray light becomes too intense. At each height the gas temperature is measured at 16 radial positions with steps of 0.2 mm. The

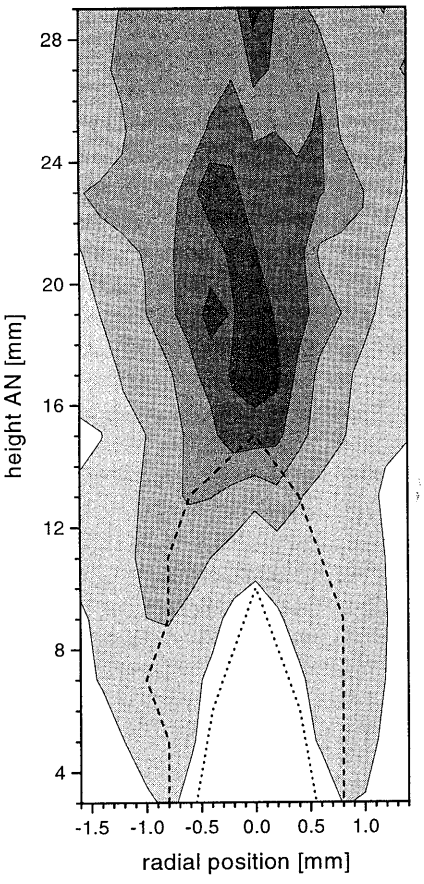

***Figure 3**: The gas temperatures in the plasma sustained by the TIA. Each grey shade denotes a temperature interval of 700 K, from white (300-1000 K) to black (3800-4500 K). The highest measured temperature equals 4480 ± 130 K at 19 mm AN. The dotted line indicates the positions of the maxima of the electron density [4], which, at each axial position, are situated more to the inside of the plasma than the maxima of the gas temperature (the dashed line). Note that the axes do not have the same scale.*

result is depicted in Figure 3. Note that the axes do not have the same scale. The maximum of T_h is situated at 19 mm AN and equals 4480 ± 130 K.

Below 12 mm AN the hottest parts of the plasma are situated on a cone, whereas at higher positions the center of the discharge has the highest temperature. The cone-like shape, as found in the upstream part, is more or less the same as that of the electron density and temperature, which were measured using spatially resolved Thomson scattering measurements [4]. However, the highest gas temperatures are situated more to the outside of the plasma than the maxima of the electron density and temperature and the top of the "T_h cone" is situated more downstream. The reason for this is discussed in section 6.

A similar axial dependence of the temperature (close to the nozzle increasing and higher in the plasma decreasing with increasing distance to the nozzle) was reported by Ricard *et al.* [12]. They used the R branch of N_2^+ to determine the rotational temperature (which was assumed to be equal to the gas temperature) and found slightly lower temperatures (up to 4000 K), probably because they used different settings (5 slm argon and 700 W microwave power). An other difference is that they only measured as function of axial and not of the radial position.

4. Nitrogen entrainment

The entrainment of nitrogen is measured using the Stokes branch of vibrational Raman scattering. In this case the scattering of a photon on a molecule coincides with a vibrational transition within the same molecule, so that the scattered photon is shifted in wavelength. Since this change in wavelength is characteristic for the molecule (and the vibrational transition) vibrational Raman scattering can be used to determine the concentration of specific molecules in a plasma and its surroundings. In the past this technique was used in our lab to determine the entrainment of nitrogen in an argon Inductively Coupled Plasma (ICP) [9].
In this paper the Stokes transition from v = 0 to v = 1 within the nitrogen molecule is used. The shift in wavelength can be calculated from the energy difference of the vibrational levels. According to Herzberg [13] the energies of the vibrational levels of N_2 can be approximated by:

$$E_{N2}^{vib}(v) \approx 0.29076v - 1.79 \times 10^{-3} v^2 \quad [eV] \tag{5}$$

This results in a shift in wavelength from 532 nm to 607 nm, see Table 1.
It should be noted that at high temperatures the signal does not only decrease because of the lower concentration of nitrogen, but also due to the excitation of N_2 to the higher vibrational levels, which corresponds to different Stokes wavelengths [13]. To correct for this we assume a Boltzmann distribution over the vibrationally excited levels, which is ruled by the gas temperature T_h:

$$n_{N2} = n_{N2}^{v=0} \sum_{v} exp\left[-\frac{E_{N2}^{vib}(v) - E_{N2}^{vib}(0)}{k_B T_h} \right] \approx \frac{n_{N2}^{v=0}}{1 - exp\left[-\frac{E_{N2}^{vib}(1) - E_{N2}^{vib}(0)}{k_B T_h} \right]} \tag{6}$$

In the approximation of the last step the vibrational energy spacing is taken constant, which is a reasonable assumption for the relatively low gas temperatures in the TIA (see previous section). Thus by combining the gas temperature obtained by Rayleigh scattering with the density in the vibrational ground state $n_{N2}^{v=0}$ as determined by Raman scattering, the density of molecular nitrogen is obtained. For a gas temperature equal to 2000 K, the correction according to equation (6) is around 23%.
During the Rayleigh scattering measurements of the previous section, scattering on particles other than argon atoms was neglected. Now the nitrogen density is known, it is possible to correct for this using an iterative procedure:

1. estimate T_h from the Rayleigh measurements,
2. calculate the N_2 density from the Raman measurements, using equation (6) and T_h,

transition	ΔE [eV]	λ [nm]
0 → 1	0.2890	607.3
1 → 2	0.2854	606.2
2 → 3	0.2818	605.2

***Table 1**: The lower three Stokes transitions of N_2. The resulting wavelength is calculated for an incident 532.0 nm photon.*

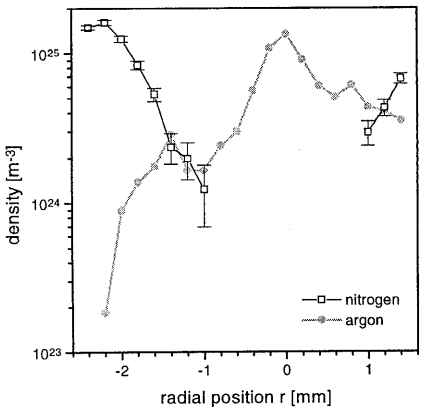

***Figure 4**: The densities of nitrogen and argon measured with the combination of vibrational Raman and Rayleigh scattering at 5 mm AN. The detection limit of N_2 (1.1×10^{24} m^{-3}) is not good enough to determine the nitrogen density inside the plasma.*

3. improve the estimation of T_h by correcting the Rayleigh signal for the (known) contribution of nitrogen and
4. in case the accuracy is not high enough repeat the procedure from step 2.

Normally the change in the nitrogen density and the gas temperature is smaller than 0.1% after two iterations.

The experimental setup is the same as described in the previous section. At every 0.2 mm in radial direction vibrational Raman and Rayleigh measurements are performed using 5000 and 300 shots, respectively. The laser power equals approximately 0.4 J per shot. The calibration is performed in pure air at room temperature. To avoid interference with dust particles (especially during the calibration of the Rayleigh measurements) a special dust free room is constructed around the detection volume.

The results are depicted in Figure 4. As expected nitrogen is the most abundant species far away from the plasma. Unfortunately the detection limit is only 1.1×10^{24} m^{-3}, which is not good enough to determine the nitrogen density inside the plasma. This high limit is due to the relatively small cross section for vibrational Raman scattering and the fact that the setup is optimised for the detection of Thomson and Rayleigh signals (i.e. at and around 532 nm).

5. Effects on the electron particle balance

The influence of the nitrogen entrainment on the electron particle balance can not be determined directly, since it is impossible to measure the concentration of nitrogen in the plasma with our setup. Therefore, an other approach has to be used. As can be seen in Figure 4, closer to the plasma the nitrogen is gradually replaced by argon. This decreasing concentration induces a net diffusion of nitrogen towards the plasma. In case the gradients in axial direction can be neglected, the amount of inward diffusing N_2 is independent of the radial position and equals the amount of nitrogen which enters the plasma. This amount can be compared with the number of electrons produced in the plasma, since the destruction of one N_2 molecule via CT and DR consumes one electron-ion pair, cf. reactions (1) and (2).

The inward flux of nitrogen molecules at given radial position r can be calculated using Fick's law:

$$\Gamma(r) = -D\nabla n_{N2} \tag{7}$$

In principle the diffusion coefficient D should be obtained from combining the diffusion coefficient of N_2 in Ar and the self diffusion coefficient of N_2:

$$\frac{1}{D} = \frac{1}{D_{N2Ar}} + \frac{1}{D_{N2}} \tag{8}$$

These two diffusion coefficients can be calculated using the hard sphere approximation [14]

$$D_{N2Ar} = \frac{2}{3}\frac{4}{\pi\left(d_{N2}+d_{Ar}\right)^2}\frac{1}{n_{Ar}}\sqrt{\frac{k_B T_h}{2\pi}\left(\frac{1}{M_{N2}}+\frac{1}{M_{Ar}}\right)} \approx \frac{1.4\times10^{19}}{n_{Ar}}\sqrt{T_h} \tag{9}$$

and

$$D_{N2} = \frac{2}{3}\frac{1}{\pi d_{N2}^2}\frac{1}{n_{N2}}\sqrt{\frac{k_B T_h}{\pi M_{N2}}} \approx \frac{1.6\times10^{19}}{n_{N2}}\sqrt{T_h} \tag{10}$$

Here d_{N2} and d_{Ar} represent the (effective) hard sphere diameter of N_2 and Ar (3.75 Å and 3.64 Å, respectively [15]). The other symbols have their usual meaning. The difference in the constants in both expressions is small compared to the inaccuracy of the hard sphere model, so that we can simplify the expression for the N_2 diffusion coefficient to

$$D \approx 1.5\times10^{19}\frac{\sqrt{T_h}}{n_{Ar}+n_{N2}} \approx 2.0\times10^{-4}\frac{T_h^{3/2}}{p} \quad [m^2 s^{-1}] \tag{11}$$

The total amount of nitrogen molecules diffusing towards the plasma at radial position r can be obtained from integrating the flux over the surface of a cylinder with radius r and height h:

$$Q_{N2}(r) = 2\pi r h \Gamma(r) \tag{12}$$

Using the results of Figure 4 this total flux can be calculated. The result is plotted in Figure 5 for h = 1 mm. The large scatter in the results is mainly due to the inaccuracies in the determination of the N_2 density ($\pm$ 6 $\times$ 10^{23} m^{-3}). Within the error margins the total flux is constant at $\overline{Q}_{N2}$ = (6 $\pm$ 3) $\times$ 10^{18} s^{-1}, so that it can be assumed that this total flux equals the

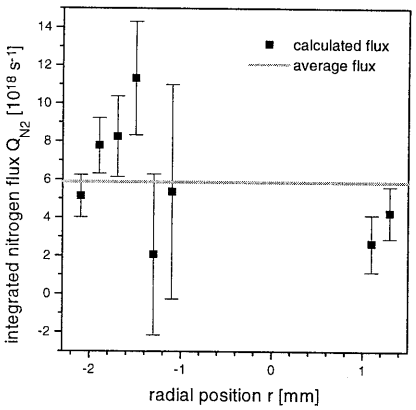

***Figure 5**: The integrated flux of nitrogen molecules diffusing towards the plasma between 4.5 and 5.5 mm AN. The error in the data points is due to the inaccuracies in the nitrogen concentration. The horizontal grey line represents the average integrated nitrogen flux: (6 $\pm$ 3) $\times$ 10^{18} s^{-1}, which is assumed to enter the plasma.*

amount of nitrogen molecules which enters the plasma between h = 4.5 and 5.5 mm AN per unit of time.
This total flux has to be compared with the number of electrons produced in that part of the plasma, which equals

$$Q_{ne} = \iiint n_e n_1 S_{CRM}(\hat{T}_e) dV \tag{13}$$

An expression for the ionisation coefficient can be found in [1]

$$S_{CRM}(\hat{T}_e) = 7.34 \times 10^{-15} \sqrt{\hat{T}_e}\, exp\left(-\frac{12.06}{\hat{T}_e}\right) \quad [m^3 s^{-1}] \tag{14}$$

which is valid for the range $0.6 < \hat{T}_e < 2.2$ eV. Note that $\hat{T}_e$ represents the electron temperature given in eV, whereas T_h is given in K.
The electron density and temperature at 6 mm AN are depicted in Figure 6 as function of the radius. Unfortunately there is no measured data available at 5 mm AN. As a good approximation for the plasma a cylinder can be taken with radius $r_p = 0.6$ mm and an average electron temperature of 1.8 eV and density of 2×10^{21} m^{-3}. From Figure 4 it can be seen that the argon density in this plasma part is around 6×10^{24} m^{-3}. Substitution of these values in equations (13) and (14) results in a production of 2×10^{20} electrons per second in the plasma part under study ($4.5 \leq h \leq 5.5$ mm AN). This is more than one order of magnitude higher than the total flux of nitrogen. The large difference is probably not caused by the relatively simple hard sphere diffusion model we used, since this is normally assumed to be accurate within a factor 2. Also the fact that in principle it is better to use the Maxwell-Stefan theory [16] instead of Fick's law to describe diffusion can not explain this discrepancy, since for gases the differences in both approaches are small [16]. Also the local creation of new nitrogen molecules via association

$$N + N + Ar \longrightarrow N_2 + Ar \tag{15}$$

can be neglected, due to the low rate constant (around 10^{-45} $m^6 s^{-1}$).
The conclusion that the entrainment of nitrogen would not influence the particle balance significantly is in contradiction with the measurements of the previous chapter [4], in which it

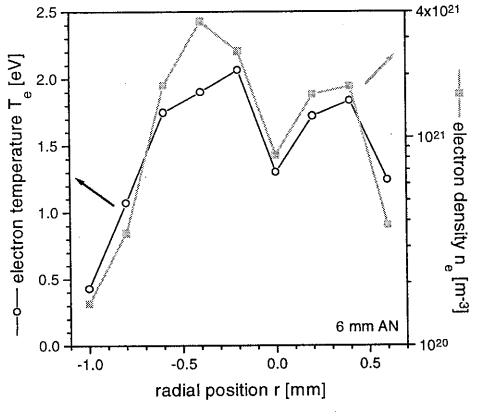

***Figure 6**: The electron density and temperature as measured with local Thomson scattering at 6 mm AN [4].*

was shown that in case the plasma is sustained in a pure argon environment the electron temperature is significantly lower. One of the possibilities is that the entrainment is not caused by ordinary diffusion but by turbulent mixing, which may be much faster. Therefore, we have to take a closer look to the Reynolds number

$$\mathrm{Re} = \frac{\rho v d}{\eta} = \frac{\rho}{\eta}\frac{4\varphi}{\pi d} \tag{16}$$

For T_h = 300 K the viscosity η of argon equals 3.685×10^{-5} kg m^{-1}s^{-1} [17] and the argon density ρ = 1.61 kg m^{-3}. Together with a gas flow φ = 3.0 slm and the diameter of the nozzle d = 1.75 mm, the typical Reynolds number is found to be around 1.6×10^3, which is higher than the critical Reynolds number above which a free jet becomes turbulent: $\mathrm{Re}_{crit} \approx 1.2 \times 10^3$ [18,19]. Due to this turbulence the entrainment of nitrogen may be much faster than the estimations based on the hard sphere diffusion model, so that the destruction of N_2 via CT and DR can become an important process in the particle balance. Unfortunately, no general information could be found on the turbulent entrainment velocity. For instance, Blevins [19] gives only expressions for a laminar jet and for the area where the turbulent jet is fully developed which is situated more downstream (see Figure 7). This is due to the fact that more upstream the flow depends on the design of the nozzle.

Simple experimental evidence for the presence of turbulence in the TIA is the noise which is created by the plasma. The noise disappears when the gas flow is reduced to 2 slm, which corresponds to $\mathrm{Re} \approx 1.1 \times 10^3$, i.e. a laminar jet. Note that this jet also draws gas from its surroundings [19]. However, the entrainment of nitrogen should be less efficient, since in this case the measured electron temperature is much lower: around 17×10^3 K [11]. Unfortunately, this result was obtained by global Thomson scattering (i.e. not radially resolved). A next step towards the complete understanding of this torch will be to determine the electron temperature and density profiles as function of the gas flow. But this is left for future studies.

The conical shape of the plasma as is shown in Figure 3 and in [4] agrees well with the theory of axisymmetric turbulent jets [18,19]. According to this theory the jet consists of a conical non-turbulent core just after the nozzle with a turbulent mixing layer around and behind it, see Figure 7. The distance of the nozzle to the top of the core equals around five nozzle diameters [18,19]. The boundary between the turbulent and non-turbulent zones coincides with the

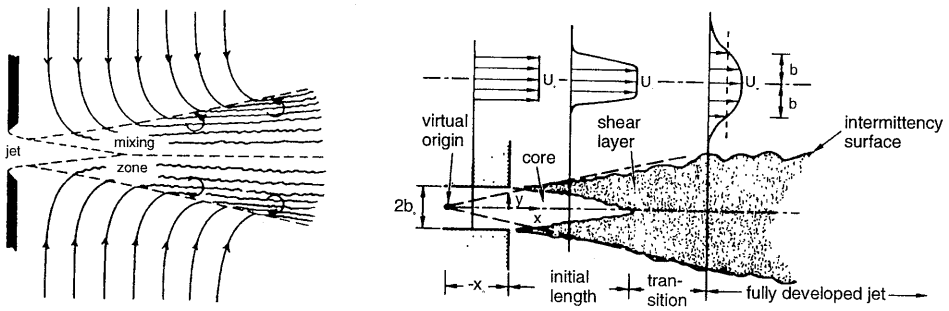

***Figure** 7: Typical examples of the structure of an axisymmetric turbulent jet, taken from [18,19]. The non-turbulent core is gradually "eaten" up by the turbulent mixing zone. The plasma (the maxima of n_e and T_e) is situated close to the boundary between these two layers (see Figure 3).*

maxima of the radial electron density profiles, cf. Figure 3. The reason for this is the competition between the electrical (microwave) field strength F_{mw} and the plasma conductivity σ, which both determine the power density absorbed by the plasma

$$\varepsilon_{EM} = \sigma F_{mw}^2 \tag{17}$$

The conductivity is an increasing function of the electron density, which is low in the turbulent zone due to the relatively short residence time of the electrons [1]. On the other hand, close to the symmetry axis the electrical field strength increases with the radial position, which pushes the plasma to the outside.

6. The heavy particle energy balance

In Figure 8 the gas temperature at 3 mm AN and the electron density at 2 mm AN [4] are depicted as functions of the radial position. The electron density (and temperature) was obtained by Thomson scattering using the same laser setup as described in section 3. It can be seen that the maxima of the electron density profile are situated closer to the center than the hottest parts of the plasma. At first sight this seems to be strange since normally the heavy particles are heated by the electrons.

A possible explanation can be the heat produced by the destruction of the entrained nitrogen molecules via charge transfer (CT), followed by dissociative recombination (DR), see reactions (1) and (2). Normally the charge transfer reaction is considered to be the rate limiting process in the reaction chain of CT and DR [20,21]. Since the number of events depends on the product of the concentrations of the electrons and nitrogen molecules, this mechanism heats especially the outer parts of the plasma. This may explain the different positions of the maxima of T_h and n_e as demonstrated in Figure 8.

In the following the amount of heat produced in this N_2 channel is compared to that of the

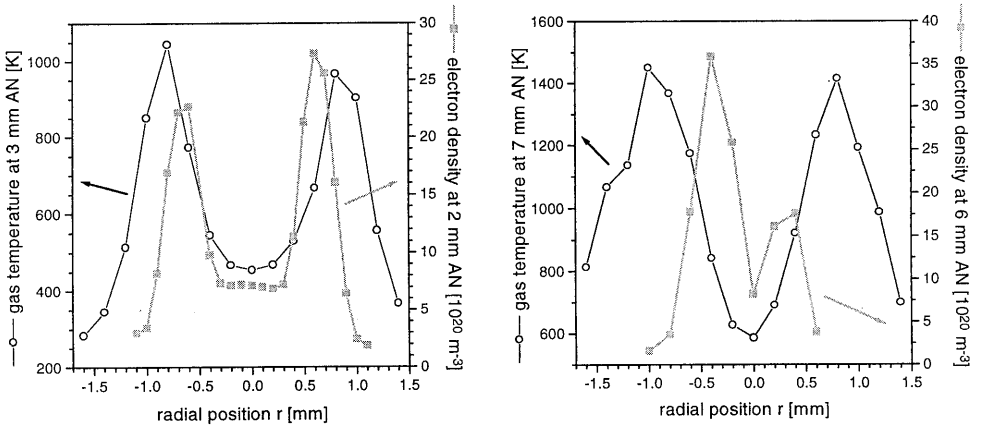

***Figure 8**: A comparison of the gas temperature and the electron density profiles [4] at two different heights above the nozzle (AN). The radial profile of the gas temperature has more or less the same structure as that of the electron density (and temperature [4]). However, the hottest part of the gas is situated more towards the outside than the maximum of the electron density.*

normal heating mechanism: electron-heavy particle collisions (the so-called elastic channel). Since there is no information available on the concentrations of nitrogen in the plasma, we have to restrict ourselves to an integrated approach for the same plasma volume as used in section 5 ($r_p = 0.6$ mm and $h = 1$ mm, situated around 5 mm AN). This is not a completely fair comparison, since the N_2 channel is concentrated at the outside of the plasma volume (see above), whereas the elastic channel is much more equally distributed (due to the relatively flat n_e, T_e and n_h profiles, cf. Figure 6 and Figure 4).
The total transfer of heat due to elastic electron-heavy particle collisions in the plasma part under study is given by

$$q_{elas} = \iiint \varepsilon_{elas} dV \approx \pi r_p^2 h \varepsilon_{elas} \tag{18}$$

in which the local heat transfer equals

$$\varepsilon_{elas} = n_e n_l \left\langle \sigma_{e-h}^m v_e \right\rangle \frac{2m_e}{M_h} \frac{3}{2} k_B (T_e - T_h) \tag{19}$$

The electron-atom collision rate coefficients for momentum transfer $\langle \sigma^m_{e\text{-}h} v_e \rangle$ can be found in, for instance, [1]:

$$\left\langle \sigma_{e-h}^m v_e \right\rangle_{Ar} = \left(0.084 + 0.537 \hat{T}_e + 1.192 \hat{T}_e^2\right) \times 10^{-14} \quad [m^3 s^{-1}] \tag{20}$$

This function is valid for the electron temperature range $0.5 \text{ eV} < \hat{T}_e < 2.5$ eV. Substituting $\hat{T}_e = 1.8$ eV, $n_e = 2 \times 10^{21}$ m^{-3} and $n_l = 6 \times 10^{24}$ m^{-3} (cf. previous section) gives that the local heat transfer equals 7×10^9 Wm^{-3}, so that in the plasma cylinder under study the heavy particles are heated by 8 W due to the elastic channel.
The amount of heat produced in the N_2 channel can be estimated by assuming that all the nitrogen, which diffuses inwards, is dissociated, so that the power of this molecular channel equals

$$q_{N2} = \overline{Q}_{N2} E_{kin} \tag{21}$$

where E_{kin} represents the total kinetic energy of the two nitrogen atoms which are produced in the dissociative recombination reaction. The exact value of this energy depends on the internal energies of the end products. Kella *et al.* [22] measured the dissociation products of the $^{15}N^{14}N^+$ molecule, which we assume to be the same as for $^{28}N_2^+$. In case the nitrogen molecular ion is in the vibrational ground state, the dominant products are either two atoms in the ^2D state or a combination of the ^2D and the ^4S states [22]. The total kinetic energy of the nitrogen atoms equals 1.05 and 3.44 eV, respectively, *plus* the energy stored in rotational excitation and the kinetic energy of the electron. We assume that the average released kinetic energy equals 2 eV.
In the previous section it is made plausible that the amount of entraining nitrogen $\overline{Q}_{N2}$ in the plasma part under study equals more or less the number of electrons produced in that part (2×10^{20} s^{-1}). The destruction of these molecules yields a heat of around 60 W, which is almost one order of magnitude larger than the heat produced by the elastic channel. Moreover, the heat of the N_2 channel is merely generated at the outer parts of the plasma cylinder, so that the maxima of the gas temperature are more situated to the outside than those of the electron density and temperature.

7. Conclusions

The entrainment of nitrogen has a significant influence on the electron particle balance of the argon plasma created by the TIA. This is probably due to the turbulent character of the plasma: the conventional Fick diffusion (estimated from a hard sphere model) is not fast enough, in spite of the small plasma dimensions.

The contour plot of the gas temperature is more or less similar to that of the electron density and temperature: at axial positions close to the nozzle the radial profiles are hollow and more downstream they gradually convert into a Gaussian shape. Probably the plasma is sustained at the outside boundary of the non-turbulent core of the jet.

However, the cone of the maxima in the gas temperature close to the nozzle contains that of the electron density (and temperature), i.e. the hottest parts of the plasma are more situated to the outside than the maxima of the electron density. This is due to the fact that the entrainment of N_2 influences also the radial dependence of the gas temperature, since the heat produced in the destruction of the nitrogen molecules (via charge transfer and dissociative recombination) is the most dominant channel for energy transfer from the electrons to the heavy particles.

References

1. Chapter 6: J. Jonkers, J.A.M. van der Mullen and D.C. Schram, *"On the difference between helium and argon plasmas operated at atmospheric pressure"*, submitted to Phys. Rev. E
2. Chapter 7: J. Jonkers, J.A.M. van der Mullen and D.C. Schram, *"The role of molecular rare gas ions in atmospheric argon and helium plasmas"*.
3. M. Moisan, G. Sauvé, Z. Zakrzewski and J. Hubert, Plasma Sources, Sci. and Techn. **3** 584 (1994).
4. Chapter 5: J. Jonkers, L.J.M. Selen, J.A.M. van der Mullen, E.A.H. Timmermans and D.C. Schram, Plasma Sources, Sci. and Techn. **6** 533 (1997).
5. M. Huang, D.S. Hanselman, Q. Jin and G.M. Hieftje, Spectrochim. Acta B **45** 1339 (1990).
6. M. Huang, D.S. Hanselman, P. Yang and G.M. Hieftje, Spectrochim. Acta B **47** 765 (1992).
7. D. Lapierre, R.J. Kearney, M. Vardelle, A. Vardelle and P. Fauchais, Plasma Chem. Plasma Process. **14** 407 (1994).
8. J.M. de Regt, F.P.J. de Groote, J.A.M. van der Mullen and D.C. Schram, Spectrochim. Acta B **51** 1371 (1996).
9. J.M. de Regt, F.P.J. de Groote, J.A.M. van der Mullen and D.C. Schram, Spectrochim. Acta B **51** 1527 (1996).
10. J.M. de Regt, R.A.H. Engeln, F.P.J. de Groote, J.A.M. van der Mullen and D.C. Schram, Rev. of Sci. Instrum. **66** 3228 (1995).
11. Chapter 3: J. Jonkers, J.M. de Regt, J.A.M. van der Mullen, F.P.J. de Groote, H.P.C. Vos and E.A.H. Timmermans, Spectrochim. Acta B **51** 1385 (1996).
12. A. Ricard, L. St-Onge, H. Malvos, A. Gicquel, J. Hubert et M. Moisan, J. Phys. III France **5** 1269 (1995).
13. G. Herzberg, *"Molecular spectra and molecular structure"*, part I: *"Spectra of diatomic molecules"*, Van Nostrand Reinhold company, New York (1950).

14. R.B. Bird, W.E. Stewart and W.N. Lightfoot, *"Transport phenomena"*, John Wiley & Sons, New York (1960).
15. J.O. Hirschfelder, C.F. Curtiss and R.B. Bird, *"Molecular theory of gases and liquids"*, John Wiley & Sons, New York (1966).
16. R. Taylor and R. Krishna, *"Multicomponent mass transfer"*, John Wiley & Sons, New York (1993) and J.A. Wesselingh and R. Krishna, *"Maxwell-Stefan apporach of mass transfer"*, (1993).
17. *"Handbook of chemistry and physics"*, CRC press, Cleveland 54th edition (1973).
18. G. Birkhoff and E.H. Zarantonello, *"Jets, wakes and cavities"*, Academic press inc., New York (1957).
19. R.D. Blevins, *"Applied fluid dynamics handbook"*, Van Nostrand Reinhold company inc., New York (1984).
20. Yu. P. Raizer, *"Gas discharge physics"*, Springer-Verlag, Berlin (1991).
21. D.C. Schram, J.A.M. van der Mullen, J.M. de Regt, D.A. Benoy, F.H.A.G. Fey, F.P.J. de Groote and J. Jonkers, J. of Anal. At. Spectrom. **11** 623 (1996).
22. D. Kella, P.J. Johnson, H.B. Pedersen, L. Vejby-Christensen and L.H. Andersen, Phys. Rev. Lett. **77** 2432 (1996).

9

The "Torche à Injection Axiale": remaining questions and possible answers

J. Jonkers, J.A.M. van der Mullen, A. Hartgers, I.A.J. Thomas and D.C. Schram

This chapter deals with possible alternatives for the conclusion of the previous chapter that the turbulent inward transport of nitrogen provides the dominant loss channel of the free electrons in the TIA. New experiments show that the spatially resolved Thomson scattering measurements of chapter 5 are most probably correct. The diffusion gradient length is found to be only 0.06 mm, which is smaller than previously estimated. Moreover, calculations show that the high energy tail of the EEDF is underpopulated with respect to a Maxwellian distribution. This lowers the ionisation frequency by a factor of 0.4 to a value which is confirmed by the electron energy balance. However, the correct production is still more than one order of magnitude higher than the losses predicted by classical ambipolar diffusion theory. This difference can not be explained by volume recombination via the formation and destruction of Ar_2^+, so that we have to conclude that turbulent mixing of the plasma with the surrounding air remains the most serious candidate.

1. Introduction

If the low excitation temperatures as obtained by the Absolute Line Intensity measurements [1] are interpreted as electron temperature values this results in a severe underproduction of charged particles. The small TIA plasmas suffer from high transport losses so that they can not be driven at an electron temperature of only 4000 K. This paradox could only be explained if the atomic state distribution function of the TIA is far from the equilibrium shape as predicted by Saha-Boltzmann. This was the reason to investigate what the real Saha densities are, i.e. to measure the electron density n_e and temperature T_e using Thomson scattering. It was indeed confirmed [2] that the excited states are heavily overpopulated so that the plasma is strongly ionising and the inverse process of ionisation (atomic three particle recombination) is unimportant. Since it was thought that this overpopulation was driven by diffusion, which should be fast due to the steep gradients, insight in the spatial structure was needed. By focusing the laser, local measurements were done [3] from which it turned out that the gradients in the electron density (and temperature) are indeed very steep, so that the diffusion is fast. However, the local electron temperature is higher than the value obtained in the global Thomson measurements, so that the ionisation frequency is much larger than the frequency at which electrons are transported out of the plasma. To state it differently, the electron particle balance does not fit; we are now faced with an apparent overproduction: the production of electrons is around four orders of magnitude larger that the efflux (outward transport), see Table 1. In this table the results of the global [1] and local [2] Thomson scattering measurements are combined with the gas temperatures as found in the ionising plasma parts [4]. The fact that the actual gas temperature T_h (500 to 800 K) is much lower than that what was estimated before (3000 K [2]) increases the mismatch of the particle balance, since a lower T_h reduces the diffusion losses and increases the ionisation frequency.

In the previous chapter it was made plausible that the imbalance may be due to entrainment of nitrogen, which is enhanced by the turbulent character of the plasma. However, no quantitative evidence could be found to support this statement.

main gas		argon	argon	argon	helium
surroundings		air	air	argon	air
reference		[2]	[3,4]	[3]	[2]
microwave power	[kW]	0.33	1.0	0.6	0.30
gas flow	[slm]	2.0	3.0	1.8	5.0
electron density	[10^{20} m^{-3}]	10	25	15	3.0
electron temperature	[eV]	1.5	2.0	1.5	2.2
gas temperature	[K]	(500)	800	(500)	(500)
ionisation frequency	[MHz]	42	230	42	10
diffusion loss frequency	[MHz]	0.007	0.014	0.007	0.08

***Table 1**: The TIA problem: the ionisation frequency is three orders larger than the diffusion loss frequency. The diffusion losses[a] are based on a gradient length of 0.2 mm [3]. The gas temperatures between brackets are estimated, based on the measurements which are presented in the previous chapter [4].*

This chapter can be seen as an error analysis: the ionisation and diffusion terms of the particle balance are scrutinised. After a thorough investigation it has to be concluded that the difference between production and losses, as given in Table 1, is overestimated, but there remains a discrepancy of more than one order of magnitude. Therefore we have to conclude that the entrainment of nitrogen is the only possible candidate to equilibrate the particle balance.
In section 2 and 3 we will focus on the validity of the results of Thomson scattering. It will be investigated whether the laser might be responsible for an additional heating of the electrons and if the gradients in the electron density are measured correctly. Section 4 is devoted to the influence of the gradient in the electron temperature on the diffusion. This is indeed important in enhancing the outward diffusion but still the outward flux of electrons is still less than the production. Therefore, we focus our attention on the ionisation in section 5. It is found that there are serious deviations from a Maxwell electron energy distribution, which reduce the production by a factor of 0.4. However, this is not sufficient to fit the particle balance. An alternative way for determining the ionisation frequency is the electron energy balance. It is shown (in section 6) that the production frequency obtained in this way agrees well with the non-Maxwell ionisation frequency based on the electron temperature and density as obtained by Thomson scattering (cf. section 5). Therefore, it has to be concluded that the most significant destruction process is missing. In section 7 one alternative loss process is studied: the formation and destruction of Ar_2^+. For this we make use of the model presented in chapter 7 [5]. This, however, is found to be insufficient. Therefore we have to conclude that turbulent mixing of ambient air with the plasma, by which a very efficient dissociative recombination channel is offered, must be responsible.

[a] Note that the fits which are used to calculate the diffusion losses [9] are not valid for these low gas temperatures. Therefore an extrapolation has been used to obtain the results listed in Table 1.

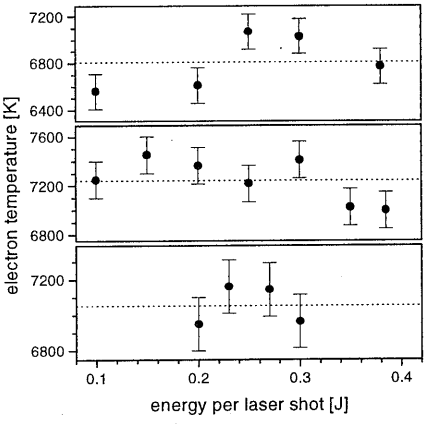

***Figure 1**: The electron temperature as a function of the energy per laser shot, measured on three different days. The horizontal dashed lines indicate the average temperature for each series. The electron temperature is apparently not affected by the laser power within one series (without switching off the ICP); the difference between the series is most likely due to the calibration and the reproducibility of the plasma.*

2. Heating of the electrons due to the laser

The Thomson scattering measurements in [3] were performed using a strongly focused laser beam. Since the small diameter of beam (0.2 mm) results in a very high irradiance (typically 10^{15} Wm^{-2}) it might be possible that the electrons are heated by the laser and that therefore the measured electron temperature is higher than the real one. The presence of this effect is investigated by performing Thomson scattering measurements on an Inductively Coupled Plasma (ICP) [6] as function of the power of the laser. An ICP is chosen since it is known [7] that laser induced heating is stronger for lower electron temperature. Moreover the stability of the ICP is better than that of the TIA.

The obtained electron temperature for various energies per laser shot are depicted in Figure 1. Three different measurement series are presented taken on three different days. Within each set of measurements the plasma is burning continuously while the laser energy is varied. It is found that the dependence of the measured electron temperature on the irradiance of the laser is not larger than the experimental uncertainty of the electron temperature (i.e. the inaccuracy of the fit) which equals 150 K. The difference between the series is probably due to the reproducibility of the plasma and the inaccuracy of the calibration of the electron density[b] (typically 7.5%), which is only done before and after each series. These two errors are systematic but different for each set of measurements and introduce an extra uncertainty of 500 K [8], which is more than enough to explain the difference between the series. Therefore, we have to conclude that the influence of the laser energy on the electron temperature could not be established.

3. Smaller gradient lengths?

From the spatially resolved Thomson scattering measurements presented in [3], it was concluded that the gradient length of the electron density profile Λ_n equals approximately 0.2 mm. However, since the spatial resolution of the setup is also around 0.2 mm [3], it might be

[b] The electron density also influences the measured electron temperature, since collective scattering is significant, so that the distribution of the Thomson scattering signal also depends on n_e.

possible that the active plasma zone has much sharper boundaries. As discussed before [3,9] a smaller gradient length would increase the diffusion loss frequency. Therefore it is necessary to check whether the measured electron density profiles are correct or not.

In case of Thomson scattering the *number* of electrons in the detection volume is determined. The electron *density* is obtained by dividing by the size of this detection volume, which is done in the calibration procedure [6]. The electron density measured in this way is thus an average over the detection volume, so that only correct values of n_e are obtained if the electron density does not fluctuate too much within this volume. However, for the plasmas created by the TIA it might be possible that the gradient length of the electron density profile is smaller than 0.2 mm. In this case the maximum of the actual electron density has to be much higher, since with Thomson scattering the average n_e over the detection volume is obtained. In order to find out whether the plasma could be much smaller we compare the results of the local Thomson scattering measurements (TS) [3] with those of a technique, which is essentially different: H_β broadening.

The hydrogen H_β Balmer spectral line (486.13 nm) is broadened due to interactions of the bound electron with the free electrons. Therefore, the width of this line can be related to the electron density. For this normally the tables of Vidal, Cooper and Smith [10] are used, which are reproduced by the fit [11]

$$log(n_e) = 22.758 + 1.478\, log(\Delta\lambda_{1/2}) - 0.144\left[log(\Delta\lambda_{1/2})\right]^2 - 0.1265\, log(T_e) \qquad (1)$$

The full width at half maximum $\Delta\lambda_{1/2}$ is expressed in nm. This fit is valid for electron densities between 3.2×10^{20} m^{-3} and 3.2×10^{22} m^{-3} and electron temperatures within the range $5000 < T_e < 20000$ K. It should be noted that in the VCS tables (and thus the fit) the Stark profile is convoluted with a Doppler profile at a gas temperature which equals T_e. In our case this results in an underestimation of the electron density being smaller than 7% (for gas temperatures $T_h > 500$ K).

The H_β line is measured using the setup described in [12]. The apparatus profile ($\Delta\lambda \approx 0.03$ nm) can be neglected, since it is much smaller than the width of H_β (around 0.3 nm). Measurements are performed at different heights above the nozzle (AN). Unfortunately, the spatial resolution of the setup does not allow radially resolved measurements, so that the

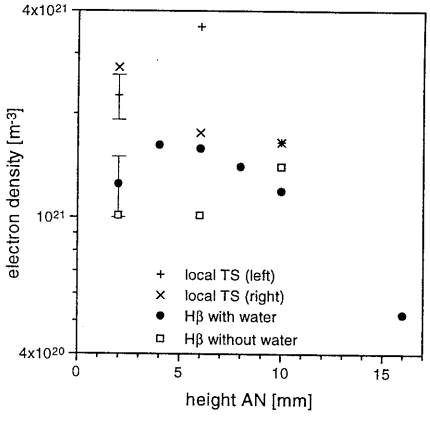

***Figure 2**: The electron density measured by H_β broadening as a function of the height above the nozzle (AN). The dots represent the measurements in which a small amount of nebulised water is added to the gas flow in order to obtain a clear and strong H_β line. Also the maxima of the electron density profiles (at both sides of the center) measured with local Thomson scattering (TS) are depicted. The values of the TS measurements are structurally higher since they are the maxima and the H_β are not spatially resolved so that they represent an average value.*

obtained electron densities represent the maximum values (see below).
Even in a "pure" argon plasma always small concentrations of hydrogen are present, due to H_2O and H_2 impurities in the used argon gas and due to the entrainment of water molecules from the surrounding air. However, in that case the noise on the H_β line is too large for an accurate fit. Therefore also measurements are performed with a small amount of nebulised water added to the argon flow. The resulting electron density, assuming T_e = 20000 K in equation (1), is depicted in Figure 2. The difference between the measurements with and without water added to the argon gas flow is within the accuracy of the measurements, so that this small amount of water is assumed to have no significant influence on the plasma.
In the same figure also the two maxima (left and right) of the electron density profile obtained by the local TS measurements [3] are plotted. The electron densities as measured using H_β broadening agree within a factor of 2.5 with the maximum n_e at each height as determined by Thomson scattering. However, the values obtained by H_β are structurally lower than those obtained by TS, which is probably due to the fact the H_β results are an average value (they are not spatially resolved) over a larger volume than the detection volume of Thomson scattering. Therefore, we have to assume that the local TS as presented in [3] are correct and no systematic errors were made with respect to the detection volume, so that the measured gradient length has the correct value.
A possible pitfall could be that most of the H_β light is not emitted by the hot active part of the plasma, but by the cold recombining parts where the electron density is lower. This can be checked by performing relative line intensity measurements of the Balmer series. As is discussed before [1,13], the Atomic State Distribution Function (ASDF) of an ionising system is characterised by a relatively low excitation temperature.
The measured relative populations are shown in Figure 3 for three different heights above the nozzle. In spite of the addition of a small amount of nebulised water it appears only to be possible to measure H_α to H_γ. The straight lines fitted to these relative populations correspond with excitation temperatures around 0.23 eV. This is in good agreement with the theoretical excitation temperature for a strongly exciting system, which is given by [13]

$$\frac{1}{\hat{T}_{exc}} = \frac{3}{\hat{I}_p} + \frac{1}{\hat{T}_e} \qquad (2)$$

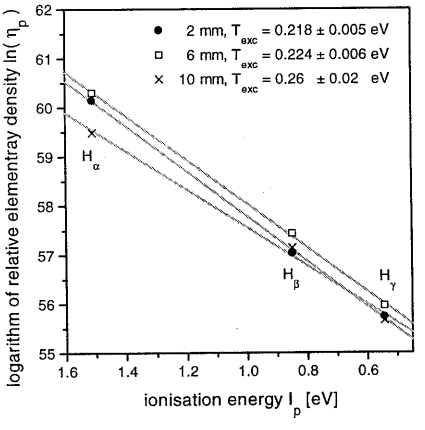

***Figure 3**: The relative densities of the second, third and fourth excited levels of hydrogen, obtained by relative line intensity measurements, at the three different heights in the plasma. A small amount of water is nebulised in the argon gas flow during the measurements, in order to be able to detect H_γ. The slope of the fitted lines yields excitation temperatures around 0.23 eV, which is much lower than the electron temperature, indicating that by far most of the light is emitted by the ionising parts of the plasma.*

For an electron temperature $\hat{T}_e$ = 2 eV (cf. Table 1) and a typical ionisation energy I_p = 0.85 eV, this formula predicts an excitation temperature $\hat{T}_{exc}$ = 0.25 eV. From this it has to be concluded that by far most of the light of the Balmer series is produced in the strongly ionising part of the plasma, i.e. at those positions where the electron temperature and density reach their maximum values. Therefore it is correct to compare the results of the H_β measurements with the maximum electron densities as found by Thomson scattering.

4. Diffusion

The expression for calculating the losses due to diffusion, as is used in [3,9], is based on the assumption that the gradient length in the electron temperature can be neglected. However, the local Thomson scattering measurements show that this is not the case for plasmas produced by the TIA, see Figure 4.

The losses due to ambipolar diffusion are obtained from solving the momentum balances of free electrons and of the ions simultaneously

$$\begin{aligned} -n_e e\vec{F}_a - \vec{\nabla}p_e - m_e n_e \nu_e^m \vec{v}_e = 0 \\ n_i e\vec{F}_a - \vec{\nabla}p_i - m_i n_i \nu_i^m \vec{v}_i = 0 \end{aligned} \tag{3}$$

in which $\vec{F}_a$ is the electric field due to the ambipolar diffusion and p_x and ν_x^m are the partial pressure and the collision frequency for momentum transfer of species x, respectively. The other symbols have their usual meaning. Normally this set of equations is solved by assuming that the densities and fluxes are equal and that the gradients in the temperature can be neglected. This yields the expression which is used in [3,9]. In case also gradients in the electron temperature are present, it follows from (3) that the diffusion losses are given by

$$\frac{D_a}{\Lambda_{diff}^2} n_e \equiv \nabla\left(\frac{D_a}{k_B T_e}\nabla p_e\right) = \nabla\left[D_a\left(\nabla n_e + n_e \frac{\nabla k_B T_e}{k_B T_e}\right)\right] \approx D_a n_e\left(\frac{1}{\Lambda_n^2} + \frac{1}{\Lambda_T^2}\right) \tag{4}$$

The last simplification is only valid for those positions where n_e or T_e reach a maximum value (i.e. $\nabla n_e = 0$ or $\nabla T_e = 0$).

In Figure 4 the electron density and temperature as obtained by local Thomson scattering at 2 mm AN are plotted. The gradient length is determined by assuming a parabolic dependence on the radial position r, like for instance

$$n_e(r) = n_e^0\left(\frac{r - r_0}{b_n}\right)^2 \tag{5}$$

Here n_e^0 represents the maximum electron density at radial position r_0 and b is the charac-

	Λ_n [mm]	Λ_T [mm]	Λ_{diff} [mm]
left	0.065	0.12	0.058
right	0.073	0.12	0.062

***Table 2**: The gradient length of the electron density and temperature profiles and the diffusion gradient length for both sides of the center of the plasma. The accuracy is typically 10%.*

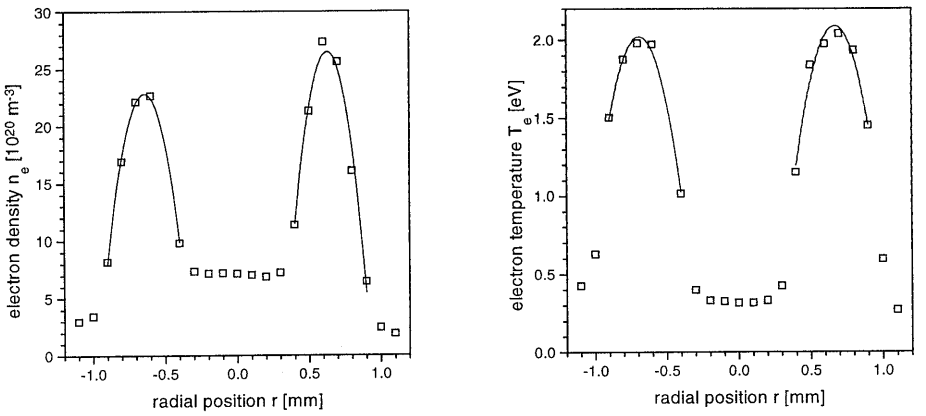

***Figure 4**: The measured electron density and temperature as functions of the radial position at 2 mm AN [3]. The solid lines are the parabolic fits to determine the gradient lengths (see text). The gradient in the electron temperature can not be neglected with respect to that in the electron density.*

teristic width of the profile. The gradient length can be found using

$$\frac{n_e^0}{\Lambda_n^2} \equiv \nabla^2 n_e\Big|_{r=r_0} = \frac{\partial}{\partial r}\left[\frac{1}{r}\frac{\partial}{\partial r}(r n_e)\right]\Bigg|_{r=r_0} = \frac{2n_e^0}{b_n^2} \tag{6}$$

As can be seen in Table 2 the diffusion gradient length which is obtained here (0.06 mm) is smaller than 0.2 mm, which was the estimated value for Λ_{diff} in [3]. This is mostly due to an overestimation of the gradient length in the electron density, since the gradient length in the electron temperature is a factor two larger, which leads only to a slight decrease of the diffusion gradient length (13%).

5. Deviations from Maxwell

In discharges at atmospheric pressure the Electron Energy Distribution Function is normally assumed to be Maxwellian. This is because the electron density is relatively high and it is the (Coulomb) collisions between the free electrons which impose a Maxwellian EEDF. However, for strongly ionising plasmas the fast electrons are lost at a high frequency (due to the excitation and ionisation processes) which can result in an underpopulation of the fast electrons with respect to Maxwell. This could certainly be the case for the plasmas sustained by the TIA since the ionisation degree is low (0.3%), so that the number of inelastic collisions is high compared to that of elastic Coulomb collisions. In this section the production and destruction of the fast electrons are compared in order to investigate whether the assumption of a Maxwell EEDF is valid or not.

In 1973 Vriens [14] introduced a relatively simple model which describes this deviation from Maxwell: the two electron group model (2EGM). The free electrons are divided in two groups: those with sufficient kinetic energy E to excite atoms in the ground state (i.e. $E \geq E_2$)

and those without ($E < E_2$). By far most of the electrons belong to the latter group and are therefore called the bulk electrons. The other group plays a crucial role in sustaining the discharge, since these tail electrons can bring the ground atoms into excited states, from which ionisation is relatively easy [9]. An important assumption in this model is that the both groups can each be described by one temperature: T_b for the bulk and T_t for the tail electrons. The EEDF has a continuous transition between bulk and tail[c] [15], which is given by

$$f^{2EGM}(E_e) = \begin{cases} f_b(E_e) & \text{for } E_e < E_2 \\ C_t(T_b, T_t) f_t(E_e) & \text{for } E_e \geq E_2 \end{cases} \tag{7}$$

in which f_x refers to a Maxwellian distribution which is governed by temperature T_x

$$f_x(E) = \frac{2}{\sqrt{\pi}} \frac{\sqrt{E}}{(k_B T_x)^{3/2}} \exp\left(-\frac{E}{k_B T_x}\right) \tag{8}$$

The normalisation constant for the tail C_t is given by

$$C_t(T_b, T_t) = \left(\frac{T_t}{T_b}\right)^{3/2} \exp\left(\frac{E_2}{k_B T_t} - \frac{E_2}{k_B T_b}\right) \tag{9}$$

The distribution of the tail electrons over the kinetic energies is governed by the tail temperature. However, the total amount of tail electrons is determined by the condition that the EEDF has to be continuous at the threshold, via the factor C_t.
In an ionising plasma, the net excitation from the ground state

$$A_1 + e_t \rightarrow A^* + e_b \tag{10}$$

converts the fast tail electrons into slow bulk electrons. The EEDF obeys Maxwell in case the net excitation frequency ν_{exc} can be neglected with respect to the population and depopulation frequencies of the tail due to elastic Coulomb collisions. For strongly exciting or ionising plasmas this might not hold anymore and the number of electrons in the tail will be below its equilibrium value, so that in the Coulomb collisions between free electrons more new tail electrons are produced than destroyed. A good example of this is the low pressure fluorescent lamp, where due to the escape of radiation, the excitation is not balanced by deexciation and the EEDF can be severely underpopulated, see for instance [14,15,16,17].
The tail temperature is obtained by solving the power balance for the tail electrons [14,15], which in case of plasmas sustained by the TIA can be simplified to

$$P_{Coul} + P_F = P_{inel} \tag{11}$$

This balance states that the power gained by the tail electrons due to Coulomb collisions (P_{Coul}) and acceleration by the electromagnetic field (P_F) equals the power lost in inelastic collisions (P_{inel}). The first term can be expressed as [15]

---

[c] In reality also the first derivative of the EEDF has to be continuous [17]. Owing to this simplification especially P_F will be overestimated. However, the influence of this term on the total energy balance of the tail is limited (see above).

$$P_{Coul} = 2\pi n_e \left(E_2 + k_B T_t\right) f^{2EGM}\left(E_2\right)\left(\frac{T_b}{T_t} - 1\right)\left(\frac{e^2}{4\pi\varepsilon_0}\right)^2 \sqrt{\frac{2}{m_e E_2}}\, ln\,\Lambda_t \tag{12}$$

The Coulomb logarithm for the tail electrons is given by [15]

$$ln\,\Lambda_t = ln\left(\frac{4\pi\varepsilon_0 E_2}{e^2}\sqrt{\frac{\varepsilon_0 k_B T_b}{e^2 n_e}}\right) \tag{13}$$

The heating of the tail electrons by the microwave electromagnetic field F_{mw} can be approximated by [15]

$$P_F \approx \left(E_2 + k_B T_t\right) f\left(E_2\right) \frac{e^2 F_{mw}^2}{2 n_1 \sigma^m k_B T_t} \sqrt{\frac{2E_2}{m_e}} \tag{14}$$

where n_1 is the ground state density and $\sigma^m \approx 1.5 \times 10^{-19}$ m^2 the cross section for momentum transfer for electrons with threshold energy E_2. A typical value of the microwave electric field strength can be calculated using the expression for the Ohmic dissipation

$$\varepsilon_{mw} = \varsigma F_{mw}^2 \tag{15}$$

in which the conductivity is given by

$$\varsigma = \frac{e^2 n_e}{m_e \nu^m} \tag{16}$$

The collision frequency for momentum transfer can be expressed as

$$\nu^m = n_+ \left\langle \sigma_{e+}^m v_e \right\rangle + n_1 \left\langle \sigma_{e1}^m v_e \right\rangle \tag{17}$$

where the rate coefficients for electron-ion and electron-atom collisions equal [18]

$$\left\langle \sigma_{e+}^m v_e \right\rangle \approx 2.91 \times 10^{-12} \hat{T}_e^{-3/2}\, ln\left(1550\sqrt{\frac{\hat{T}_e^3}{\hat{n}_e}}\right) \quad [m^3 s^{-1}] \tag{18}$$

and [9]

$$\left\langle \sigma_{e1}^m v_e \right\rangle = \left(0.084 + 0.537\hat{T}_e + 1.192\hat{T}_e^2\right) \times 10^{-14} \quad [m^3 s^{-1}] \tag{19}$$

respectively. Substituting the typical values of the plasma parameters, cf. Table 1, results in a conductivity $\sigma \approx 1.2 \times 10^2\ \Omega^{-1} m^{-1}$. Together with equation (15) and a power density and $\varepsilon \approx 5 \times 10^{11}$ Wm^{-3} (estimated in section 6) results in a typical microwave electrical field strength $F_{mw} \approx 7 \times 10^4$ Vm^{-1}. For this rough estimation it is found that the power gained by the tail electrons from the electrical field is less than 20% of that by Coulomb collisions (cf. Table 3), so that the value of the exact field strength is not important.
The inelastic losses are given by:

$$P_{inel} = \sum_i n_e n_1 k_{1i} \Delta E_{1i} \approx n_e n_1 S_{CRM}^{2EGM} \Delta E \approx n_e n_1 S_{CRM}^{2EGM} E_{12} \tag{20}$$

In the second step it is assumed that (radiative and deexcitation) transitions back to the ground state can be neglected, i.e. that each excitation process leads to ionisation. Note that this is valid for the TIA plasmas (due to the high density of atoms in the ground state), but not for the

low pressure lamps for which the 2EGM was originally developed. In the third step we make use of the fact that in the plasmas under study step wise excitation is dominant [9,19], so that the mean value of the typical energy lost ΔE will be the excitation potential of the first excited level E_{12}. The ionisation coefficient for a 2EGM EEDF (S_{CRM}^{2EGM}) is related to the ionisation coefficient for a Maxwellian EEDF [9]:

$$S_{CRM}^{Maxw}\left(\hat{T}_e\right) = 7.34\times10^{-15}\sqrt{\hat{T}_e}\,exp\left(-\frac{12.06}{\hat{T}_e}\right) \quad [m^3s^{-1}] \tag{21}$$

which is valid for the temperature range $0.6 < \hat{T}_e < 2.2$ eV.
However, it is not correct to replace only the electron temperature in the expression for S_{CRM}^{Maxw} by the tail temperature, since in this case the number of electrons in the tail is underestimated. To correct for this S_{CRM}^{Maxw} should also be multiplied with C_t:

$$S_{CRM}^{2EGM}\left(T_b, T_t\right) = \left(\frac{T_t}{T_b}\right)^{3/2} exp\left(\frac{E_2}{k_B T_t} - \frac{E_2}{k_B T_b}\right) S_{CRM}^{Maxw}\left(T_t\right) \tag{22}$$

Using the equations given above, the tail temperature and the ionisation coefficient can be calculated, provided that the bulk temperature and the electron density are known.
The electron densities were measured using Thomson scattering. As discussed in [2] this technique is not able to detect deviations from Maxwell at high energies. Therefore, we assume that the measured electron temperatures equal the temperatures of the bulk electrons.
The results of the calculations are given in Table 3. The tail of the EEDF is underpopulated with respect to a Maxwellian distribution based on the (measured) electron temperature.

		argon in air	argon in argon
n_e	[m^{-3}]	2.5×10^{21}	1.5×10^{21}
T_h	[K]	800	500
$\hat{T}_b = \hat{T}_e$	[eV]	2.0	1.5
$\hat{T}_t$	[eV]	1.40	1.00
$\hat{T}_t / \hat{T}_b$		0.70	0.67
P_F / P_{Coul}		0.14	0.18
S_{CRM}^{2EGM}	[$m^{-3}s^{-1}$]	1.1×10^{-17}	1.1×10^{-18}
$S_{CRM}^{2EGM} / S_{CRM}^{Maxw}$		0.44	0.37
$n_1 S_{CRM}^{2EGM}$	[MHz]	100	16
ν_{diff}	[MHz]	0.16	0.08

***Table 3**: The results of the 2EGM applied to argon plasmas created by the TIA. The calculated ionisation frequency is relatively sensitive to the bulk (or electron) temperature: a 5% temperature change results in typically a 35% change in S_{CRM}^{2EGM}. The influence of the electron density, which determines T_b/T_t, via the ionisation degree, is less important: a 10% increase in n_e results in a 4% increase in S_{CRM}^{2EGM}.*

However, the influence on the ionisation coefficient is not very large: for the conditions listed in Table 1, the ionisation frequency is only a factor of 0.4 lower, so that deviations from Maxwell can not explain the imbalance between ionisation and loss processes of electron in argon plasmas created by the TIA. It should be noted that the resulting ionisation coefficient depends strongly on the bulk (or electron) temperature (a 5% change in T_b results in a 35% change in S_{CRM}^{2EGM}), since this temperature determines the threshold value $f^{2EGM}(E_2)$.
It should be noted that the underpopulation of the tail of the EEDF with respect to Maxwell, which is found here, is not in agreement with the results of Huang *et al.* [20]. They claim to have measured an overpopulation in the tail of the EEDF in a similar microwave plasma torch. However, according to our opinion it is not straightforward to detect deviations in the tail of the EEDF using Thomson scattering, since this weak signal is disturbed by (the shot noise of) stray light from the nozzle of the torch.

6. The electron energy balance

A thorough investigation of the measurements and the diffusion and ionisation terms shows that there is still an imbalance between the production and loss terms on the electron particle balance. In this section a different approach is used to determine the production (or loss) frequency of the electrons in the TIA plasma: the electron energy balance.
In a strongly ionising plasma, like the TIA, the power gained by the electrons in the microwave field is (almost) completely used for the creation of new free electrons:

$$\varepsilon_{mw} = \frac{P_{mw}}{V} = n_e n_1 S_{CRM} I_1 = n_e \nu_{ion} I_1 \tag{23}$$

From this simplified electron energy balance it is possible to determine the ionisation frequency

$$\nu_{ion} = \frac{1}{n_e I_1} \frac{P_{mw}}{V} \tag{24}$$

The plasma volume V can be estimated by assuming that the plasma has the shape of a (hollow) cone, cf. Figure 5. The volume is given by:

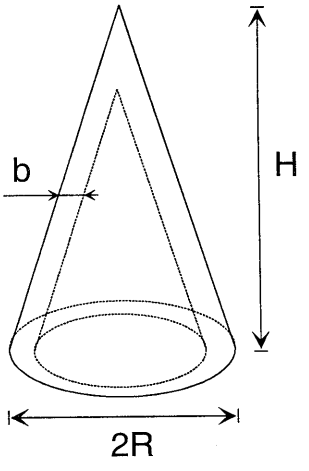

***Figure 5**: The simplified shape of the plasma in order to estimate its volume.*

$$V = \pi RHb \tag{25}$$

Substitution of the typical dimensions: height H = 10 mm, radius R ≈ 0.88 mm (the radius of the nozzle) and a typical width b equal to the gradient length of the electron density profile Λ_n = 0.07 mm, results in a plasma volume of 2 mm^3. For the applied power P_{mw} = 1.0 kW this results in the power density $\varepsilon_{mw} = 5 \times 10^{11}$ Wm^{-3}, which is used in the previous section to estimate the electrical field strength. If we assume that the average electron density in this plasma volume equals 2×10^{21} m^{-3} (cf. Figure 4), the production rate according to equation (24) equals 100 MHz, which is in good agreement with the calculated production frequency (94 MHz, see Table 3). Therefore, we have to conclude that the production frequency as determined in the previous section is correct and since it is more than two orders larger than the losses due diffusion, an other mechanism has to be responsible for the destruction of the electrons.

7. Molecular ions

The presence of molecular ions offers a fast destruction channel for electrons via dissociative recombination (DR):

$$X_2^+ + e \xrightarrow{DR} X + X^* \tag{26}$$

Possible ways to form molecular ions are charge transfer (CT) with a foreign molecule, such as N_2:

$$Ar^+ + N_2 \xrightarrow{CT} Ar + N_2^+ \tag{27}$$

and the formation of molecular rare gas ions (MRI):

$$Ar^+ + Ar + Ar \longrightarrow Ar_2^+ + Ar \tag{28}$$

The influence of nitrogen on the plasmas was discussed in the previous chapter [4]. The formation of MRI is favoured by the high pressure and the low gas temperature. The electron loss frequency due to this MRI channel has to be calculated by taking more processes into account than the formation and the DR of Ar_2^+ [5]. Especially dissociation by atom impact, the inverse reaction of (28), or by electron impact plays an important role as well. For a

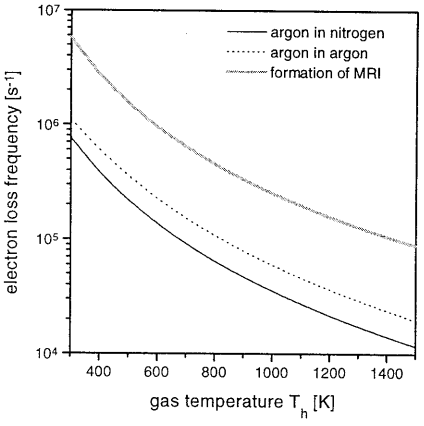

***Figure 6**: The electron loss frequency due to the formation and destruction of Ar_2^+ as a function of the gas temperature [5]. The curves "argon in air" and "argon in argon" corresponds to the plasma conditions as given in the second and third column of Table 1, respectively. The grey line represents the loss frequency in case the formation of Ar_2^+, cf. equation (28), would have been the bottle-neck.*

complete outline we refer to chapter 7 [5]. The resulting electron loss frequency for the conditions as present in the TIA is depicted in Figure 6. The electron loss frequency is strongly dependent on the gas temperature and equals around 10^5 Hz for the conditions of interest (T_h = 500 to 800 K, see also Table 1). Although this loss channel is much faster than the diffusion (typically 10^4 Hz, cf. Table 1), it is by far not sufficient to be significant for the particle balance, since the production terms are around 10^7 to 10^8 Hz (cf. Table 3).

8. Conclusions

The results of the spatially resolved Thomson scattering measurements presented in the previous chapter are correct: no significant heating of the electrons could be found and the size of the plasma is apparently measured correctly. From these measurements it can be concluded that the diffusion gradient length is very small: 0.06 mm. However, in spite of this steep gradient the diffusion is not fast enough to explain the huge production of electrons, which corresponds to the measured electron temperature. Other calculations show that the EEDF is probably not Maxwellian, and the number of electrons in the tail is considerably lower than the equilibrium value corresponding to the bulk temperature T_e. This lowers the ionisation frequency by a factor of 0.4 to a value which is confirmed by the electron energy balance. However, this production frequency is still higher than the losses is predicted by classical ambipolar diffusion theory. One alternative process of volume recombination, the formation and destruction of Ar_2^+, is also found to be insignificant. Therefore, we have to conclude that the most serious candidate to solve this problem is turbulent mixing of the plasma with the surrounding air.

References

1. Chapter 2: J. Jonkers, H.P.C. Vos, J.A.M. van der Mullen and E.A.H. Timmermans, Spectrochim. Acta B **51** 457 (1996).
2. Chapter 3: J. Jonkers, J.M. de Regt, J.A.M. van der Mullen, F.P.J. de Groote, H.P.C. Vos and E.A.H. Timmermans, Spectrochim. Acta B **51** 1385 (1996).
3. Chapter 5: J. Jonkers, L.J.M. Selen, J.A.M. van der Mullen, E.A.H. Timmermans and D.C. Schram, Plasma Sources, Sci. and Techn. **6** 533 (1997).
4. Chapter 8: J. Jonkers, A. Hartgers, L.J.M. Selen, J.A.M. van der Mullen and D.C. Schram, *"The influence of nitrogen entrainment on argon plasmas created by the Torche à Injection Axiale"*
5. Chapter 7: J. Jonkers, J.A.M. van der Mullen and D.C. Schram, *"The role of molecular rare gas ions in atmospheric plasmas"*
6. J.M. de Regt, *"Fundamentals of inductively coupled plasmas: a spectroscopic study"*, Ph.D. Thesis, Eindhoven University of Technology (1996).
7. P. Jauernik, *"Thomsonstreulichtmessung der räumlichen Verteilung der Temperatur und Dichte eines Niederdrucklichtbogenplasmas mit hilfe eines Vierkanalspektrometers"*, Ph.D. Thesis, University of Düsseldorf (1986).
8. J.M. de Regt, R.A.H. Engeln, F.P.J. de Groote, J.A.M. van der Mullen and D.C. Schram, Rev. of Sci. Instrum. **66** 3228 (1995).

9. Chapter 6: J. Jonkers, J.A.M. van der Mullen and D.C. Schram, *"On the differences between atmospheric, strongly ionising helium and argon plasmas"*, submitted to Phys. Rev. E.
10. C.R. Vidal, J. Cooper and E.W. Smith, Astrophys. J. suppl. **25** 37 (1973).
11. A. Czernichowski and J. Chapelle, Acta Phys. Pol. A **63** 67 (1983).
12. J.M. de Regt, F.P.J. de Groote, J.A.M. van der Mullen and D.C. Schram, Spectrochim. Acta B **51** 1371 (1996).
13. Chapter 4: J. Jonkers and J.A.M. van der Mullen, *"On the excitation temperature in helium plasmas"*, submitted to J. Quant. Spectrosc. Radiat. Transf.
14. L. Vriens, J. Appl. Phys. **44** 3980 (1973).
15. F.A.S. Ligthart and R.A.J. Keijser, J. Appl. Phys. **51** 5295 (1980), in contrast to the present paper the expressions by Lighthart and Keijser are *not* given in SI units.
16. J.F. Waymouth, *"Electric discharge lamps"*, The M.I.T. Press, Massachusetts (1971).
17. J. Maya and R. Lagushenko in *"Advances in atomic, molecular and optical physics"*, D. Bates and B. Bederson (editors), **26** 321 (1989).
18. M. Mitchner and C.H. Kruger, *"Partially ionized gases"*, Wiley & sons, New York (1973).
19. J.A.M. van der Mullen, Phys. Rep. **191** 109 (1990).
20. M. Huang, D.S. Hanselman, Q. Jin and G.M. Hieftje, Spectrochim. Acta B **45** 1339 (1990).

10

Absorption measurements on a low pressure, inductively coupled, argon/mercury discharge for lighting purposes: 1. Gas temperature and argon metastable density

J. Jonkers, M. Bakker and J.A.M. van der Mullen, J. Phys. D: Appl. Phys. **30** 1928 (1997).

The gas temperature and the absolute density of the argon $4s^3P_2$ level in an 80 W inductively coupled low pressure argon/mercury plasma are determined for three different argon filling pressures. This is done by measuring the line profile of the $4s^3P_2 \rightarrow 4p^3D_3$ transition in argon, using a tuneable laser diode. Since the width of this argon line is found to depend on the kinetic heavy particle temperature only, radial profiles of the gas temperature can be obtained. It turns out that the maximum gas temperature in this discharge (550 to 810 K depending on the filling pressure) is significantly higher than that in a common tubular fluorescent lamp. From the radial distribution of the argon 4s density it can be concluded that the maxima of the electron density and of the electron temperature are situated close to the coil. It is also found that the position of these maxima depends on the argon filling pressure.

1. Introduction

There is an increasing interest in electrodeless lamps because reactions between the electrodes and the plasma are avoided. Owing to this the life time is considerably longer than that of conventional discharge lamps and the choice of the filling is less restricted.

One special class of electrodeless lamps is that formed by the inductive fluorescent lamps. For some years commercial lamps of this type have been available: the "QL-lamp" of Philips since 1992 and the "Genura" of General Electric since 1994 [1]. Recently the third major lighting company Osram Sylvania announced the "Endura", which will be available around 1998. With respect to the mechanism of light generation these lamps are similar to the well known tubular lamp. Inside a fluorescent lamp mainly UV radiation is created which is converted into visible light by a fluorescence powder, which is situated at the wall of the bulb [2,3]. However, a main difference between the electrodeless and the conventional fluorescent lamps is (besides the lack of electrodes) the plasma current. A typical current in the tubular lamp is 400 mA, which is much lower than that in the inductively coupled lamps: 5 to 10 A.

During the last decade all major lighting companies presented models in which the inductive lamp is described as a relatively simple one-dimensional transformer [1,4,5,6,7]. In these models the plasma is assumed to be similar to that of the tubular lamp. For instance a zeroth-order Bessel function is taken as the radial electron density profile, according to the theory of Schottky [8]. This is a reasonable assumption for the conventional tubular lamps, but highly questionable for inductively coupled lamps. It fixes the position of the maximum of the electron density halfway the radius, whereas most of the power is dissipated much closer to the coil.

Most of the experimental work on inductive lamps deals with measurements on *global* (plasma) parameters [1,4,6,7], such as the total impedance of the coil or the efficacy (the efficiency of a light source taking the eye sensitivity curve into account [2,3]). However, experimentally obtained *local* plasma parameters, like the electron density and temperature, are needed for a proper understanding.

In this paper measurements of the local gas temperature in the QL-lamp are presented. Using a tuneable diode laser radial temperature profiles for several argon filling pressures are obtained by measuring the absorption profile of the argon $4s^3P_2 \rightarrow 4p^3D_3$ transition (811.531 nm). This technique is based on the fact that Doppler broadening is the dominant broadening mechanism

for this line, so that its width is directly related to the kinetic temperature of argon atoms in the $4s^3P_2$ state. This temperature is assumed to be equal to the gas temperature.
Since the wall temperature varies between 400 and 500 K, it is expected (and found) that the gas temperature in this lamp is significantly higher than inside the conventional tubular lamp. In this case the wall temperature equals approximately 315 K and the maximum gas temperature is typically 360 K [2,9].
Another parameter which can be deduced from these measurements is the density of the argon metastable $4s^3P_2$ state. In a next paper this density and the gas temperature will be used to determine the electron temperature and density.

2. The Philips QL-lamp

The QL-lamp consists of a coil of 15 windings with a ferrite core (the antenna) surrounded by a bulb, cf. Figure 1. An RF generator (not depicted) feeds the coil with an alternating current of 2.65 MHz and an amplitude of typically 1 A. This induces a plasma current of approximately 10 A. The ferrite core ($\mu_r \approx 40$) enhances the coupling between coil and plasma. The power delivered by the RF generator is held constant at 80 W.
The bulb contains a mixture of argon and mercury. In this paper experiments are presented and discussed on bulbs with different argon filling pressures (33, 66 and 133 Pa at room temperature). The mercury pressure is ruled by the temperature of the amalgam which is situated at the bottom of the bulb. In steady state it equals approximately 0.8 Pa. Like in all fluorescent lamps [2,3] mercury is the active species in the lamp, which means that most of the inelastic collisions take place between free electrons and mercury atoms. This is because the energy gap between the ground state and the first excited state is much lower for mercury than for argon (4.67 versus 11.55 eV respectively). The argon has to be present as buffer gas, since otherwise the gas pressure would be too low and electrons and ions would easily diffuse to the wall, where recombination takes place.

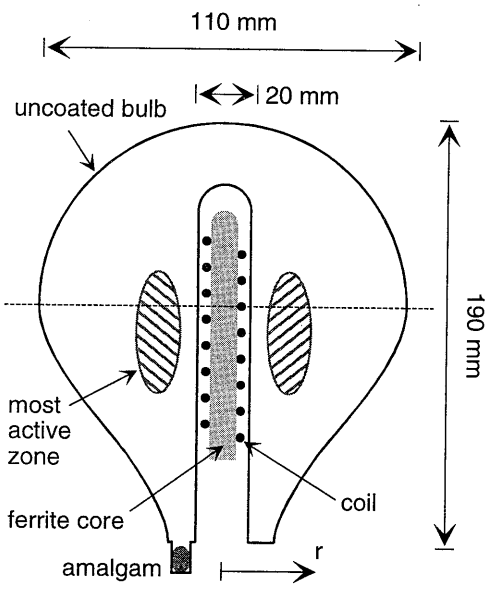

Figure 1: A schematic drawing of the Philips' QL-lamp. The horizontal dashed line indicates the median plane in which the measurements are performed. Note that in contrast with the commercially available lamps, the bulb of this test lamp is uncoated.

The plasma current is concentrated in a torus close to the coil, which is depicted as the hatched area in Figure 1. Since by far most of the power is coupled into this most active zone, it is expected that the electron temperature and density reach their maximum values at this position. This area can easily be recognised during the start up phase of the lamp. Due to the much lower mercury pressure during this phase, the mercury atoms in the most active zone are depleted [10,11] and the typical purple light emitted by argon can be observed in this area of the discharge. During steady state the density of excited argon also peaks in this region, as is shown in this paper.

3. Experimental

3.1 Diode laser setup

The setup is depicted in Figure 2. The laser beam is generated by a Sharp LT016MD0 IR diode laser, which is mounted on a Peltier element to fix the temperature within 1 mK. The wavelength of the laser depends on the diode laser current and temperature. The temperature is chosen such that the wavelength is close to the central wavelength of the argon $4s^3P_2 \rightarrow 4p^3D_3$ transition: 811.531 nm. The current through the diode laser is used for scanning the wavelength and is controlled by the computer. This current can be changed with steps of 50 μA, which corresponds to wavelength steps of $\Delta\lambda = 0.3$ pm [12].
The intensity after passing through the lamp $I_b(\lambda)$ (see Figure 2) is measured by a photo diode (BPW34), digitised and stored on the computer's hard disk for later analysis. A neutral density filter is used to avoid stimulated emission (see section 3.2). Note that the light originating from the lamp has to be subtracted. In order to minimise the contribution of this background, the photo diode is positioned as far away as possible from the lamp (approximately 1 m).

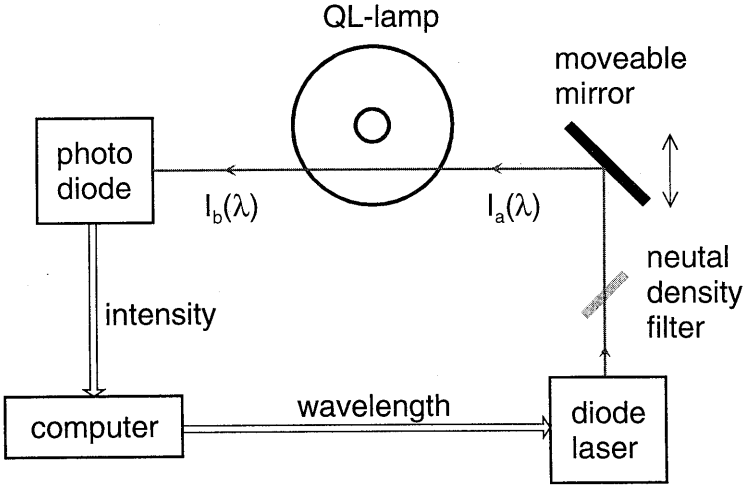

***Figure 2**: The diode laser setup. Wavelength scans can be performed automatically with a computer which controls the resonance wavelength of the laser diode and records the remaining intensity (after the beam has passed through the lamp). Before the beam enters the lamp its intensity is decreased by a neutral density filter to avoid stimulated emission (see text).*

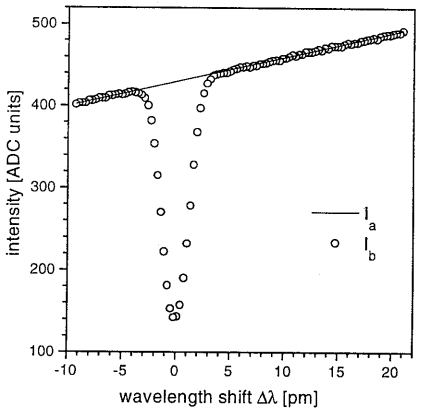

***Figure 3**: A typical wavelength scan. The measured intensity I_b is depicted by the open circles; the full line represents the fitted intensity without any absorption I_a. The horizontal scale represents the shift with respect to the central wavelength: 811.531 nm.*

A typical result is depicted in Figure 3. The bandwidth of the laser (< 0.1 pm [12]) is much smaller than the typical width of the absorption signal (3 pm), so that an apparatus profile deconvolution procedure is not needed. The absorption results in a dip on an otherwise straight line. The slope of this line is not equal to zero since the diode laser current not only changes the wavelength of the laser beam but also its intensity. The incident intensity $I_a(\lambda)$ is obtained from a linear fit to the intensities shifted away at least 6 pm from the central wavelength (see Figure 3).

3.2 Line areas and profiles

The intensity of the laser beam after it has passed through the lamp equals:

$$I_b(\lambda) = I_a(\lambda)\, exp\left[-\tau_{ab}(\lambda)\right] \tag{1}$$

in which the optical depth $\tau_{ab}(\lambda)$ is the integral of the absorption coefficient $\kappa_x(\lambda)$ over the "line of sight":

$$\tau_{ab}(\lambda) = \int_a^b \kappa_x(\lambda)\mathrm{d}x \tag{2}$$

The absorption coefficient [13]

$$\kappa(\lambda) = \frac{\lambda_0^4 A}{8\pi c}\frac{g_{4p}}{g_{4s}}\left(1 - \frac{g_{4s}}{g_{4p}}\frac{n_{4p}}{n_{4s}}\right) n_{4s}\phi(\lambda) \tag{3}$$

depends on the density of the lower state n_{4s} and its statistical weight g_{4s}. The central wavelength of the transition is represented by λ_0 and A is its transition probability for spontaneous emission (0.331×10^8 s^{-1} [14]). The area of the "line shape function" $\phi(\lambda)$ is normalised to 1. The second term between brackets in equation (3) represents stimulated emission and is only important if the density n_{4p} per statistical weight g_{4p} of the upper level becomes comparable with that of the lower level: n_{4s}/g_{4s}. For low intensities of the laser beam we assume that this is not the case, so that equation (3) directly links the absorption coefficient to the density of the lowest excited state of argon. However, at higher laser intensities the population of the 4p level will increase (due to the absorption) and the contribution of stimulated emission becomes significant. In this case the absorption

coefficient is a function of the laser power, since n_{4p} will depend on the intensity. It is found that a neutral density filter is needed to reduce the laser power (of about 30 mW) 50 times.
In general the shape of the absorption profile $\phi(\lambda)$ is mainly effected by three mechanisms:

1. Stark broadening, which is due to the interaction between the bound and the free electrons, results in a Lorentzian absorption profile with a full width at half maximum of [15] (in SI units):

$$\Delta\lambda_S = 2\times10^{-22} n_e w\left[1+5.5\times10^{-6}\alpha\sqrt[4]{n_e}\left(1-6.8\times10^{-3}\frac{\sqrt[6]{n_e}}{\sqrt{T_e}}\right)\right] \quad (4)$$

   In which α and w are the ion broadening parameter (approximately 0.021) and the electron impact parameter (5.5 pm) respectively. For typical conditions inside the QL-lamp (n_e = 3 $\times 10^{19}$ m^{-3} and T_e = 15000 K) this formula predicts a Stark width of about 0.033 pm.
2. Van der Waals or pressure broadening results from the interaction between atoms and molecules and it can be estimated by [16]

$$\Delta\lambda_V = \gamma n_a \quad (5)$$

   The Van der Waals broadening coefficient γ equals around 5×10^{-27} nm/m^{-3} [12,17], so that this effect results in a maximum broadening of 0.16 pm (for 133 Pa filling pressure).
3. Doppler broadening, which stems from the thermal motion of the atoms, results in a Gaussian shaped absorption profile with a full 1/e width given by [13,15]:

$$\Delta\lambda_D = \lambda_0\sqrt{\frac{8k_B T_g}{m_{Ar}c^2}} \quad (6)$$

   in which m_{Ar} represents the mass of an argon atom. This equation predicts a Doppler broadening of 2.7 pm for an argon gas of 600 K.

Thus Doppler broadening is by far the most significant broadening process. This means that the line shape function $\phi(\lambda)$ is to a good approximation a Gaussian, which width is related to the gas temperature by equation (6).

3.3 Procedure

In order to obtain the local gas temperature and 4s density Abel inversion has to be performed. This technique is well known for emission experiments to deduce the (cylindrically symmetric) local emission coefficient j from measurements of the lateral intensity I [18]. These two quantities are related to each other via

$$I_{ab}(\lambda) = \int_a^b j(\lambda, x)dx \quad (7)$$

So in fact Abel inversion is the inverse process of the integration over the line of sight. In case of absorption experiments the integration of the *local* absorption coefficient over the "line of sight" equals the *laterally* obtained optical depth (cf. equation 2). Therefore not the measured intensity after passing through the lamp $I_b(\lambda)$ is Abel inverted but the corresponding optical depth

$$\tau_{ab}(\lambda) = ln\left[\frac{I_a(\lambda)}{I_b(\lambda)}\right] \quad (8)$$

By performing this Abel inversion separately for each wavelength the local absorption coefficient is obtained, as a function of the wavelength. After this the 4s density and the gas temperature can be determined from the area and the width (of the Gaussian) respectively. However, Abel inversion usually increases the noise on the data points. In our case the absorption profile is relatively small so that there are not enough points for an accurate fit after Abel inversion. Therefore, we apply a different procedure to determine the gas temperature and the 4s density.

As stated before the local absorption profile is almost a pure Gaussian, since Doppler broadening is the dominant broadening process. Since the temperature gradients are not very large (see section 4), the widths of the line profiles do not vary a lot along the line of sight. Moreover, the variation in line width is even smaller than the variation in temperatures, because the width of the Gaussian is proportional to the square root of the gas temperature, see equation (6). Thus the lateral wavelength profile, being the "summation" of Gaussians with approximately the same shape, results in almost a Gaussian as well. This can be seen in Figure 4, where the Gaussian shape appears to be a good fit to the lateral measurement of the line profile.

Using a Gaussian fit the area and the width can be determined for each lateral measurement. By performing Abel inversion on the (laterally measured) areas local values for the 4s density of argon are obtained. However, the local gas temperature can not be calculated from Abel inversion of the widths of the lateral profiles, since the width is not an additive quantity, i.e. the width of the lateral wavelength profile is not an integral of the local widths over the line of sight. Fortunately, the width of a Gaussian is proportional to the quotient of its area and its height, and these are both additive quantities. So by performing Abel inversion on the area and the height of the lateral absorption profiles local values are obtained for the 4s density and the gas temperature.

An other problem is the scatter of the values for the width and the height of the lateral measurements. As discussed previously, Abel inversion increases the noise on the data points. Especially the noise on the points close to the centre is increased drastically. In order to obtain values with an acceptable accuracy, the lateral measurements of the width and the height of the absorption profiles have to be smoothed by fitting a fifth-order polynomial through the

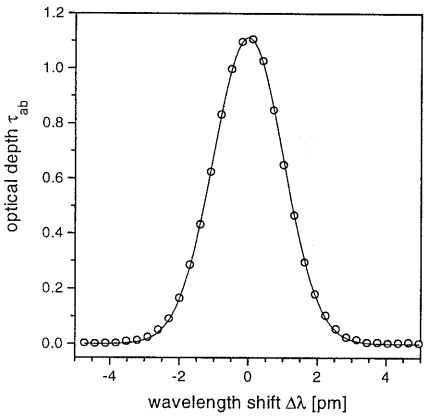

***Figure 4**: A typical lateral absorption profile (open circles). The full line is a Gaussian fit to obtain the area and the height. This figure is obtained from the data of Figure 3.*

data points. This also allows us also to extrapolate to the outer plasma edge (at r = 54 mm), where it is difficult to do measurements as the laser beam is close to grazing incidence on the glass lamp housing and the laser beam is distorted.
The absorption profile is determined every 1 mm for r between 10.5 and 47.5 mm. The lower limit for the lateral range is set to 10 mm by the inner wall of the bulb, see Figure 1. Note that the extrapolation to the outer wall will not introduce large errors, since the 4s density in this region is low.

4. Results

In Figure 5 the density of the argon $4s^3P_2$ state is plotted as a function of the radial position for three values of the argon filling pressure. At higher pressures only a part of the radial distribution is depicted, since the noise due to Abel inversion in the other points is too large.
The trend that the density of the excited argon is lower at higher filling pressures (namely, at higher argon densities) is opposite to that which might be expected. However, the energy gap between the ground state and this first excited state is very large (11.55 eV), so that small changes in the electron temperature will influence the 4s density drastically.
An other trend which can be observed in Figure 5 is that for increasing filling pressure the maximum of the radial density profile shifts inwards (from r = 22.5 mm at 33 Pa to 17.5 mm at 133 Pa). Since this density reflects the electron density and temperature, this means that the most active zone (see Figure 1) is situated closer to the coil at higher filling pressures. As a result the coupling between coil and plasma [1,4,6,7] will be better at higher filling pressures[a].
After Abel inversion of the height of the lateral absorption profiles, the gas temperature can be calculated from the quotient of the local area and height. The result is depicted in Figure 6. For each filling pressure only a part of the radial profile is shown. This is because the result is obtained from the quotient of the Abel inverted height and area, which introduces extra

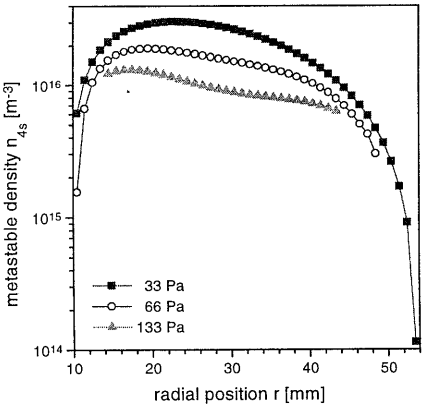

***Figure 5**: The radial density profile of argon in the $4s^3P_2$ state for three different argon filling pressures. The RF input power equals 80 W. The walls of the bulb are situated at 10 and 54 mm (see Figure 1).*

[a] As is discussed in the next chapter the argon metastable density is much more sensitive to the electron temperature. An impression of the radial electron density profile can be obtained from the gas temperature profile, see Figure 6, which shows that the maximum is situated more to the outside for higher argon filling pressures, resulting in a less efficient coupling.

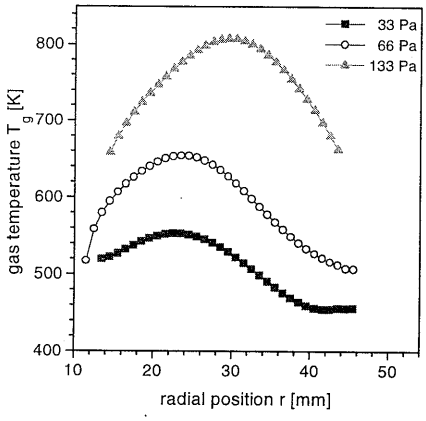

***Figure 6**: The gas temperature as a function of the radial position for three different argon filling pressures. The distributions are depicted only partially, because of the large inaccuracies due to the two Abel inversion procedures (see section 3.3).*

inaccuracies.

As expected, the gas temperatures are significantly higher than the typical gas temperature in the tubular lamp (360 K [2,9]). This is probably due to the higher plasma current and therefore higher electron density. From Figure 6 it can also be concluded that the higher the filling pressure the higher the gas temperature. This is because at higher argon density the number of collisions between the free electrons and the heavy particles increases, whereas the heat conductivity of argon is independent of the gas density.

5. Conclusions

Radial profiles of the gas temperature and the argon 4s density in Philips' QL-lamps are presented as functions of the argon filling pressure at constant RF power (80 W). The maximum temperature (550 K at 33 Pa to 810 K at 133 Pa filling pressure) is significantly higher than the maximum temperatures found in the conventional tubular lamp (361 K at 466 Pa). This is most likely due to a much higher electron density in the QL-lamp.

From the argon 4s density profiles it can be concluded that the maximum of the electron density and temperature is situated close to the coil, probably there where most of the power is dissipated. This is in contrast with the simple models presented in various other papers. At higher argon filling pressures this maximum shifts closer to the coil, which causes an increase in the coupling between the plasma and the coil.

References

1. D.O. Wharmby and S.-A. El-Hamamsy, Proceedings of the 7th International Symposium on the Science and Technology of Light Sources, Kyoto Japan, p27 (1995).
2. J.F. Waymouth, *"Electrical discharge lamps"*, The MIT Press, Massachusetts (1971).
3. W. Elenbaas, *"Light sources"*, The MacMillan Press Ltd., London (1972).
4. J.W. Denneman, J. Phys. D: Appl. Phys. **23** 293 (1990).
5. G.G. Lister and M. Cox, Plasma Sources, Sci. and Techn. **1** 67 (1992).
6. R.B. Piejak, V.A. Godyak and B.M. Alexandrovich, Plasma Sources, Sci. and Techn. **1** 179 (1992).
7. V.A. Godyak, R.B. Piejak and B.M. Alexandrovich, J. Illum. Eng. Soc. **23** 40 (1994).

8. W. Schottky, Phys. Z. **25** 635 (1924).
9. C. Kenty, M. Easley and B.T. Barnes, J. Appl. Phys. **22** 1006 (1951).
10. W. Uyterhoeven, Philips Techn. Rev. **3** 197 (1938).
11. D.Y. Fang and C.H. Huang, J. Phys. D: Appl. Phys. **21** 1490 (1988).
12. J.M de Regt, R.D. Tas and J.A.M. van der Mullen, J. Phys. D: Appl. Phys. **29** 2404 (1996).
13. M. Mitchner and C.H. Kruger, *"Partially ionised gases"*, Wiley Interscience, New York (1973).
14. W.L. Wiese and G.A. Martin, *"Wavelengths and transition probabilities for atoms and atomic ions"*, part 2: *"Transition probabilities"*, U.S. Government Printing Office, Washington (1980).
15. H. Griem, *"Spectral line broadening by plasmas"*, Academic Press, New York (1974).
16. V.W. Lelevkin, D.K. Otorbaev and D.C. Schram, *"Physics of non-equilibrium plasmas"*, North-Holland Amsterdam (1992).
17. K. Tachibana, H. Harima and Y. Urano, J. Phys. B: At. Mol. Phys. **15** 3169 (1982).
18. C.A. Kak and M. Slaney, *"Principles of computerized tomographic imaging"*, IEEE Press, New York (1988).

11

Absorption measurements on a low pressure, inductively coupled, argon/mercury discharge for lighting purposes: 2. Electron density and temperature

J. Jonkers, J.A.M. van der Mullen, J. van Dijk, M. Bakker and D.C. Schram

Typical values for the electron density and temperature in the QL lamp are obtained from the radially resolved measurements of the gas temperature profile and the density of the lowest argon metastable state, as presented in the previous chapter. The results agree very well with the electron density and temperature as found by the size-stabilised plasma theory of chapter 6, which has been adapted to describe the argon/mercury discharge. For increasing argon filling pressure a lower electron temperature and a higher electron density are found, which are due to an increased residence time of the charged particles.

1. Introduction

In the previous chapter [1] Diode Laser Absorption (DLA) measurements were presented, from which the argon $4s^3P_2$ metastable density and the gas temperature were obtained, both as function of the radial position. Measurements were performed at fixed RF power (80 W) and for three different argon filling pressures: 33, 66 and 133 Pa.

In this chapter we will deduce the electron density n_e and temperature T_e from these results. This is possible since the argon metastable state is mainly populated via inelastic electron collisions and the gas is heated by elastic electron collisions, so that n_e and T_e can be obtained by solving a set of two equations (cf. section 2). In this chapter we focus on the center of the most active zone, i.e. where the electron density reaches its maximum value, which is assumed to coincide with the maximum of the measured gas temperature. This center is situated at r_{max} from the axis of the plasma, with see Figure 1.

The electron density and temperature can also be determined using the theory of chapter 6 [2], i.e. solving the electron particle and energy balances. It is found that n_e and T_e depend on the characteristic size of the plasma Λ, the power density ε and the argon and mercury pressures p^{Ar} and p^{Hg}. We will refer to this as the "size-stabilised plasma theory". In chapter 6 this theory was applied to atmospheric helium and argon plasmas. Since the QL-plasma is mainly a mercury discharge (with argon as buffer gas), the various terms of the electron particle and energy balance have to be adjusted. This is discussed in section 3. It is found that the values of n_e and T_e found by both methods agree fairly well.

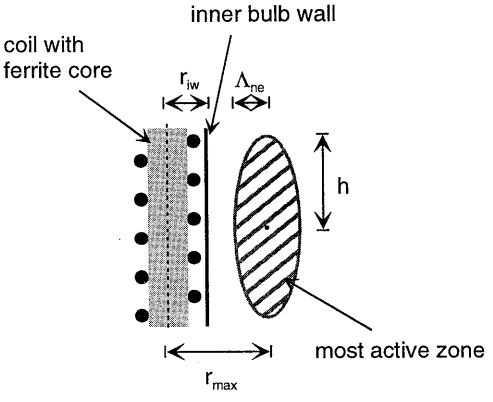

***Figure 1**: A schematic of the most important part of the QL-lamp. This chapter deals with the electron density and temperature in the center of the most active zone (denoted by a black dot). A drawing of the complete lamp can be found in chapter 10.*

2. The absorption measurements

In this section we use the experimental results of chapter 10 [1] to determine the electron density and temperature. The electron density is obtained from the heavy particle energy balance, which states that the heavy particles are heated by collisions with the electrons and cooled by heat conduction to the walls. The value of this heat conduction term can be estimated from the measured gas temperature profiles, cf. section 2.1.
An other result of chapter 10 is the density of the lowest argon $4s^3P_2$ metastable state n_2^{Ar} from which the electron temperature can be deduced by taking the ratio of this density with that of the argon ground state n_1^{Ar} and using a Collisional Radiative Model (CRM), see section 2.2.
It is found that both equations (the heavy particle balance and the ratio n_2^{Ar} / n_1^{Ar}) depend on T_e and n_e. This makes an iterative procedure necessary, which is discussed in section 2.3. In the same section the results and their sensitivity to the assumptions and to the inaccuracies of the measurements and the model are presented.

2.1 Heavy particle energy balance

The heavy particles are heated by the free electrons via elastic collisions and cooled by conduction of heat to the wall. This is described by the energy balance of the heavy particles:

$$n_e n^{Ar} \left\langle \sigma^m_{e-Ar} v_e \right\rangle \frac{2m_e}{m_{Ar}} \frac{3}{2} k_B T_e = -\nabla(\kappa \nabla T_h) = \frac{\kappa}{\Lambda^2_{Th}} T_h \qquad (1)$$

in which κ represents the heat conductivity (0.030 $Wm^{-1}K^{-1}$ [3]). The gradient length of the gas temperature profile Λ_{Th} is determined from the measurements (see Figure 6 of chapter 10) using the equation

$$\frac{-T_h(r_{max})}{\Lambda^2_{Th}} \equiv \left[\frac{\partial^2 T_h}{\partial r^2} + \frac{1}{r} \frac{\partial T_h}{\partial r} \right]_{r=r_{max}}$$
$$= \frac{T_h(r_{max}+\Delta r) - 2T_h(r_{max}) + T_h(r_{max}-\Delta r)}{\Delta r^2} + \frac{1}{r_{max}} \frac{T_h(r_{max}+\Delta r) - T_h(r_{max}-\Delta r)}{2\Delta r} \qquad (2)$$

in which Δr represents the difference in radial position between two measurement points (1.0 mm). We assume that the error in the gradient obtained in this way equals 10%.
The left hand side of equation (1) represents the heating by elastic collisions between electrons and argon atoms. The cross section for momentum transfer averaged over a Maxwellian EEDF is given by [2]

$$\left\langle \sigma^m_{e-Ar} v_e \right\rangle = \left(0.084 + 0.537\hat{T}_e + 1.192\hat{T}_e^2\right) \times 10^{-14} \quad [m^3 s^{-1}] \qquad (3)$$

The influence of collisions with other heavy particles (Hg and Hg^+) can be neglected due to their much lower densities ($p^{Ar} / p^{Hg} > 10^2$).

2.2 Argon metastable density

The electron temperature is obtained from the ratio of the densities of the metastable and the ground state of argon[a]:

[a] In this section the various argon states are denoted by a number and the superscript "Ar" is dropped.

$$\rho = \frac{\eta_2}{\eta_1} = \frac{n_2}{n_1}\frac{g_1}{g_2} \tag{4}$$

where η_p represents the density of level p per statistical weight g_p. In equilibrium this ratio would have been given by Boltzmann's formula. However, as for many other plasmas this is not the case in the QL-lamp. In order to understand the global trends of ρ on the electron temperature and density, we consider a simple model of four levels: the argon atom and ion ground states (1 and +), the metastable level (2) and an other excited level (3). The interactions between these levels are depicted in Figure 2.
The population of the metastable state can be obtained from a particle balance of this state

$$n_1 n_e k(1,2) + n_3\left[n_e k(3,2) + A(3,2)\right] = n_2 n_e\left[k(2,1) + k(2,3)\right] \tag{5}$$

which states that the production of metastable atoms via electron (de)excitation and radiative decay processes equals the destruction via electron (de)excitation. Note that the diffusion of metastable states is neglected, since the corresponding time scale is much larger than the life time.
Equation (5) can be written as

$$\rho = \frac{n_2}{n_1} = \frac{k(1,2)}{k(2,1) + f \times k(2,3)} \tag{6}$$

in which the factor

$$f = \frac{k(3,+)}{k(3,+) + k(3,2) + \dfrac{A(3,2)}{n_e}} \tag{7}$$

corrects for the fact that a destruction event of the metastable state by excitation towards level 3 can be followed by a radiative or collisional backward process. For low electron density radiative decay is the most probable so that f approaches to 0 and equation (6) reduces (in theory) to

$$\rho = \frac{n_2}{n_1} = \frac{k(1,2)}{k(2,1)} = \frac{g_2}{g_1} exp\left(\frac{I_2 - I_1}{k_B T_e}\right) \tag{8}$$

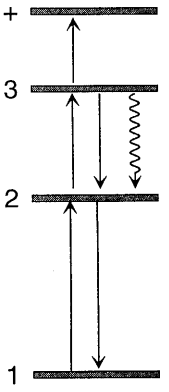

***Figure 2**: A simplified picture of the population and the depopulation processes of the metastable level. The straight and wavy arrows indicate electron induced transitions (excitation and deexcitation) and radiative decay respectively.*

i.e. the density ratio ρ is given by the Boltzmann relation. In case the electron density is higher, so that the (de)excitation processes are significant, the factor f is higher which reduces the metastable density. For increasing electron temperature this simple model predicts that the density ratio increases, since the excitation rates scale with [2,4,5]

$$k(p,q) \propto \sqrt{k_B T_e}\, exp\left(\frac{I_q - I_p}{k_B T_e}\right) \tag{9}$$

so that the rate with the largest energy gap (i.e. from ground to metastable state) increases faster than the rates with smaller energy gaps (note that the deexcitation rates hardly depend on the electron temperature).

This simple model is good enough to explain the density ratio ρ qualitatively, but not quantitatively. In reality the metastable level does not interact with only one single other excited state, but with many others. In order to take all these interactions into account we use the Collision Radiative Model (CRM) which was developed by Benoy *et al.* [6]. The density ratio ρ as calculated with this model is depicted in Figure 3 as function of the electron temperature for three different electron densities. As can be seen ρ obeys the same trends as are given above: increasing with increasing electron temperature and decreasing electron density.

The solid lines in Figure 3 represent the fit we will use to determine the electron temperature

$$log\rho = -11.73 + 4.64\hat{T}_e - 0.897\hat{T}_e^2 + 0.163 log\,\hat{n}_e + 0.452(log\,\hat{n}_e)^2 \tag{10}$$

This expression reproduces the data points of Figure 3 within 4%, which is much better than the typical accuracy of the model (20%).

Note that in the CRM model of Benoy *et al.* [6] it is assumed that the whole EEDF obeys a Maxwell distribution. It is well known that the high energy tail of the EEDF in a conventional tubular fluorescent lamp is underpopulated with respect to a Maxwellian distribution [7,8,9]. Indications for similar deviations in a pure argon plasma at atmospheric pressure were found in chapter 9 [10]. This significant underpopulation is necessary to create a large net production of fast electrons by electron-electron Coulomb collisions to compensate the losses of fast electrons due to excitation of ground state atoms. Therefore, we can state that the

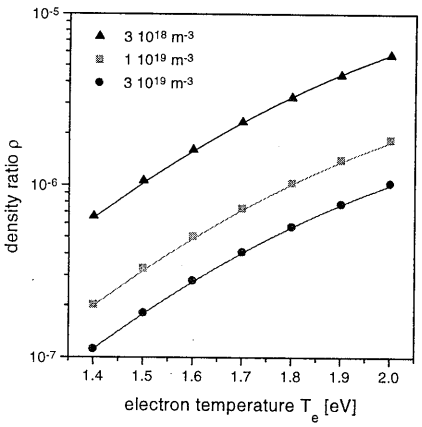

***Figure 3**: The ratio of the densities of the argon metastable and ground states as function of the electron temperature for various electron densities. The solid lines are the fits according to equation (10).*

underpopulation of the tail increases with decreasing ratio n_e / n_1. In chapter 9 indications were found that in the argon plasmas created by the TIA the number of fast electrons is a factor two lower than what is expected for a Maxwellian distribution. The ratio n_e / n_1 in this plasma equals around 1.7×10^{-4} ($n_e \approx 2 \times 20^{21}$ and $n_1 \approx 1.2 \times 10^{25}$ m^{-3} [10]), which is smaller than in the QL-lamp 1.0×10^{-3} ($n_e \approx 1.5 \times 20^{19}$ and $n_1 \approx 1.5 \times 10^{22}$ m^{-3}, cf. section 2.3), so that in the QL-lamp the deviations are even smaller than a factor two. Since the number of tail electrons depends exponentially on the electron temperature, the underestimation of the electron temperature due to this error is negligible.

2.3 Procedure and results

In the two previous sections it is shown that it is only possible to obtain the electron density when the electron temperature is known and vice versa. Therefore two coupled equations, the electron particle and energy balance, are solved iteratively, using the following steps:

1. start with $\hat{T}_e = 1.5$ eV,
2. estimate n_e from the heavy particle energy balance (1) using T_e,
3. improve the estimation of T_e by applying one bisection iteration [11] to equation (10), using the measured density of the argon metastable state and the value of n_e and
4. in case no convergence is reached, repeat from step 2.

The convergence criterion is that the inaccuracy in the electron temperature has to be smaller than 10^{-4} eV and the relative change in the electron density smaller than 10^{-3}, which is reached after typically 10 iterations.

The results are presented in Figure 4. It can be seen that for increasing argon filling pressure the electron temperature decreases whereas the electron density increases. This is a consequence of the fact that a higher argon pressure obstructs the diffusion, so that a lower production of electrons, and thus lower electron temperature, is required. Moreover, the corresponding longer residence time of the electrons in the plasma benefits the electron density [2]. A more quantitative discussion of these arguments is given in section 3.

The errors in the results are estimated from the inaccuracies of the measurements and the model and from the assumption that the argon pressure during operation equals twice the

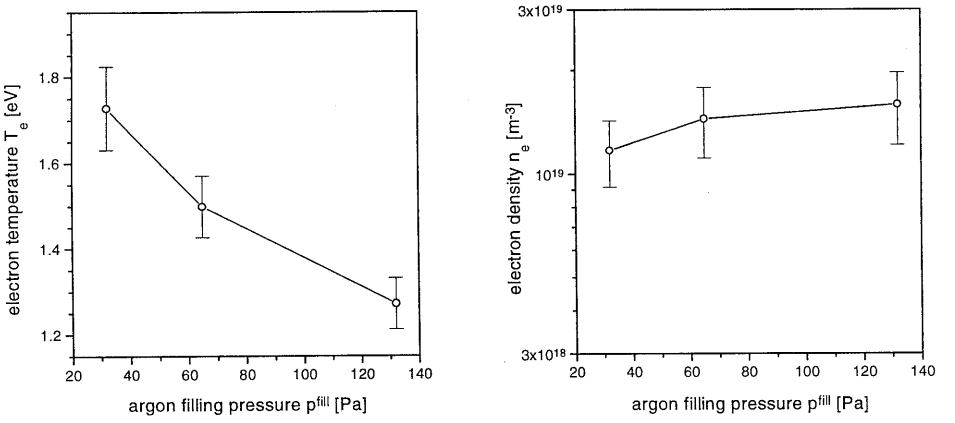

***Figure 4**: The electron temperatures and densities as determined from the results of the diode laser absorption (DLA) experiments. The error bars are estimated in Table 1.*

filling pressure [Pa]		$\Delta T_e / T_e$ [%]			$\Delta n_e / n_e$ [%]		
		33	66	133	33	66	133
p^{Ar}	$(2.0 \pm 0.3) \times p^{fill}$	3.2	2.9	2.8	6.4	7.3	7.6
$\Delta\rho$	$\pm 20\%$	2.5	2.4	2.4	7.0	6.6	6.4
Δn_2	$\pm 5\%$	0.6	0.6	0.6	1.7	1.6	1.6
ΔT_h	$\pm 10\%$	3.0	2.6	2.5	12	13	13
Δr_{max}	± 1 mm	0.0	0.0	0.0	0.1	0.0	0.0
$\Delta\Lambda_{Th}$	$\pm 10\%$	1.7	1.4	1.3	16	16	17
total		5.6	4.8	4.7	22	23	24

Table 1: *The sensitivity of the estimated electron temperatures and densities to the inaccuracies of the various assumptions for the different argon filling pressures.*

filling pressure, see Table 1. The relatively large error of the model does not result in a strong influence on the electron temperature and density. The inaccuracy of the electron temperature is also determined by Δp^{Ar} and ΔT_h which both affect the accuracy of the ground state density value. The uncertainty in n_e is mainly caused by the error in the gradient length of the gas temperature profile.

3. The size-stabilised plasma theory

In chapter 6 [2] it was shown that it is possible to obtain the electron temperature from the electron particle balance, in case that the ambipolar diffusion of ion and electrons is the dominant loss process. This condition is satisfied for atmospheric argon plasmas provided that the size is small enough. For low pressure plasmas this condition is more easy to fulfil, since a low pressure facilitates the diffusion and the corresponding low electron density makes that three particle recombination can be neglected [5,12]. With the same assumption it is also possible to calculate the electron density using the electron energy balance.
In this section we will apply this theory to the QL-lamp. Since this plasma is an argon/mercury mixture most of the terms of the particle and energy balances are different from the ones used in chapter 6. In section 3.1 the electron particle balance is adapted to the QL discharge. Section 3.2 deals with the electron energy balance. Just like in section 2 two coupled equations are found, which are solved iteratively. The results and their accuracy will be discussed in section 3.3.

3.1 Electron particle balance

In atomic low pressure plasmas the dominant loss process of the free electrons is diffusion towards the walls of the vessel, where recombination takes place. In steady state these losses have to be compensated by a production of electrons in the plasma. This is given by the (simplified) electron particle balance [2]

$$n_e n_1^{Hg} S_{CRM}^{Hg} = -\nabla\left(D_a \nabla n_e\right) \qquad (11)$$

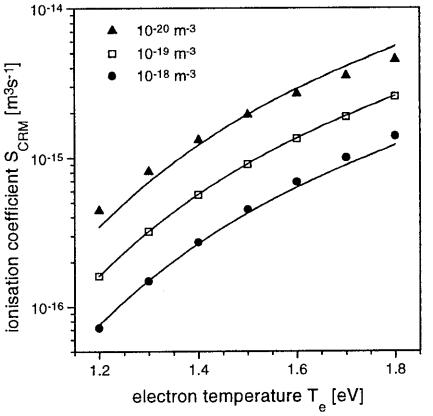

Figure 5: *The ionisation coefficient of mercury as function of the electron temperature for three different electron densities [13]. The lines represent the fit according to equation (12).*

The right hand side represents the diffusion losses, which depend on the ambipolar diffusion coefficient D_a and the gradient in the electron density n_e. The production (the left hand side) is proportional to the mercury ground state density n_1^{Hg} and the ionisation coefficient of mercury S_{CRM}^{Hg}. Only the ionisation of mercury has to be taken into account, since its ionisation potential is much lower than that of argon (10.43 versus 15.76 eV) so that mercury is by far the dominant ion [12]. The various coefficients are discussed below. Since the production depends exponentially on the electron temperature and the losses only linearly, equation (11) can be solved using the bisection method [11].

The ionisation coefficient of mercury for a Maxwellian EEDF is calculated by Herben [13] and can be reproduced by the fit

$$log\, S_{CRM}^{Hg} = \left(-27.06 + 17.83\hat{T}_e - 8.99\hat{T}_e^2 + 1.63\hat{T}_e^3\right) + 0.318\, log\left(\frac{n_e}{10^{19}}\right) \qquad (12)$$

This expression is accurate within 25% for the electron temperature range $1.2 < \hat{T}_e < 1.8$ eV and the electron density range $10^{18} < n_e < 10^{20}$ m^{-3}. The data points and the fit are given in Figure 5. In contrast with the ionisation coefficient of argon at atmospheric pressure (see Figure 1 of chapter 6) it is found that for mercury at low pressure the ionisation coefficient depends on the electron density. In atmospheric (argon) plasmas each excitation of an atom in the ground state leads to ionisation, whereas at low pressure there are two main channels after the first excitation has taken place: (step-wise) ionisation or radiative decay. The latter route is, of course, crucial for a lamp.

As discussed before [7,8,9,10] in strongly ionising plasmas an underpopulation of the tail of the EEDF can be found. In section 2.2 it is made plausible that these deviations depends on the ratio of Coulomb and inelastic collisions, i.e. in this case on n_e / n_1^{Hg}. Herben [13] used the "two electron group model" [7,8] to investigate the influence of possible deviations on the ionisation coefficient for QL-lamp conditions. He found that the systematic error is smaller than 20% provided that n_e / $n_1^{Hg} > 2.5\%$. In the QL-lamp this ratio is much larger: 9 to 45%, depending on the argon filling pressure.

The mercury density is determined by the mercury vapour pressure p^{Hg} of the amalgam which is situated at the bottom of the lamp. In the calculation of the ground state it has to be taken into account that a significant part of the mercury is ionised (see section 3.3):

$$n_l^{Hg} = \frac{p^{Hg}}{k_B T_h} - n_e \tag{13}$$

For the gas temperature the values as found by the measurements [1] are used.
The expression for the diffusion losses is obtained by simplifying the right hand side of equation (11) to

$$\nabla(D_a \nabla n_e) \approx \frac{D_a}{\Lambda_{ne}^2} n_e \tag{14}$$

The gradient length of the electron density profile Λ_{ne} is taken equal to one third of the distance from the center of the most active zone to the inner wall of the vessel (r_{max} - r_{iw}).
The ambipolar diffusion coefficient is given by the Einstein relation

$$D_a = D_+ \left(1 + \frac{T_e}{T_h}\right) \approx \mu_+ \frac{k_B T_e}{e} \tag{15}$$

where the second step is valid, since the electron temperature is much higher than the gas temperature. For mercury in argon the ion mobility μ_+ is given by Chanin and Biondi [14]:

$$\mu_{Ar}^{Hg} = 6.13 \times 10^{-2} \frac{T_h}{p^{Ar}} \approx \frac{4.44 \times 10^{21}}{n^{Ar}} \quad [m^2 V^{-1} s^{-1}] \tag{16}$$

which agrees within 7% with the expression used by Lister and Coe [3].
When the plasma is switched on the gas temperature is (much) higher than room temperature [1]. Since the lamp is a closed system this means that the argon pressure during operation p^{Ar} is significantly higher than the argon filling pressure p^{fill}. Note that due to this effect the argon density in the hottest part of the discharge, i.e. the most active zone, is lower than in the cooler parts.

3.2 Electron energy balance

The electron energy balance

$$\underset{I}{\varepsilon_{RF}} = \underset{II}{\varepsilon_{rad}} + \underset{III}{n_e n_l^{Hg} S_{CRM}^{Hg} I_l^{Hg}} + \underset{IV}{n_e n_l^{Ar} \left\langle \sigma_{e-Ar}^{m} v \right\rangle \frac{2m_e}{m_{Ar}} \frac{3}{2} k_B T_e} \tag{17}$$

describes that in steady state the electrons are heated by the electromagnetic RF field (I) and cooled by inelastic collisions, which result in radiation (II) and in ionisation (III), and by elastic collisions (IV). The various terms are discussed in more detail below. Since the last two terms at the right hand side scale with n_e whereas the others are n_e independent, the electron energy balance offers the possibility to determine the electron density.

I) The power density as dissipated by the RF field can be estimated from

$$\varepsilon_{RF} = \frac{\chi_{active} P_{RF}}{V} \tag{18}$$

in which P_{RF} is the total power of the lamp (80 W) of which a fraction χ_{active} (50%) is dissipated in the most active plasma volume V. This volume can be approximated by an elliptical torus (see Figure 1)

$$V = 2\pi r_{max} * \pi \Lambda_{ne} h \tag{19}$$

II) The first term at the right hand side, the radiation "losses" ε_{rad}, can be obtained from a Collisional Radiative Model, like the ionisation coefficient in the previous section. However, it is difficult to obtain an accurate value in this way since ε_{rad} is very sensitive to the escape factor of resonance radiation. A better approach is to use the UV conversion efficiency

$$\chi_{UV} = \frac{\varepsilon_{rad}}{\varepsilon_{RF}} \tag{20}$$

For the conventional tubular fluorescent lamp this conversion factor equals 65% [15]. However, the QL-lamp is a slightly less efficient light source than the tubular fluorescent lamp (65 lm/W versus 85 lm/W), so that we take $\chi_{UV} = (50 \pm 3)\%$.

III) The energy losses due to ionisation are given by the left hand side of the electron particle balance (11) multiplied by the ionisation energy for mercury I_1^{Hg}.

IV) The last term of equation (17) represents the kinetic energy transfer from electrons to the heavy particles. Note that it is the same as the left hand side of equation (1), i.e. the heating of the heavy particles is a loss term on the electron energy balance.

3.3 Procedure and results

As discussed in the preceding sections the electron temperature can be determined in case the electron density is known and vice versa. In order to solve these two equations we use an iterative procedure similar to the one in section 2.3:

1. start with $\hat{T}_e = 1.5$ eV,
2. estimate n_e from the electron energy balance (17) using T_e,

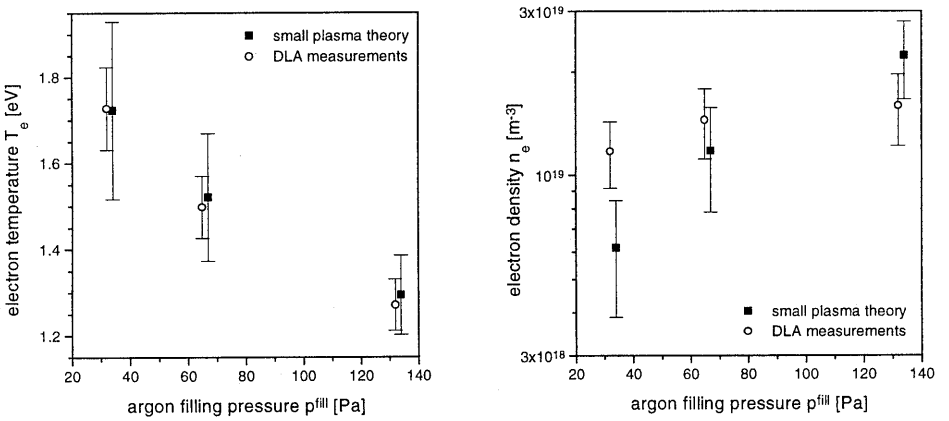

Figure 6: The electron temperature and density as estimated from the size-stabilised plasma theory. The error bars stem from the estimated inaccuracies of the model, the measurements and the used assumptions (see Table 2). For comparison the electron temperatures and densities as determined from the results of the diode laser absorption (DLA) experiments, cf. section 2.3, are also depicted. The points at the same argon filling pressure are plotted next to each other, so that the error bars do not interfere.

filling pressure		[Pa]	$\Delta T_e / T_e$ [%] 33	66	133	$\Delta n_e / n_e$ [%] 33	66	133
p^{Hg}	0.50 ± 0.10	[Pa]	5.4	5.1	4.8	5.6	5.6	6.8
p^{Ar}	(2.0 ± 0.3)	$\times p_{fill}$	4.4	3.1	1.5	18.7	16.4	9.4
ΔS_{CRM}	$\pm 20\%$		4.9	4.0	2.6	5.1	4.4	3.7
χ_{UV}	0.50 ± 0.03		0.3	0.1	0.4	6.3	6.1	5.4
χ_{active}	0.50 ± 0.10		1.1	0.3	1.3	21.1	20.2	18.1
Λ_{ne}	(0.33 ± 0.03)	$\times (r_{max} - r_{iw})$	4.8	3.6	2.0	13.6	11.9	7.3
Δr_{max}	± 1 mm		4.0	2.9	1.4	7.3	5.4	1.1
ΔT_h	$\pm 10\%$		5.5	4.5	3.3	15.5	13.8	9.6
total			12.0	9.7	7.1	37.0	33.6	25.5

***Table 2**: The sensitivity of the calculated electron temperatures and densities to the inaccuracies of the various assumptions for three argon filling pressures.*

3. improve the estimation of T_e by inserting this n_e value in the electron particle balance (11) and
4. in case no convergence is reached, repeat from step 2.

The convergence criterion is that the inaccuracy in T_e has to be smaller than 10^{-4} eV and the relative change in the electron density smaller than 10^{-3}. Convergence is reached after typically 10 iterations.

The results are presented in Figure 6. The trends are the same as found in section 2.3: a decreasing electron temperature and an increasing electron density for increasing argon filling pressure. The agreement between the temperatures as found by both methods is striking: the differences are much smaller than the estimated error bars. Also the electron densities agree fairly well with each other. It should be noted that apart from the fact that a higher argon pressure obstructs the diffusion, it is also found that the center of the most active zone is situated more to the outside so that (in our simple model) the characteristic size of the plasma Λ is larger. Both effects (lower diffusion coefficient D_a and larger Λ) benefit the residence time of the charged particles, so that the electron temperature is lower and the density higher.

The relatively large error bars in Figure 6 are due to the fact that we made some assumptions in order to be able to solve the electron particle and energy balance. These assumptions and their estimated errors are listed in Table 2 together with the inaccuracies of the measured gas temperature and center of the most active zone. It appears that the electron density is very sensitive to the exact amount of power dissipated in the most active zone (χ_{active}) and the argon pressure during operation (p^{Ar}). The electron temperature is mainly influenced by the mercury ground state density (ruled by p^{Hg} and T_h).

4. Conclusions

It is possible to determine an electron density and temperature from the radial gas temperature profile and the density of the lowest argon metastable state. Measurements of these latter two

quantities were presented in the previous chapter. The values of T_e match very good with the results obtained from solving the electron particle and energy balances, whereas the agreement between the values of n_e is fairly well. For this latter method four input parameters are necessary: the characteristic size Λ and the power density ε of the plasma and the partial pressures of the argon buffer gas p^{Ar} and of the mercury p^{Hg}.
For increasing argon pressure a lower electron temperature and a higher electron density are found, which are due to an increased residence time of the charged particles. This residence time increases with increasing buffer gas pressure because of two reasons:

1. the corresponding higher argon density obstructs the outward diffusion and
2. from the measurements it is found that the maximum of the gas temperature (and thus electron density) profile shifts outwards, so that the characteristic size increases.

References

1. Chapter 10: J. Jonkers, M. Bakker and J.A.M. van der Mullen, J. Phys. D: Appl. Phys. **30** 1928 (1997).
2. Chapter 6: J. Jonkers, J.A.M. van der Mullen and D.C. Schram, *"On the difference between ionising helium and argon plasmas at atmospheric pressure"*, submitted to Phys. Rev. E.
3. G.G. Lister and S.E. Coe, Comp. Phys. Commun. **75** 160 (1993).
4. J.A.M. van der Mullen, Phys. Rep. **191** 109 (1990).
5. M.A. Lieberman and A.J. Lichtenberg, *"Principles of plasma discharges and plasma processing"*, John Wiley & Sons, New York (1994).
6. D.A. Benoy, J.A.M. van der Mullen and D.C. Schram, J. Quant. Spectrosc. Radiat. Transf. **46** 195 (1991).
7. L. Vriens, J. Appl. Phys. **44** 3980 (1973).
8. F.A.S. Ligthart and R.A.J. Keijser, J. Appl. Phys. **51** 5295 (1980), in contrast to this paper the expressions given here are in SI units.
9. J. Maya and R. Lagushenko in *"Advances in atomic, molecular and optical physics"*, D. Bates and B. Bederson (editors), **26** 321 (1989).
10. Chapter 9: J. Jonkers, J.A.M. van der Mullen, A. Hartgers, I.A.J. Thomas and D.C. Schram, *"The Torche à Injection Axiale: remaining questions and possible answers"*.
11. E. Kreyszig, *"Advanced engineering mathematics"*, Wiley, Chichester (1993).
12. J.F. Waymouth, *"Electrical discharge lamps"*, The MIT press, Massachusetts (1971).
13. P.G.J.M. Herben, *"Towards a plasma simulation model for the Philips QL-lamp"*, M.Sc. Thesis, Eindhoven University of Technology, VDF/NT 97-29 (1997).
14. L.M. Chanin and M.A. Biondi, Phys. Rev **107** 1219 (1957).
15. M. Koedam, A.A. Kruithof and J. Riemens, Physica **29** 565 (1963).

12

General conclusions

The central theme of this thesis is a special class of small plasmas, the so-called size-stabilised plasmas. These are plasmas for which, in relation to the pressure, the dimensions are so small that in the active zone diffusion is the dominant loss process. The size of the plasma is determined by either an external wall or the combination of electric field and gas flow patterns. The conclusions of this work are listed in more detail below.

- Ordening of the class of size-stabilised plasmas is achieved by solving the electron particle and energy balances. This provides the basis for a direct relation between on the one hand the operation parameters by which the plasma is controlled externally, such as pressure, composition, power density and size, and on the other hand the internal plasma parameters, like electron density and temperature and the degree of equilibrium departure. *(Chapters 6 and 11)*

- The influence of the chemical composition of the gas can be examined using the concept of equi-operational plasmas, i.e. plasmas which are operated at identical external conditions but with different plasma gas. A comparison between atmospheric argon and helium plasmas shows that the ratio of electron temperatures is mainly determined by the ratio of the energy gaps between the ground and the first excited states and that the electron density is strongly related to the mass of the atoms (or ions). Especially due to the lower atomic mass of helium, the deviations from equilibrium are always larger in a helium than in an equi-operational argon plasma. *(Chapter 6)*

- The criterion for a size-stabilised plasmas is that diffusion is the main loss process of the charged particles. Three particle recombination of atomic ions can be neglected for a wide range of combinations of operation parameters. However, molecules can offer, via dissociative recombination, a fast volume loss channel, which limits the validity of the size-stabilised plasma theory. For atmospheric rare gas plasmas the formation of molecular ions (like for instance Ar_2^+) is found not to have a large influence on the plasma. However, there are still some uncertainties in the formation and destruction rates of these molecules, so that this picture is not complete yet. *(Chapters 6, 7 and 8)*

- In size-stabilised plasmas the Saha balance of ionisation and three particle recombination is far from equilibrium and the net ionisation flow through the atomic system is related to an overpopulation of the lower excited states with respect to their (Saha) equilibrium population densities. This overpopulation decreases with decreasing ionisation potential and above a certain level it becomes negligible. The position of this boundary can be related to the external parameters. For helium it is found that in general the observable states are strongly overpopulated with respect to Saha, so that the excitation temperature becomes level dependent and saturates to a value determined by the ionisation potential of the levels under study. *(Chapters 2, 4 and 6)*

- Application of the size-stabilised plasma theory to the atmospheric plasmas created by the "Torche à Injection Axiale" (typical sizes: 2 mm in diameter and 15 mm long) results in higher electron densities and much lower temperatures than are obtained using Thomson scattering. For a correct estimation of the diffusion losses radially resolved measurements are necessary. The difference between the theoretical and experimental values is most likely caused by the entrainment of nitrogen molecules from the surrounding air. From radially resolved measurements of the nitrogen concentration (using vibrational Raman scattering) it is concluded that classical inward diffusion is not fast enough, so that it is likely that the particle transport is enhanced by turbulence, which is found to be present in case of TIA. *(Chapters 5, 8 and 9)*

- In contrary to what normally is assumed for atmospheric plasmas, the high energy tail of the Electron Energy Distribution Function in the TIA plasmas is most probably significantly underpopulated with respect to a Maxwell equilibrium distribution. This is because the rate of the ground state excitation processes is larger than that of equilibrium restoring processes. The deviation from Maxwell reduces the ionisation within a factor of about three. *(Chapters 3 and 9)*

- For the QL-lamp the electron density and temperature as predicted by the size-stabilised plasma theory agree well with the values deduced from the measurements of the radial gas temperature profile and the argon metastable density. Both the electron density and temperature are found to be higher than in a conventional tubular fluorescent lamp, which is due to the much higher power density and the lower pressure of the buffer gas, respectively. *(Chapters 10 and 11)*

Summary

Within the wide variety of plasmas, those with a volume smaller than 1 dm^3 are the topic of this thesis. Because of the relative small dimensions, transport of (charged) particles plays a central role. These so-called size-stabilised plasmas are widely used for the generation of light, the deposition of thin layers and in the spectrochemical analysis.
For an optimal performance in these applications, knowledge about key plasma parameters, like the electron density and temperature, is crucial. The most simple and therefore also most popular way to obtain experimental values for these parameters is to deduce them from the intensities of some spectral lines emitted by the plasma. However, this is only possible if the plasma is in or close to equilibrium, which is often not the case for small plasmas. Especially for helium plasmas, these "characteristic" excitation temperatures have no relation with plasma parameters but only with the atomic structure of helium, as is shown in this thesis.
The electron density and temperature can also be obtained from the operation parameters of the plasma: the characteristic size, the power density, the pressure and the composition of the gas. The fact that in steady state the losses of charged particles due to diffusion have to be compensated by a production in the plasma, offers a powerful method to determine the electron temperature, because it is strongly related to the ionisation. The dissipated power is used to create free electrons and light and to heat the gas. Since the electrons are the intermediate step in these processes, the electron energy balance can be used to estimate the electron density. For those combinations of operation parameters for which the transport of charged particles plays an important role, i.e. small size, light (and thus mobile) ions and low pressure and power density, a high electron temperature, a low electron density and severe deviations from equilibrium are found.
The size-stabilised plasma theory is tested on two totally different plasmas. The first one is the TIA: a microwave induced plasma, which is sustained in the open air. Due to the small dimensions (around 2 mm in diameter and 15 mm long) transport of particles is important and the plasma is found to be far from equilibrium. The plasma is characterised by measuring the electron density and temperature and the gas temperature using advanced laser diagnostics, like Thomson and Rayleigh scattering. The spatial resolution of the setup has been improved to about 0.1 mm, since radially resolved measurements are necessary for a good interpretation of the results. It is found that besides outward transport of charged particles also inward transport of (nitrogen) molecules plays an important role. Moreover strong indications are found that the particle transport is enhanced by turbulence.
The other plasma under study is the Philips QL-lamp. The generation of light in this lamp is identical to the well known tubular fluorescent lamp. The most important difference is that due to inductive power incoupling no electrodes are needed, which benefits the life time. Compared to the TIA this plasma is much larger (the diameter of the bulb equals 11 cm), but also much tenuous (the typical argon filling pressure equals 100 Pa), so that also in this case huge deviations from equilibrium are induced by the transport of particles. Using a diode laser the gas temperature and the density of the lowest metastable state of argon are measured as function of the radial position and the argon filling pressure. From these results typical values for the electron densities and temperatures are determined, which agree well with the values obtained from the size-stabilised plasma theory.

Samenvatting

Plasma's zijn er in vele soorten en maten. In dit proefschrift worden de eigenschappen van plasma's die een volume hebben van minder dan ruwweg 1 dm^3 bekeken. Vanwege de relatief kleine afmetingen speelt transport van (geladen) deeltjes een centrale rol. De toepassingen van dit soort plasma's vindt men voornamelijk in verlichting, depositie van dunne lagen en spectrochemische analyse.

Kennis over plasma-parameters, zoals de dichtheid van de vrije elektronen en hun temperatuur, is van cruciaal belang voor het optimaal afstemmen van deze plasma's op hun toepassingen. De meest eenvoudige en daarom ook meest toegepaste manier om deze parameters te weten te komen is via het meten van de intensiteiten van een aantal spectrale lijnen. Voor een plasma dat in of dicht bij evenwicht is, kunnen hier de elektronentemperatuur en -dichtheid van afgeleid worden. Echter, dit gaat vaak niet op voor kleine plasma's en vrijwel nooit voor heliumplasma's. De in de literatuur gepresenteerde "karakteristieke" excitatie-temperaturen hebben geen enkel verband met plasmaparameters, maar des te meer met de atomaire struktuur van helium, zoals is aangetoond in dit proefschrift.

De elektronendichtheid en -temperatuur kunnen ook afgeschat worden op basis van de afmetingen van het plasma, de vermogensdichtheid, de druk en de samenstelling van het gas. In stationaire toestand moet het verlies van elektronen en ionen door diffusie gecompenseerd worden door een productie in het plasma. Dit levert een goede schatting van de elektronen-temperatuur omdat deze sterk gerelateerd is aan de productie. Het ingekoppelde vermogen wordt gebruikt om nieuwe geladen deeltjes en licht te creëren en het gas te verwarmen. Omdat de elektronen hierbij als intermediair optreden biedt deze vergelijking de mogelijkheid om de elektronendichtheid te bepalen. Het blijkt dat onder die omstandigheden waarbij de invloed van het transport van geladen deeltjes groot is (kleine afmetingen, lage vermogensdichtheid en druk en lichte -en dus bewegelijke- ionen) de elektronentemperatuur hoog, de elektronen-dichtheid laag en de afwijkingen van evenwicht groot zijn.

Deze "kleine-plasma-theorie" is getoetst aan twee totaal verschillende plasma's. Het eerste is een microgolf-plasma, genaamd TIA, dat expandeert in de open lucht. De kleine afmetingen (ongeveer 2 mm in diameter en 15 mm lang) zorgen ervoor dat transport van deeltjes een belangrijke rol speelt. Hierdoor is het plasma ver van evenwicht en zijn meer geavanceerde laserdiagnostieken zoals Thomsonverstrooiing noodzakelijk. Het is gebleken dat een goede interpretatie van de resultaten niet mogelijk is zonder ruimtelijk opgeloste metingen. De plaatsresolutie van de bestaande Thomsonverstrooiingsopstelling is hiertoe verbeterd tot circa 0.1 mm. Uit de metingen volgt dat niet alleen de diffusie van geladen deeltjes naar buiten, maar ook van (stiktof) moleculen naar binnen een belangrijke rol speelt. Tevens zijn er sterke aanwijzingen gevonden dat het deeltjestransport versneld wordt door turbulentie.

Het andere plasma dat aan bod is gekomen is de QL-lamp van Philips. Qua lichtproductie werkt deze lamp net zoals een TL-buis. Een groot verschil is echter dat de energie inductief ingekoppeld wordt en niet met behulp van elektroden, hetgeen de levensduur ten goede komt. Vergeleken met de TIA is dit plasma een stuk groter (de diameter van de lamp is 11 cm), maar ook veel ijler (een typische argon afvuldruk is 100 Pa), zodat ook hier het transport van geladen deeltjes er voor zorgt dat het plasma ver van evenwicht is. In verschillende lampen zijn de gastemperatuur en de dichtheid van het laagste metastabiele niveau van argon gemeten

als funktie van de plaats. Uit deze resultaten zijn typische elektronendichtheden en -temperaturen bepaald, die goed overeenstemmen met de waarden die verkregen zijn uit de "kleine-plasma-theorie".

Stellingen

behorende bij het proefschrift

Excitation and Transport in small scale Plasmas

door

Jeroen Jonkers

I

De geringe massa van de ionen is de voornaamste reden dat helium plasma's veelal ver van lokaal thermodynamisch evenwicht verwijderd zijn. Dit laatste verklaart tevens waarom voor helium plasma's meestal excitatie-temperaturen rond de 4000 K worden gerapporteerd.

(dit proefschrift)

II

De stelling dat in kleine atmosferische plasma's de kinetische-energieverdeling van de vrije elektronen wordt beschreven door een Maxwell-verdeling is onjuist.

*(M. Huang et al., Spectrochim. Acta **45B** 511 (1990), D.A. Benoy, "Modelling of thermal argon plasmas", proefschrift Technische Universiteit Eindhoven (1993), en dit proefschrift)*

III

Ten onrechte wordt vaak verondersteld dat bij het verlies van vrije elektronen door de vorming en vernietiging van moleculaire edelgasionen de vorming de bepalende stap is.

(dit proefschrift)

IV

Plasma's met een van nature hoge verliesfrequentie van de vrije elektronen zijn zeer goed bestand tegen de introductie van moleculaire gassen.

V

De mogelijkheden die Adaptive Noise Cancellation biedt voor het verbeteren van de signaal/ruis-verhouding in analytisch-chemische routinebepalingen worden, ten onrechte, tot op heden niet benut.

(E.P.P.A. Derks, B.A. Pauly, J. Jonkers, E.A.H. Timmermans en L.M.C. Buydens, "Adaptive noise cancellation on inductively coupled plasma spectroscopy", geaccepteerd voor publicatie in Chemometrics and intelligent laboratory systems)

VI

Bij de ontwikkeling van een plasmabron voor de *on line* analyse van rookgassen zijn flexibiliteit en robuustheid van groter belang dan het behalen van goede detectielimieten

(J.A.M. van der Mullen, J. Jonkers, E.A.H. Timmermans, H.M.M. de Jong, "Het on-line monitoren van een chemische afvalverbrandings-installatie met behulp van (inductief gekoppelde) plasma's", studiedag georganiseerd door het Belgisch Instituut voor Regeltechniek en Automatizering (BIRA), 1996).

VII

Om de hoeveelheid kwik te reduceren die als gevolg van verlichting in het milieu terecht komt, is het beter om energiezuinige dan kwikarme lampen te ontwikkelen.

(H.P. Stormberg, The 7th international symposium on the science & technology of light sources, Kyoto, 1995)

VIII

Het spectrum van de hoge-druk zwavellamp kan niet volledig worden beschreven door de produktie en het transport van de $B^3\Sigma_u^- \rightarrow X^3\Sigma_g^-$ straling te modelleren onder de aanname van lokaal thermisch evenwicht.

IX

De populariteit van de ingenieur in het bedrijfsleven is gedeeltelijk te verklaren door de zeer onevenwichtige man/vrouw verhouding onder de studenten van technische studies.

X

De term "zinloos geweld" als omschrijving van geweld op straat bagatelliseert de gevolgen voor het slachtoffer.

XI

Om eerstejaars wedstrijdroeiers zo hard mogelijk te laten roeien is het beter om ze een kortere haal aan te leren dan door de Koninklijke Nederlandsche Roeibond wordt gepropageerd.